

Department of the Navy  
Bureau of Ships  
Contract Nonr-220(12)

EXPERIMENTAL AND THEORETICAL INVESTIGATIONS OF  
A SUPERCAVITATING HYDROFOIL

R. L. Waid and Z. M. Lindberg

This research was carried out under the Bureau of Ships  
Fundamental Hydromechanics Research Program  
Project NS 715-102, David Taylor Model Basin

Reproduction in whole or in part is permitted for any  
purpose of the United States Government

Engineering Division  
California Institute of Technology  
Pasadena, California

Report No. 47-8  
April, 1957

Approved:  
M. S. Plesset

## TABLE OF CONTENTS

	<u>Page</u>
ABSTRACT	1
INTRODUCTION	1
APPARATUS AND TEST PROCEDURE	2
A. Model	2
B. Experimental Procedures	2
C. Data Analysis Procedure	5
D. Experimental Results	6
THEORETICAL CALCULATIONS	11
A. Application of Nonlinear Theory to the General Case	11
B. Theoretical Force Coefficients for the Supercavitating Hydrofoil	17
C. Experimental Comparison	19
CONCLUSIONS	22
APPENDICES	
A. Approximations and Corrections for Span- wise Twist of the Model Hydrofoil	23
B. Minimum Experimental Cavitation Number	27
BIBLIOGRAPHY	29
FIGURES	
TABLES	
DISTRIBUTION LIST	

# EXPERIMENTAL AND THEORETICAL INVESTIGATIONS OF A SUPERCAVITATING HYDROFOIL

## ABSTRACT

An experimental investigation of the two-dimensional hydrodynamic characteristics of a thin, supercavitating hydrofoil is described. The effects of twist and vibration of the thin hydrofoil model are considered, and experimental techniques for investigating spanwise twist and leading edge vibration and data correction methods are described. The theory of Wu for the forces on fully cavitating hydrofoils was used to calculate the forces on this profile. The calculated lift is in good agreement with the experimental results; however, the measured drag differs appreciably from the theoretical values.

## INTRODUCTION

Extremely high-speed operation of a conventional hydrofoil may make the occurrence of cavitation on the hydrofoil unavoidable with a resulting increase in drag and decrease in lift. If the hydrofoil is to operate successfully at high speeds, it is usually desirable for stable operation either to suppress the cavity formation entirely or to design the hydrofoil to have acceptable characteristics in the cavitating condition. In extreme operating conditions it may be necessary to operate the hydrofoil in a supercavitating state.

Theoretical<sup>1, 2, 3</sup> and experimental<sup>4</sup> investigations of the hydrodynamic forces on sharp-edged, flat plate and circular arc hydrofoils in full cavity flow have been reported. The present tests are an extension of this investigation to a more complex supercavitating hydrofoil profile. The results of experiments in the two-dimensional test section of the High Speed Water Tunnel are presented and compared with the theoretical values. Details of the mathematical procedure are presented together with the calculated lift and drag coefficients in fully cavitating flow.

## APPARATUS AND TEST PROCEDURE

A. Model

The hydrofoil model (cf. Fig. 1) tested has a 3.00-in. chord and 2.90-in. span. The coordinates of the profile, as specified by the David Taylor Model Basin, are given in Table I; Fig. 2a shows a sketch of the profile.

The hydrofoil tested differed slightly from the specified profile due to errors in fabrication. Since the hydrofoil was designed for full cavity operation, the contour of the lower surface is of primary importance. The principal errors on the lower surface occurred at the leading edge where the profile was approximately .001 in. too thick, and at the trailing edge where the profile was flattened by the removal of approximately .003 in. excess material in the final finishing process. These differences between the prescribed profile and the model are shown in the sketches given in Figs. 2b, c, and d. The model was later modified to obtain a more nearly correct profile; several repeat tests, however, showed the differences in the results to be insignificant.

The model and mounting disk were machined from a single piece of stainless steel (17-4 PH). After the model had been finished to its final contour, it was heat treated to increase its yield strength to 176,000 psi. This high strength was necessary in order to test the thin hydrofoil at high velocities with sufficiently high angles of attack.

B. Experimental Procedures

The experiments were conducted in the two-dimensional test section<sup>5</sup> of the High Speed Water Tunnel. During the tests the water temperature varied between 74.6 and 77.2°F. The vapor pressures of water for these temperatures are 0.42 and 0.46 psia. The air content of the water, as measured with a Van Slyke gas content analyzer, was approximately seven parts of air per million parts of water throughout the tests. The measured cavity pressure for vapor cavitation was approximately 0.5 psia. The excess pressure above vapor pressure of the water was caused by diffusion of air into the cavity. The methods

of mounting the hydrofoil and disk, tare corrections, and testing and data recording techniques are described in Refs. 4 and 5.

Because of the thinness of the hydrofoil, sizeable deflections occurred under hydrodynamic loading. Since it was impractical to compute this angular twist from the hydrodynamic forces, the deflections were determined experimentally for each data point by means of a catheter telescope mounted outside the test section window. The vertical position of the leading and trailing edges of the tip were measured (Fig. 3) and the twist angle determined to  $\pm 0.05^\circ$  by this method when the foil was reasonably steady. Vibration of the leading edge of the foil often made it impossible to make accurate measurements at the leading edge; therefore, a third measurement near the center of the model chord, where there was essentially no vibration, provided twist data which were also accurate to  $\pm 0.05^\circ$ .

Photographs of the cavitating hydrofoil were taken at each data point. Figures 3 and 4 are typical examples of these pictures which were taken with a 1/30-second exposure and show the extent of the cavitation on the hydrofoil. The chordwise bending of the model can be detected in these photographs as well as the tip twist.

Figure 3 shows the location of the cavity pressure probe and air feed line with respect to the hydrofoil. The air line was used during some of the runs to inject air into the cavities in order to obtain lower cavitation numbers than could be obtained with vapor cavities. The cavity pressure,  $p_k$ , was measured whenever the cavity was sufficiently free of water to obtain valid manometer readings. The free stream static pressure and the nozzle differential pressure for velocity determination were also read from manometers for each data point.<sup>4</sup>

Two cavitation numbers,  $\sigma_k$  and  $\sigma_v$ , are used in this report. The cavitation number,  $\sigma_k$ , was based on the cavity pressure,  $p_k$ , whenever it could be measured. When it was impossible to measure the cavity pressure, the cavitation number was based on the vapor pressure,  $p_v$ , of water and is called the vapor pressure cavitation number  $\sigma_v$ . These cavitation numbers are defined as follows,

$$\sigma_k = \frac{p_o - p_k}{\frac{\rho}{2} V^2} \quad \text{and} \quad \sigma_v = \frac{p_o - p_v}{\frac{\rho}{2} V^2}$$

where

$p_o$  is the free stream static pressure, lb/ft<sup>2</sup>

$p_k$  is the measured cavity pressure, lb/ft<sup>2</sup>

$p_v$  is the water vapor pressure at the temperature of the test, lb/ft<sup>2</sup>

$V$  is the free stream velocity, ft/sec

and

$\rho$  is the density of the water, slugs/ft<sup>3</sup>.

The experimental program was begun with force tests in fully wetted flow at a tunnel velocity of 20 fps in order to check the data system and to verify the tip twist and vibration characteristics of the hydrofoil. The model was tested at angles of attack from  $-5^\circ$  to  $+12^\circ$  with a sufficient working section static pressure to suppress all cavitation.

Most of the cavitation tests were made at a free stream velocity of 30 fps at twelve attack angles from  $-2^\circ$  to  $+10^\circ$ , including the design angle of  $2.722^\circ$ . At each angle of attack the working section static pressure was varied to obtain data over the range from noncavitating,  $\sigma = 3.0$ , to full cavity flow. Air was injected into the cavity during some of the tests in an attempt to decrease  $\sigma_k$  (see Appendix B). A few test runs were also made at a free stream velocity of 40 fps at angles of attack of  $2.722^\circ$ ,  $3^\circ$ , and  $4^\circ$ . During most of the tests at 40 fps and greater, the leading edge of the foil vibrated so violently that the vertical position of the leading edge could not be measured. The vertical measurement at the midchord of the foil was used during these runs.

Additional test runs were made at a free stream velocity of 45 fps for attack angles from  $2.722^\circ$  to  $6^\circ$ . To avoid violent force fluctuations which occur while developing a full cavity at this higher speed, the full cavity was produced at a lower velocity and maintained while the free stream velocity was increased to 45 fps. Therefore only the fully

cavitating regime, with cavitation numbers between 0.082 and 0.200, was investigated in these tests. Air-supported cavities were also used in some of the tests at 45 fps.

A final series of test runs were made for the purpose of observing the instantaneous cavitation patterns. The thin leading edge of the model had been observed to vibrate considerably during most of the previously described force tests. Single flash (15 microsecond duration) photographs were taken of the hydrofoil at tunnel velocities of 30 and 40 fps for various attack angles and cavitation numbers. The only data recorded for these tests were the pressures necessary to compute  $\sigma_v$ .

### C. Data Analysis Procedure

The measured force and moment data were corrected for balance pressure sensitivity and the tare forces on the mounting disk, as described in Ref. 5. The data were then reduced to coefficient form as follows:

$$C_L = \frac{\text{Lift}}{\frac{\rho}{2} V^2 A}, \quad C_D = \frac{\text{Drag}}{\frac{\rho}{2} V^2 A}, \quad C_{M_o} = \frac{\text{Moment}}{\frac{\rho}{2} V^2 A c}$$

where

V is the free stream velocity, ft/sec

$\rho$  is the density of the water, slugs/ft<sup>3</sup>

A is the plan area of the hydrofoil model, ft<sup>2</sup> (chord x span)

c is the hydrofoil chord, ft.

The moment coefficients are referred to the leading edge of the hydrofoil.

The model coefficients, computed directly from the force data, do not represent the section characteristics of the profile because of deflection of the hydrofoil. The chordwise deflection (or uncambering) has been estimated to have only a small influence on the measured lift coefficient, and although this effect on the drag coefficient can become appreciable, no attempt has been made to correct for it. Leading edge vibration undoubtedly has some effect on the model coefficients, but it was beyond the scope of the present investigation to evaluate it. The spanwise twist has a definite and predictable effect on the forces and

moments. The model coefficients were corrected for twist so that the resulting coefficients would represent the characteristics of the untwisted hydrofoil section. These are called the section characteristics and are different from the model characteristics.

The twist corrections which were applied to the data were based on a first order approximation that the entire hydrofoil was operating at an effective angle of attack which was greater than the angle of attack at the spindle end of the foil. A numerical correction of the coefficients would entail a tedious operation involving the coefficients, the rate of change of the coefficients with attack angle, and the effective twist angle, all of which vary with the base angle, the velocity, and the cavitation number. Therefore, it was expedient to correct the data by a graphical method.

The model coefficients and the effective attack angles for each spindle attack angle and tunnel velocity were plotted as functions of the cavitation numbers, and curves faired through the data. From these curves, graphs then were made of the coefficients as functions of the effective attack angle at constant cavitation number. The coefficients for each data point were then corrected by plotting the model coefficients at the effective attack angle and translating them to the base angle at a constant cavitation number. The twist-corrected data have been designated  $C_D$ ,  $C_L$ , and  $C_{M_0}$ . None of the data was corrected for tunnel blockage or other wall effects.

Table II presents the data, including the cavitation numbers, the model coefficients, the twist angle measurements, the hydrofoil section coefficients, and the lift-drag ratios. The data are referred to by data numbers which correspond to the numbers of the reference photographs. The data for the experiments in which air was injected into the cavities are not plotted in any of the figures.

#### D. Experimental Results

Force coefficients in noncavitating flow. The section lift, drag, and moment coefficients of the hydrofoil in noncavitating flow at 20, 30 and 40 fps are shown as functions of the attack angle in Fig. 5.

Force coefficients in cavitating flow ( $V=30$  fps). The section coefficients in fully wetted to fully cavitating flow at 30 fps are presented in Figs. 6 through 9. The solid symbols in these figures denote data for which only the vapor pressure cavitation number,  $\sigma_v$ , could be obtained. Whenever it was possible, the measured cavity pressure cavitation number was used to plot the data (open symbols). A discussion of this method of presenting cavitating force data is given in Ref. 4. With the exception of the data at fully wetted conditions ( $\sigma_v \approx 3.0$ ), all of the other data points represent cavitating flow. Partial cavitation on the upper surface and trailing edge of the hydrofoil had only a small effect on the force and moment coefficients. The maximum values of the coefficients occurred when the upper surface of the cavity became long enough to join the wake cavity from the blunt trailing edge. As the cavity extended beyond the hydrofoil in the full cavity region, the forces steadily decreased. At  $-2^\circ$  and  $0^\circ$  the leading edge cavity formed on the lower surface of the foil and thus produced negative lift forces. Although the leading edge cavity was also formed on the lower surface at  $+1^\circ$  angle of attack, the cavity was too short to enclose the entire lower surface, and the positive lift force was maintained. At an attack angle of  $2^\circ$  the upper surface of the foil showed some cavitation, but it was not completely enclosed by a cavity at even the minimum attainable cavitation number.

The hydrofoil section coefficients in the fully cavitating region ( $\sigma < 0.6$ ) are presented in Figs. 10 through 13. Only the data for the attack angles which produced positive lift forces are shown in these figures. The dashed portions of the faired curves join the region of data (open symbols) for measured cavitation numbers  $\sigma_k$  and the region of the data of vapor cavitation numbers  $\sigma_v$  (solid symbols). The dashed lines are used to indicate the portions of the data in which different methods of determining the cavitation number were used.<sup>4</sup>

Much of the data for cavitating conditions at attack angles less than  $4^\circ$  was taken with only a portion of the upper surface of the foil covered by cavities. Often only 50 per cent of the upper surface was wetted as the cavitation formed numerous unjoined finger-like cavities at the leading edge which partially collapsed near midchord and then redeveloped

near the trailing edge. These cavities were uniform in size and were distributed along the leading edge of the model leaving sizeable wetted regions between them. At  $4^\circ$  attack angle, the upper surface of the hydrofoil was sufficiently below the full cavity contour so that the surface of the model did not interfere with the formation of long uninterrupted cavities.

Cross-plots of the faired curves of Figs. 6 through 13 were made at selected  $\sigma$  values in order to show the coefficients as functions of the angle of attack, as shown in Figs. 14 through 17. Figure 18 is a polar diagram of section lift and drag coefficients at constant cavitation numbers. The symbols used in these figures are not experimental data points, but are used to denote regions of measured and vapor cavitation number, as in Figs. 6 through 13.

Effect of velocity on full cavity force coefficients. The experimental tests at tunnel velocities of 40 and 50 fps were made to attain lower cavitation numbers (Appendix B) and to establish the velocity dependence, if any, of the force coefficients in full cavity flow. Figures 19 and 20 present the data obtained with vapor cavities at tunnel velocities of 40 and 45 fps as compared with the results obtained at 30 fps (faired curves from Figs. 6 and 7). The lift coefficients, Fig. 19, show no velocity effect. The shift of some of the groups of data is due to the slight differences in the actual attack angle as is noted on the figures. The drag coefficients, Fig. 20, are in fair agreement at low attack angles. The data for  $3^\circ$  attack angle at 45 fps, where  $.09 < \sigma < .10$ , show smaller drag coefficients than the 30 and 40 fps data at 2.8 degrees. A review of the data film showed that these low drag points were obtained without the leading edge vibration which resulted from the absence of the tip cavity. The interaction between a cavity extending over the full span and the leading edge vibration was noted several times during the tests. It was observed that when the cavity near the tip gap of the model was absent, the frequency of the leading edge vibration was changed significantly (Fig. 29) and in some cases the vibration was eliminated entirely (Fig. 28). The shedding of the tip end of the cavity appeared to be random. This phenomenon was responsible for the

observed 8 per cent decrease in the drag coefficient, Fig. 20, without a significant decrease in the lift coefficient, Fig. 19. It is not known whether the observed change in drag can be attributed to the absence of vibration, the loss of the cavity or a combination of both. The drag coefficients for large attack angles at 45 fps are significantly different from those at 30 fps. This discrepancy may be due to the fact that the uncambering effect becomes more severe with an increase in velocity and attack angle. The chordwise deflection is concentrated near the leading edge of the foil so that it should not have an appreciable effect on the lift coefficients. On the other hand, this deflection should have a more pronounced effect on the drag coefficients. This view seems to be verified by the experimental data (Figs. 19 and 20) and the theoretical calculations (see Sec. B of "Theoretical Calculations" for the effects of camber and entry on the force coefficients). It should be noted that, in addition to the uncambering effect produced by high velocities, the amplitude of the leading edge vibration appeared to increase with an increase in velocity. The amplitude of this vibration for an attack angle of  $4^{\circ}$  and a tunnel velocity of 45 fps has been estimated from the data photographs to be 0.025 inch.

Force coefficients for the modified model. The section lift and drag coefficients for the hydrofoil with the modified leading edge are presented in Fig. 21. The symbols represent the data points while the curves are interpolated from those shown in Figs. 6 and 7. The discrepancies between the data for the two models were not considered significant enough to require more extensive testing. The differences in the data for fully wetted flow are small and the partial cavitating data are in reasonable agreement considering the violent force fluctuations which occur in that region. The data in the full cavity region at an attack angle of 3.8 degrees were taken without a tip cavity and without leading edge vibration, which caused a difference only in the drag coefficient.

Photographs of cavities from the vibrating leading edge. Most of the experimental data were taken with the leading edge or the entire model vibrating. A series of single flash photographs were taken of the modified model at tunnel velocities of 30 and 40 fps in order to study this

vibration. Figures 22 through 25 show an oblique view looking from the tip of the hydrofoil toward the mounting disk. The tip cavitation can be seen as a sheet of cavitation caused by the flow through the tip clearance gap. This cavity partially obscures the cavity on the hydrofoil; however, the wave-like surface of the main cavity can still be seen in the photograph. A similar though smaller sheet-type cavity forms at the intersection of the foil and the mounting disk.

Plan view photographs of the cavitation pattern are shown in Figs. 26 through 33. The leading edge of the foil is near the right side of the photographs and the trailing edge near the center with the free tip at the bottom of the photographs.

Figures 26 through 30 are for a tunnel velocity of 30 fps and an attack angle of  $2.73^\circ$ . A variety of flow patterns is produced by the model at this attack angle. Finger-like cavities are seen in Figs. 28, 29 and 30 which show extensive wetted regions between the cavities. The wave-like cavities in Fig. 27 show a node in the vibrating leading edge which causes the cavities on either side of it to be phase displaced. This node is located at the two-thirds span position. A check of twenty photographs indicates that when the cavitation extends to the tip of the foil the node appears in this same span position. The frequency of shedding of the wave-like cavities is approximately 800 cps (range 740-930 cps) as long as the single node exists. This frequency seems to be independent of the angle of attack. When there is no tip cavitation, there is usually no node and the frequency of shedding is increased. Only one good photograph, Fig. 29, was obtained without tip cavitation. The wave frequency for this photograph is approximately 1400 cps.

Figures 31 and 32 show the wave-like cavities with full cavity flow at an attack angle of 5.73 degrees and a velocity of 30 fps. The front half of the upper surface of the foil is intermittently wetted. The shedding frequency in these figures is 750 and 800 cps respectively. The frequency calculations are based on the assumption that the cavity surface disturbance is moving at the velocity of the cavity wall,  $\left[ V_0(1+\sigma)^{1/2} \right]$ .

Large attack angles, 8 and  $10^\circ$ , produced cavities which separated smoothly from the leading edge of the foil without detectable upper

surface waves. The wave pattern of the lower surface of these cavities can be seen through the clear upper cavity surfaces in Figs. 34 and 35. These waves developed on the cavity wall approximately 1/4-inch downstream from the trailing edge of the foil with a frequency of approximately 15,000 cps and a wave length of 0.025 inch which is several times the estimated boundary layer displacement thickness. It has been suggested that these lower surface waves might be surface tension waves, or be associated with Tollmein-Schlichting laminar boundary layer oscillations.

Simple tests were made to determine the approximate natural frequencies of vibration of the hydrofoil in air. Resonance occurred at frequencies between 750 and 850 cps, at 1000 cps, and at higher multiples of these frequencies.

## THEORETICAL CALCULATIONS

### A. Application of the Nonlinear Theory to the General Case

A significant part of the present program is a comparison of the experimental results with Wu's nonlinear theory for two-dimensional fully cavitated hydrofoils.<sup>1</sup> The equations for these calculations are derived here on the basis of this theory.

The theoretical calculations are based on the assumption that the foil has sharp leading and trailing edges which are the separation lines of the free streamlines. Therefore, in full cavity flow the upper surface may have any profile which lies below the upper free streamline. In addition, it is also assumed that the lower surface of the foil is concave with a continuous, slowly changing slope (a nearly constant curvature in the center region and small changes in curvature at the leading and trailing edges).

With the points A and B at the leading and trailing edges respectively (cf. Fig. 36), the following boundary conditions are specified:

$$i) \theta_A = \pi - \alpha + \phi_1$$

$$\text{ii) } \theta_B = -(\alpha + \varphi_2)$$

$$\text{iii) Radius of curvature at } A = R_A = \frac{-(1 + \varphi_1^2)^{3/2}}{\left(\frac{d^2 \bar{y}}{d \bar{x}^2}\right)_A} \equiv \frac{1}{K_A}$$

$$\text{iv) Radius of curvature at } B = R_B = \frac{-(1 + \varphi_2^2)^{3/2}}{\left(\frac{d^2 \bar{y}}{d \bar{x}^2}\right)_B} \equiv \frac{1}{K_B}$$

Applying these boundary conditions in the same manner as is done in deriving Eqs. (4.3) - (4.6) of Ref. 1, we obtain

$$A_1 + A_3 = \frac{\varphi_1 + \varphi_2}{2} + \frac{1}{2} \left\{ \left[ (\alpha + \varphi_2)^2 + \epsilon^2 \right]^{1/2} - (\alpha + \varphi_2) \right\} + \frac{\epsilon^2}{4\pi}, \quad (1)$$

$$\beta + A_2 = \alpha + \frac{\varphi_2 - \varphi_1}{2} + \frac{1}{2} \left\{ \left[ (\alpha + \varphi_2)^2 + \epsilon^2 \right]^{1/2} - (\alpha + \varphi_2) \right\} - \frac{\epsilon^2}{4\pi}, \quad (2)$$

$$A_1 + 4A_2 + 9A_3 \approx \frac{2K_B}{J} \frac{(\alpha + \varphi_2)}{\left[ (\alpha + \varphi_2)^2 + \epsilon^2 \right]^{1/2}} (1 + \cos \beta), \quad (3)$$

and

$$A_1 - 4A_2 + 9A_3 = \frac{2K_A}{J} (1 - \cos \beta). \quad (4)$$

The quantity  $J$  appearing in the above equations is

$$J = 4 + \pi \sin \beta + A_1 \left( \pi + \frac{8}{3} \sin \beta \right) + \frac{\pi}{2} A_2 \cos \beta - \frac{8}{15} A_3 \sin \beta \quad (5)$$

which is the same as given in Eq. (3.18) of Ref. 1. In solving for  $\beta$ ,  $A_1$ ,  $A_2$ , and  $A_3$  in Eqs. (1) - (4), it is necessary to make an approximation of  $J$ .

When  $\alpha$  is small, then  $\beta$  is small, and we can make the approximations

$$J \cong 4 + \pi \sin \beta + \pi A_1 \cong 4 + \pi(\beta + A_1). \quad (6)$$

Solving Eqs. (1) - (4), we obtain

$$\beta = \alpha + \frac{\varphi_2 - \varphi_1}{2} + \frac{1}{2} \delta - \frac{\epsilon^2}{4\pi} - \frac{1}{2} \frac{1}{J} (K_B \psi \cos^2 \frac{\beta}{2} - K_A \sin^2 \frac{\beta}{2})$$

and

$$A_1 = \frac{9}{8} \left( \frac{\varphi_1 + \varphi_2}{2} + \frac{1}{2} \delta + \frac{\epsilon^2}{4\pi} \right) - \frac{1}{4} \frac{1}{J} (K_B \psi \cos^2 \frac{\beta}{2} + K_A \sin^2 \frac{\beta}{2})$$

where

$$\delta = \left[ (\alpha + \varphi_2)^2 + \epsilon^2 \right]^{1/2} - (\alpha + \varphi_2),$$

$$\psi = \frac{\alpha + \varphi_2}{\left[ (\alpha + \varphi_2)^2 + \epsilon^2 \right]^{1/2}},$$

and

$$\epsilon = \frac{1}{2} \ln(1 + \sigma).$$

Since  $\beta$  and  $A_1$  are small, we can now obtain a usable approximation of  $J$  to solve for  $\beta$ ,  $A_1$ ,  $A_2$  and  $A_3$  by substituting the first two terms in the equation for  $\beta$  and the first term in the equation for  $A_1$  into Eq. (6) to obtain

$$J \cong 4 + \pi \sin(\alpha + \varphi_2) = \lambda.$$

Now solving Eqs. (1)-(4) and substituting  $\lambda$  for  $J$ , we obtain

$$\beta \cong \alpha + \frac{\varphi_2 - \varphi_1}{2} + \frac{1}{2} \delta - \frac{\epsilon^2}{4\pi} - \frac{1}{2\lambda} (K_B \psi \cos^2 \frac{\alpha}{2} - K_A \sin^2 \frac{\alpha}{2}), \quad (7)$$

$$A_1 \approx \frac{9}{8} \left( \frac{\varphi_1 - \varphi_2}{2} + \frac{1}{2} \delta + \frac{\epsilon^2}{4\pi} \right) - \frac{1}{4\lambda} (K_B \psi \cos^2 \frac{\beta}{2} + K_A \sin^2 \frac{\beta}{2}), \quad (8)$$

$$A_2 \approx \frac{1}{2\lambda} (K_B \psi \cos^2 \frac{\beta}{2} - K_A \sin^2 \frac{\beta}{2}), \quad (9)$$

$$A_3 \approx -\frac{1}{8} \left( \frac{\varphi_1 + \varphi_2}{2} + \frac{1}{2} \delta + \frac{\epsilon^2}{4\pi} \right) + \frac{1}{4\lambda} (K_B \psi \cos^2 \frac{\beta}{2} + K_A \sin^2 \frac{\beta}{2}). \quad (10)$$

A discussion of the accuracy of this procedure may be found in Ref. 1, sec. IV.

With  $\beta$ ,  $A_1$ ,  $A_2$ , and  $A_3$  given by Eqs. (7)-(10) and  $J$  by Eq. (5), we can now calculate  $C_D$  and  $C_L$  by a slight modification of Eqs. (4.12) and (4.13) of Ref. 1. Replacing  $\gamma^2$  by  $[(\varphi_1 + \varphi_2)/2]^2$ , we obtain

$$C_D \approx \frac{2\pi}{J} \left[ 1 + \sigma + \frac{\epsilon^2}{6} + \frac{(\varphi_1 + \varphi_2)^2}{24} \right] \left( \sin \beta + \frac{A_1}{2} \right)^2 \quad (11)$$

and

$$C_L \approx \frac{2\pi}{J} \left[ 1 + \sigma + \frac{\epsilon^2}{4} + \frac{(\varphi_1 + \varphi_2)^2}{24} \right] \left\{ \left[ \sin \beta \cos \beta + A_1 \cos \beta + \frac{A_2}{2} \right] + \frac{\epsilon^2}{4} \frac{\cos \beta}{(\sin \beta + A_1/2)^4} \left[ \left( \sin \beta + \frac{A_1}{2} \right)^3 + \left( \frac{A_1}{2} + \frac{5}{4} A_2 + A_3 \right) \left( \sin \beta + \frac{A_1}{4} \right) \right] \sin \beta \right\}. \quad (12)$$

It should be pointed out that, in order to avoid the more tedious computation which would result from taking more terms in the expansion of Eq. (3.3) of Ref. 1, the above expressions for  $C_L$  and  $C_D$  are calculated by taking only three terms, as was done in Ref. 1. The four unknown coefficients  $\beta$ ,  $A_1$ ,  $A_2$  and  $A_3$  are then determined as shown above by applying boundary conditions (i) to (iv). They assert that the streamlines leaving the leading and trailing edges should have the same slopes and curvatures as those of the wetted surface at the two edges. The solution so obtained in turn determines the whole flow field and the

cavity boundary as a function of cavitation number  $\sigma$  and attack angle  $\alpha$ . However, it must be determined whether or not the resulting flow satisfies the boundary conditions at other points on the wetted surface. For example, since it is assumed that the streamline on the wetted side of the hydrofoil does not separate from the surface between the two edges, it would be of interest to see how well the curvature of the theoretically determined streamline agrees with the curvature of the profile at some point. For simplicity, we shall choose in particular the point  $\eta = \pi/2$ , a point somewhere near the midchord section. By using the definitions and notations adopted in Ref. 1, the radius of curvature of the streamline at  $\eta = \pi/2$  is given by

$$R = 2b^2 \cos \beta \left\{ e^{-\tau(\eta)} \frac{d\eta}{d\theta} \right\}_{(\eta = \pi/2)} \quad (13)$$

$$\Omega = -\sqrt{\omega^2 + \epsilon^2} = -\omega - \frac{\epsilon^2}{2\omega}$$

where

$$\omega = \theta + i\tau .$$

$$\Theta + iT = -\theta - i\tau - \frac{\epsilon^2(\theta - i\tau)}{2(\theta^2 + \tau^2)} ,$$

by neglecting the term in  $\epsilon^2$  this relation becomes

$$\Theta + iT = -\theta - i\tau .$$

In the present case the range of applicability of  $\sigma$  is likely to be less than  $\sigma = 0.3$ . The experimental tests showed that a full cavity was not developed for  $\sigma = 0.3$ , consequently  $\epsilon = 1/2 \ln(1 + \sigma)$  is less than 0.135 and thus the term neglected is very small. It then follows that

$$\theta = -\Theta = -(\beta + A_1 \cos \eta + A_2 \cos 2\eta + A_3 \cos 3\eta) ,$$

$$\left(\frac{d\theta}{d\eta}\right)_{\eta=\pi/2} = -(-A_1 \sin \eta - 2A_2 \sin 2\eta - 3A_3 \sin 3\eta)_{\eta=\pi/2} \quad (14)$$

$$= A_1 - 3A_3 ,$$

and

$$(\tau)_{\eta=\pi/2} \cong (-T)_{\eta=\pi/2} \cong -\left(\frac{1}{2} \ln \frac{1+\sin \beta}{1-\sin \beta} + A_1 - A_3\right) . \quad (15)$$

From Eqs. (13)-(15)

$$R = 2b^2 \cos \beta \sqrt{\frac{1+\sin \beta}{1-\sin \beta}} e^{A_1 - A_3} \frac{1}{(A_1 - 3A_3)} ,$$

where

$$b^2 = \frac{S}{J} .$$

Therefore,

$$\frac{R}{S} \cong \frac{2}{J} \cos \beta \sqrt{\frac{(1+\sin \beta)^2}{1-\sin^2 \beta}} (1+A_1-A_3) \frac{1}{A_1-3A_3}$$

which reduces to

$$\frac{R}{S} \cong \frac{2}{J} \frac{(1+A_1-A_3+\sin \beta)}{(A_1-3A_3)} .$$

For the circular arc (see Fig. 37a)

$$S = R(2\gamma) ,$$

and therefore

$$K = \frac{S}{R} = 2\gamma .$$

For the supercavitating hydrofoil for  $\sigma \leq 0.3$ ,

$$K_{\pi/2} \cong \frac{J(A_1 - 3A_3)}{2(1 + A_1 - A_3 + \sin \beta)} \quad (16)$$

$K_{\pi/2}$  in Eq. (16) is not the exact curvature of the profile streamline, but for small  $\varphi_1$ ,  $\varphi_2$ ,  $K_{\pi/2}$  and  $\sigma$  it is a good approximation (Fig. 37b). It may be used as a check to see if the boundary conditions at A and B as applied in deriving Eqs. (7)-(12) produce an approximate curvature at  $\eta = \pi/2$  which is near that of the profile at  $\eta = \pi/2$ . When this process of checking, along with some of the approximation methods adopted in choosing  $\varphi$ 's and  $K$ 's, fails to yield a  $K_{\pi/2}$  within a reasonable degree of accuracy, it may imply that more terms in the expansion, Eq. (33) of Ref. 1, should be taken and that more points should be suitably chosen on the profile to which the boundary conditions are to be applied.

#### B. Theoretical Force Coefficients for the Supercavitating Hydrofoil

The application of Wu's theoretical equations to this complex hydrofoil presents more difficult problems than the geometrically simple cases presented in Ref. 1.  $\varphi_1$  and  $\varphi_2$  were small and therefore were assumed to be equal to the slopes at A and B. The slopes of the lower surface of the foil were measured from the enlarged graph from which the model offsets were obtained. These slopes were then plotted to a large scale and a curve of the second derivative was obtained from them. Neither the prescribed nor the model profile had contours near the leading edge which satisfied the conditions specified in the derivation of the equations. The slopes changed rapidly in this region and consequently the curvatures were large for both profiles (Fig. 38). A further complication was the fact that the curvatures became negative near the leading edge. This occurred for approximately the first .03 chord of the prescribed profile and for approximately the first .06 chord of the model profile. The trailing edge contour of the prescribed profile was as specified. The model profile near the trailing edge deviated from the specified contour in a manner similar to that at the leading edge.

The rapidly changing slopes and large negative curvatures near the leading and trailing edges presented a considerable problem in

choosing the values of the  $\phi$ 's and  $K$ 's which should be substituted into Wu's equations. It was suggested that sets of  $\phi$ 's and  $K$ 's be approximated by a root mean square average where they deviated from the specified contours. Root mean square  $\phi_1$ 's and  $K_A$ 's were computed over the first 0.05 chord for both the prescribed and model profiles and rms  $\phi_2$  and  $K_B$  computed over the last 0.10 chord for the model profile. This method still gave negative curvatures at these points. These  $\phi$ 's and  $K$ 's, Table IIIa, were then substituted into Eqs. (5), (7)-(12), and (16) to calculate  $C_L$ ,  $C_D$  and  $K_{\pi/2}$ , Table IIIb. There were large differences in these values, and furthermore the negative curvature at the trailing edge produced a streamline curvature at the midchord which was almost twice that of the profile. Since these conditions were unsatisfactory, it was proposed by Dr. Wu that geometric mean and rms curvatures over the first and last halves of the profiles be determined. The two methods of averaging over the last half of the prescribed profile gave the same result to two decimal places, Table IIIa, and this differed from the measured curvature at  $\bar{x} = 1.0$  chord by 0.01. The model profile average curvatures over the last half differed by 0.01, the geometric mean being larger. However, these average curvatures of the model profile at the trailing edge were only a little more than half as large as those computed in the same region for the prescribed profile. The agreement of the two methods of averaging over the first half of the profile was poor for both the prescribed and model profiles, Table IIIa.

A systematic variation of the values of  $\phi$ 's and  $K$ 's obtained from the averaging methods along with the maximum and minimum  $\phi$ 's was made to discover the effect of each of these parameters on  $C_L$ ,  $C_D$  and  $K_{\pi/2}$  for  $\alpha = 3^\circ$  and  $\sigma = 0$ . It was concluded from Table IIIb and Fig. 39 that

1. for increasing  $\phi_1$ ,  $C_L$  increases and  $C_D$  decreases ;
2. for increasing  $\phi_2$ , both  $C_L$  and  $C_D$  increase ;
3. for increasing  $K_B$ , both  $C_L$  and  $C_D$  decrease ;
4.  $K_A$  had a negligible effect on  $C_L$  and  $C_D$  .

An interesting point shown by Fig. 39 is that  $C_L$  and  $C_D$  are

apparently linear functions of the parameters  $\phi_1$ ,  $\phi_2$  and  $K_B$  for the ranges calculated for this report. This fact could possibly be helpful in designing other hydrofoils of a similar nature.

The parameters chosen for computing the coefficients of the prescribed model were

$$\phi_1 = .065, \quad \phi_2 = .100, \quad K_A = 0, \quad \text{and} \quad K_B = .22 ;$$

and for the model profile

$$\phi_1 = .058, \quad \phi_2 = .079, \quad K_A = 0, \quad \text{and} \quad K_B = .13 .$$

The  $\phi$ 's chosen in both cases were r m s  $|\overline{dy}/\overline{dx}|$  from  $\overline{x} = 0$  to  $\overline{x} = .05$  chord. The prescribed profile  $\phi_2$  was  $|\overline{dy}/\overline{dx}|$  at  $\overline{x} = 1.0$  chord since the  $\overline{dy}/\overline{dx}$  curve, Fig. 38a, had no inflections in this region.  $\phi_2$  for the model profile was a r m s  $|\overline{dy}/\overline{dx}|$  from  $\overline{x} = .9$  chord to  $\overline{x} = 1.0$  chord. This decision was arbitrary, but it was considered to be the most realistic approximation.  $K_A$  was chosen to be equal to zero because it appeared to have a negligible effect on the coefficients. There was no problem in choosing  $K_B$  for the prescribed profile since its  $\overline{d^2y}/\overline{dx^2}$  behaved properly at the trailing edge. The  $K_B$  chosen for the model was arbitrarily the geometric mean over the last .50 chord. Figures 40-42 show the calculated  $C_L$ ,  $C_D$  and  $L/D$  plotted as a function of  $\sigma$  for both profiles at attack angles from 1 to  $10^\circ$ .

### C. Experimental Comparison

Graphical comparisons of the experimentally determined section lift and drag coefficients and the lift-drag ratio with the theoretical computations for the model profile are shown in Figs. 43-45. The open data symbols denote  $\sigma_K$ , which is based on measured cavity pressure. When the cavity pressure could not be measured and  $\sigma_V$  (solid symbols) was computed, the cavity was usually too short and frothy to provide valid comparison with the theory. The theoretical curves shown are for  $3^\circ, 4^\circ, 6^\circ$  and  $10^\circ$  attack angle, while the experimental data are for  $3^\circ, 4.2^\circ, 6^\circ$  and  $10^\circ$ .

The theoretical lift coefficients, Fig. 43, are in very good

agreement with the experimental data in the region of comparable flow conditions (open symbols). At small attack angles,  $3^\circ$  and  $4^\circ$ , the experimental data are less than 3 per cent higher than the theoretical curves. At an attack angle of  $10^\circ$ , the theory is less than 5 per cent higher than the experimental data.

The comparison of the drag coefficients, Fig. 44, shows marked discrepancies between the theory and the data. For attack angles of  $3^\circ$  and  $4^\circ$ , the discrepancy can be explained by the lack of consideration of the viscous drag force in the theoretical calculations. The experimental drag coefficients at  $3^\circ$  are about .003 (28 per cent) higher than the theoretical curve. At the Reynolds number of these data ( $7.5 \times 10^5$ ) the laminar skin friction drag coefficient is .0015 while the turbulent skin friction drag coefficient is .0046. (The dashed curves in Fig. 44 represent the theoretical drag with the friction drags included). Thus the comparison at small attack angles appears to be quite reasonable when the entire lower surface and small portions of the upper surface of the foil are wetted. Hydrofoil attack angles of 6 and 10 degrees, however, show experimental drag coefficients which are as much as 11 per cent smaller than the theoretical drag coefficients without considering the skin friction drag in the theory. The addition of the skin friction drag would increase this discrepancy to about 15-20 per cent of the experimental values.

Figure 45 shows a comparison of the experimental and theoretical lift-drag ratios. The trends of the theoretical curves are opposite to those of the experimental data.

The poor agreement between experiment and theory for drag suggests that either the leading and trailing edge approximations which were used in the theoretical calculations, or the two point theoretical analysis which was made, did not provide an adequate representation of the model that was tested. Although this statement appears to be contradicted by the good lift agreement, it must be remembered that the leading edge angle of the lower surface of the foil,  $\phi_1$ , has a greater effect on drag than it does on lift, (Fig. 39). The slope of the profile deviated from the assumed (continuous slowly changing) slope of the theory by a larger

amount near the leading edge than it did near the trailing edge, Fig. 38a. Therefore, the approximation for  $\phi_1$  was probably less valid than the approximations for  $\phi_2$  and  $K_B$ . It is possible that the end condition approximations could be adjusted to provide a better over-all agreement between the experimental data and the theory and between the calculated curvature,  $K_{\pi/2}$ , and the model contour. The experimental and theoretical agreement may be improved by this type of manipulation, but the fact remains that the end condition approximations which were used in the theoretical computations were based on reasonable methods of approximation. The necessity of adjusting these approximations suggests the desirability for either a different method of approximating the end conditions or the use of more points on the wetted contour to better establish the full cavity flow field.

The foregoing discussion has been based on the assumption that the theoretical results are valid if the actual flow conditions can be well represented by the theory. Parkin<sup>4</sup> has observed that in spite of the fine agreement between the lift and drag data for flat plate and circular arc hydrofoils and the theory, the experimental lift-drag ratio has an entirely different trend than the theory predicts. The supercavitating hydrofoil lift-drag ratio results show similar discrepancies. It does not appear that these differences in trend are a result of the approximations which were made for the  $\phi$ 's and  $K$ 's. The two sets of boundary conditions (prescribed and model profiles) for which lift and drag coefficients were computed produced curves which were very similar to each other in shape (Figs. 40 and 41). Therefore, the lift-drag ratios of the two profiles have similar trends. It appears from these tests and from those made by Parkin that the extension of Wu's theory to more points on the profile of the wetted surface would be necessary before a rigorous evaluation of the theoretical and experimental data can be made. However, the computations for this expanded theory would only be practical if they could be done on a high-speed computing device.

The above discussion assumes that the theoretical and experimental results are directly comparable. Parkin has suggested that the discrepancies between the theory and the experiments may be due to tunnel

wall effects. Wu's analysis is for a hydrofoil operating in an infinite free stream, while in the experimental case this situation does not exist. Tunnel wall effects surely exist;<sup>5</sup> however, they have not been fully investigated either theoretically or experimentally for fully cavitating hydrofoils except at zero cavitation number with a linearized theory.<sup>6</sup>

## CONCLUSIONS

The theoretical calculations of lift coefficient compared very favorably with the experimental data. There was reasonable agreement between the drag data and theory at low angles of attack ( $\alpha < 5^\circ$ ). However, drag data at high attack angles and all lift-drag ratio data were decidedly different from the theory. The over-all agreement between the theoretical and experimental results might be improved by extending Wu's analysis to more boundary points on the wetted profile and by adapting the theoretical computations to high-speed computing devices.

In addition, further studies, both theoretical and experimental, of tunnel wall effects in cavitating flow would be useful in understanding the discrepancies between the experimental and theoretical lift-drag ratios.

## APPENDIX A

Approximations and Corrections for Spanwise Twist  
of the Model Hydrofoil

A simplified approximation of the spanwise twist of the model hydrofoil and its effects on the experimental force measurements are described in this section.

The model is considered to be a cantilever beam of the prescribed profile. The hydrodynamic forces are assumed to act as two distributed loads on this beam (Fig. 46). One load, the drag, acts in the direction of the free stream velocity and to a first approximation, has a negligible contribution to the twisting of the hydrofoil. The other load, the lift, acts normal to the flow direction. This distributed load is assumed to be a linear function of the section attack angle and to be applied at the center of pressure of the section, which for this profile is significantly displaced from the center of twist. For the purpose of this simplified analysis the cantilever beam is considered to be composed of a number of spanwise elements. Because of the cantilever construction each element is assumed to be twisted in proportion to the integrated spanwise torque at that element. Then

$$\frac{d^2 \alpha}{dx^2} = -h \frac{1}{2} \rho V^2 c \left( \frac{\partial C_L}{\partial \alpha} \alpha + C_{L_0} \right) kc$$

where

$\alpha$  is the elemental attack angle

$x$  is the spanwise position of the element

$h$  is the elastic constant =  $\frac{1}{KG}$

$\frac{1}{2} \rho V^2$  is the dynamic pressure of the fluid

$c$  is the hydrofoil chord

$kc$  is the distance from the elemental center of pressure  
to the section center of twist

$C_{L_0}$  is the lift coefficient at zero attack angle.

The equation can be solved for the elemental twist angle. Upon expansion of the elemental lift as a linear function of the elemental attack angle, the total lift of the twisted foil can be computed. A comparison of the total lift of the twisted foil with that of an untwisted foil yields a trigonometric relation which can be expanded in the form

$$\frac{\text{untwisted lift}}{\text{twisted lift}} = 1 - \frac{2}{3} \mu + \frac{7}{15} \mu^2 + \dots$$

where

$$\mu = \frac{C_{L_T} - C_{L_a}}{C_{L_a}}$$

$C_{L_T}$  = lift coefficient at the attack angle of the tip of the foil,

$C_{L_a}$  = lift coefficient at the attack angle of the base of the foil.

With neglect of the higher order terms, the twisted foil can be considered to have operated at an effective angle of attack ( $\alpha_e$ ) which is equal to the base angle of attack ( $\alpha_a$ ) plus two thirds of the tip twist angle ( $\alpha_{T_e}$ ). The lift coefficients were corrected for the contribution of the effective twist angle to the lifting force. Full cavity operation resulted in approximately a 1 per cent correction to the lift coefficients, while in partially cavitating flow the correction approached 10 per cent.

This correction procedure was also applied to the drag coefficients although they actually involve a slightly more complex analysis. The additional considerations are not warranted because of the other approximations which were made. The drag coefficient corrections amounted to several per cent in full cavity operation and up to 15 to 20 per cent in fully wetted flow.

It appeared that the uncambering effect at 20 and 30 fps was small enough that the twist angle corrections could be applied on the basis of the leading-to-trailing edge twist angle ( $\alpha_{T_{LE}}$ ). The uncambering effect became so great at 40 and 45 fps that the leading-to-trailing edge twist angle could

not adequately represent the average twist of the entire model. Therefore, the midchord-to-trailing edge angle ( $\alpha_{T_M}$ ) was used in the twist corrections at these velocities. The spanwise<sup>M</sup> twist corrections discussed here were applied to all of the experimental data regardless of the flow conditions. This was done for the simple reason that there is no existing procedure for correcting hydrofoil data for spanwise twist throughout the entire cavitating flow regime. The only established corrections at the present time are those for the fully wetted case, which consider not only the geometric twisting of the foil but also the induced effects of the spanwise twist upon the entire flow field. Since these induced effects have not, as yet, been evaluated for full cavity flow, it is impractical to attempt to make corrections for anything but the geometric twisting as outlined above.

## APPENDIX B

## Minimum Experimental Cavitation Number

It was desirable with this supercavitating hydrofoil to extend the experiments to the minimum attainable cavitation number. The High Speed Water Tunnel test procedure for obtaining small cavitation numbers is to reduce the working section pressure at constant free stream velocity until the tunnel diffuser cavitation produces tunnel blockage. This results in a large drop in the free stream velocity and an increase in pressure. This velocity decrease, which occurs while the pump motor speed control is maintaining constant rotating speed, is accompanied by an unstable flow condition which makes it difficult to obtain data. Several methods of reducing the minimum attainable cavitation number were tried. The principal methods attempted were high-speed operation and air injection to increase cavity pressure. Smaller cavitation numbers can generally be obtained with small models; however, this approach was impractical in these tests.

A comparison of Figs. 10 and 18 shows that the minimum cavitation numbers which were obtained with vapor cavities occurred during the lower velocity (30 fps) tests.

Air injection had two different effects. It was found that by injecting air into the cavity, the cavitation number could be reduced approximately 0.01 below its value without air injection. However, the externally supplied air collected in the high regions of the tunnel after being entrained from the cavity. These air pockets allowed the static pressure of the entire water tunnel circuit to fluctuate causing the cavity to pulsate and the forces to oscillate. Thus, it was difficult to obtain simultaneous groups of force and pressure data. The added complications associated with the air injection method were not warranted, since the minimum cavitation number could be reduced only 0.010.

The results of these tests show that the useful minimum cavitation number in the High Speed Water Tunnel can best be obtained at a low tunnel velocity and an extremely low static pressure without the addition of air to the cavity region. The minimum cavitation number for these conditions with the supercavitating hydrofoil was 0.052.

## BIBLIOGRAPHY

1. Wu, T. Yao-tsu, "A Free Streamline Theory for Two-Dimensional Fully Cavitated Hydrofoils", Hydrodynamics Laboratory, California Institute of Technology, Report No. 21-17, July 1955.
2. Wu, T. Yao-tsu, "A Note on the Linear and Nonlinear Theories for Fully Cavitated Hydrofoils", Hydrodynamics Laboratory, California Institute of Technology, Report No. 21-22, 1956.
3. Tulin, P., "Supercavitating Flow Past Foils and Struts", National Physical Laboratory, Teddington, England, Symposium on Cavitation in Hydrodynamics, Report No. 16, September 1955.
4. Parkin, B. R., "Experiments on Circular Arc and Flat Plate Hydrofoils in Noncavitating and in Full Cavity Flow", Hydrodynamics Laboratory, California Institute of Technology, Report No. 47-6, 1956.
5. Kermeen, R. W., "Water Tunnel Tests of NACA 4412 and Walchner Profile 7 Hydrofoils in Noncavitating and Cavitating Flows", Hydrodynamics Laboratory, California Institute of Technology, Report No. 47-5, 1956.
6. Cohen, H. and Tu, Yih-O, "Wall Effects on Supercavitating Flow Past Foils", Rensselaer Polytechnic Institute Math. Report No. 6, October 1956.

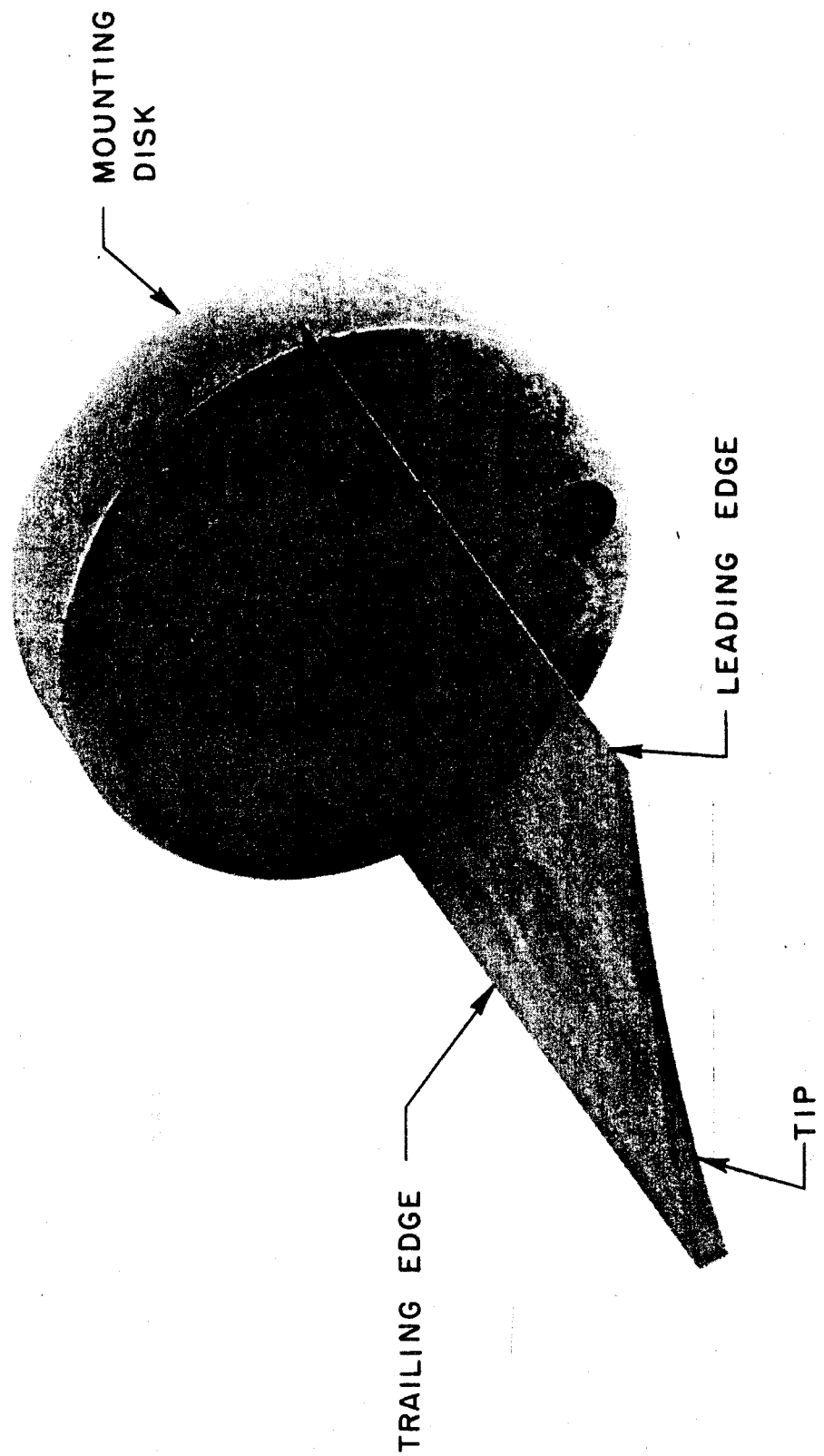


Fig. 1 3.00-in. chord by 2.90-in. span model supercavitating hydrofoil.

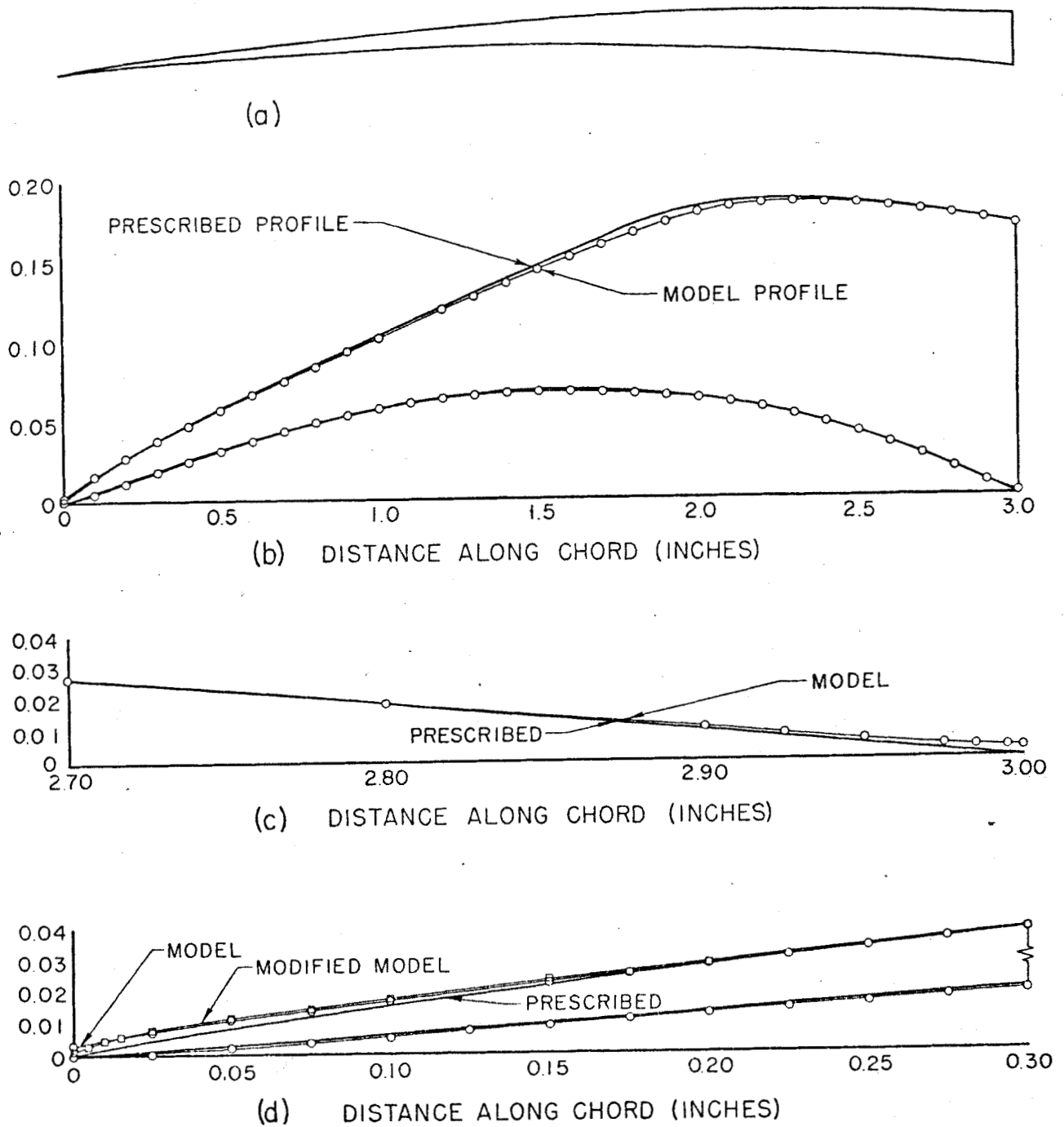


Fig. 2 Profiles of prescribed and model hydrofoil.  
 a. 1 by 1 scale  
 b. 5 by 1 scale  
 c. Bottom surface detail at trailing edge, 1 by 1 scale  
 d. Leading edge detail, 1 by 1 scale

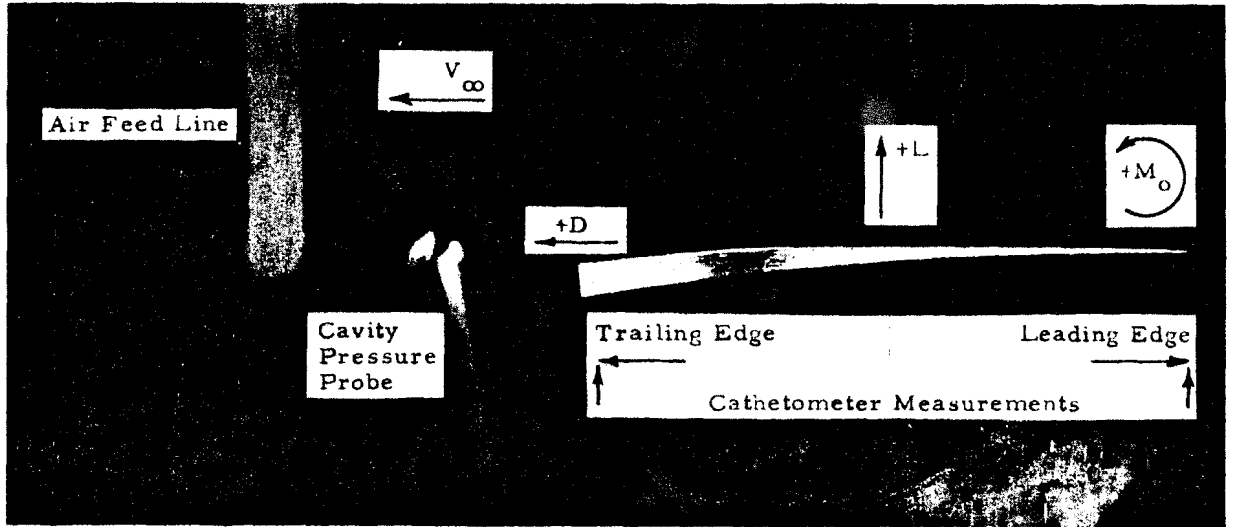


Fig. 3 Photograph of model in working section showing sign conventions.

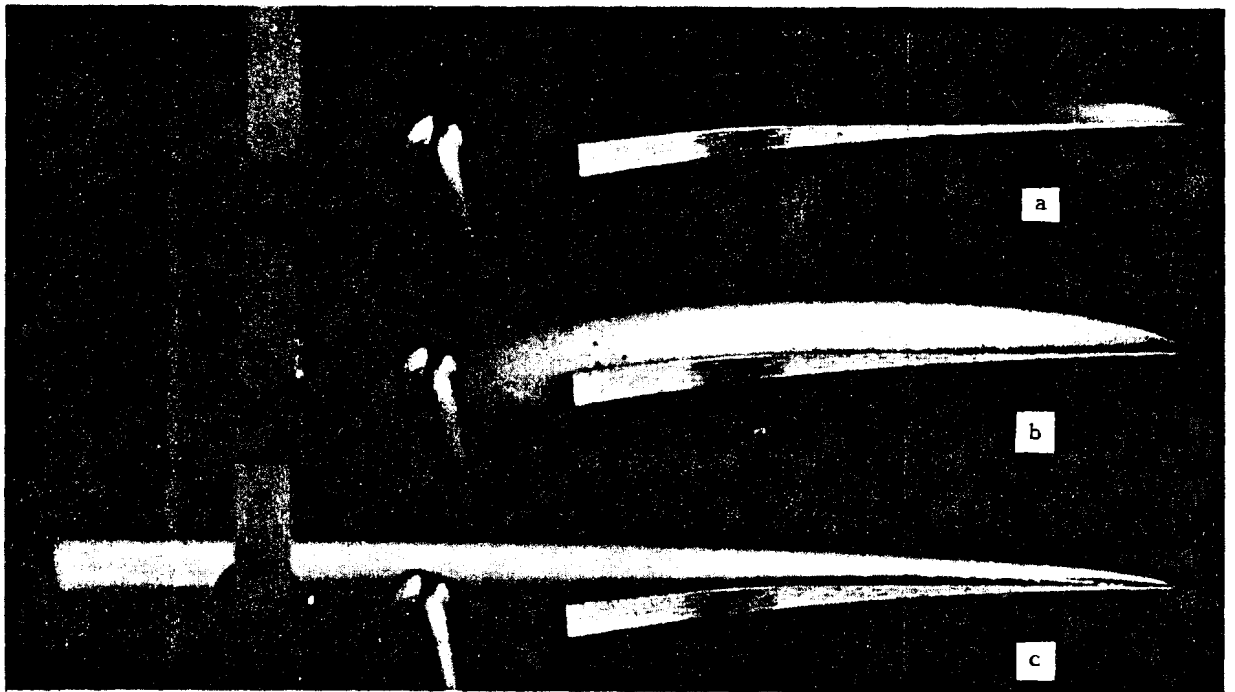


Fig. 4 Typical data record photographs.  $V = 30$  fps,  $\alpha = 5^\circ$

a.	$\sigma_v = 1.604$	$V = 30.7$
b.	$\sigma_v = .657$	$V = 30.9$
c.	$\sigma_v = .126, \sigma_k = .117$	$V = 29.2$

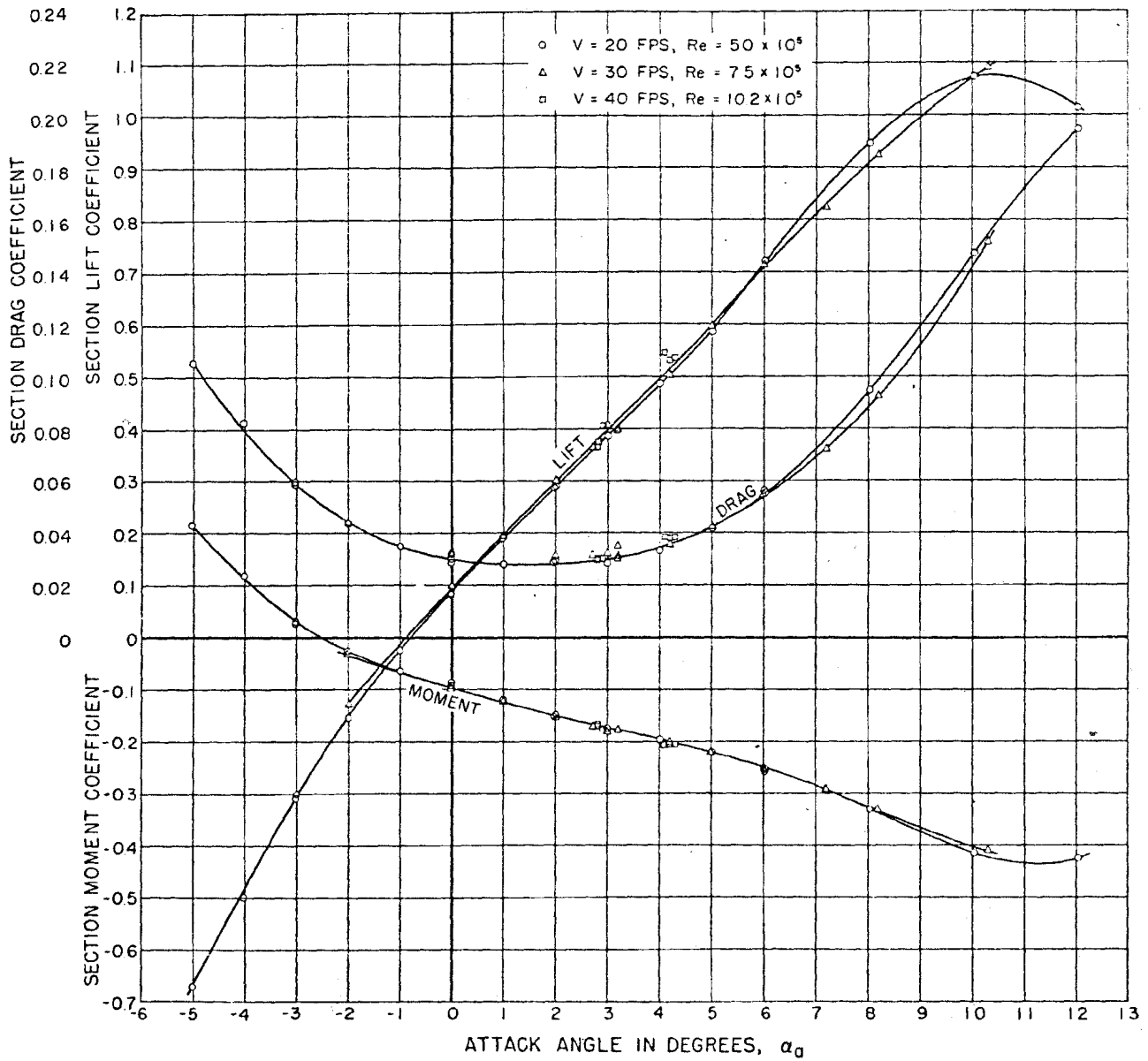


Fig. 5 Lift, drag, and moment coefficients for hydrofoil in noncavitating flow.

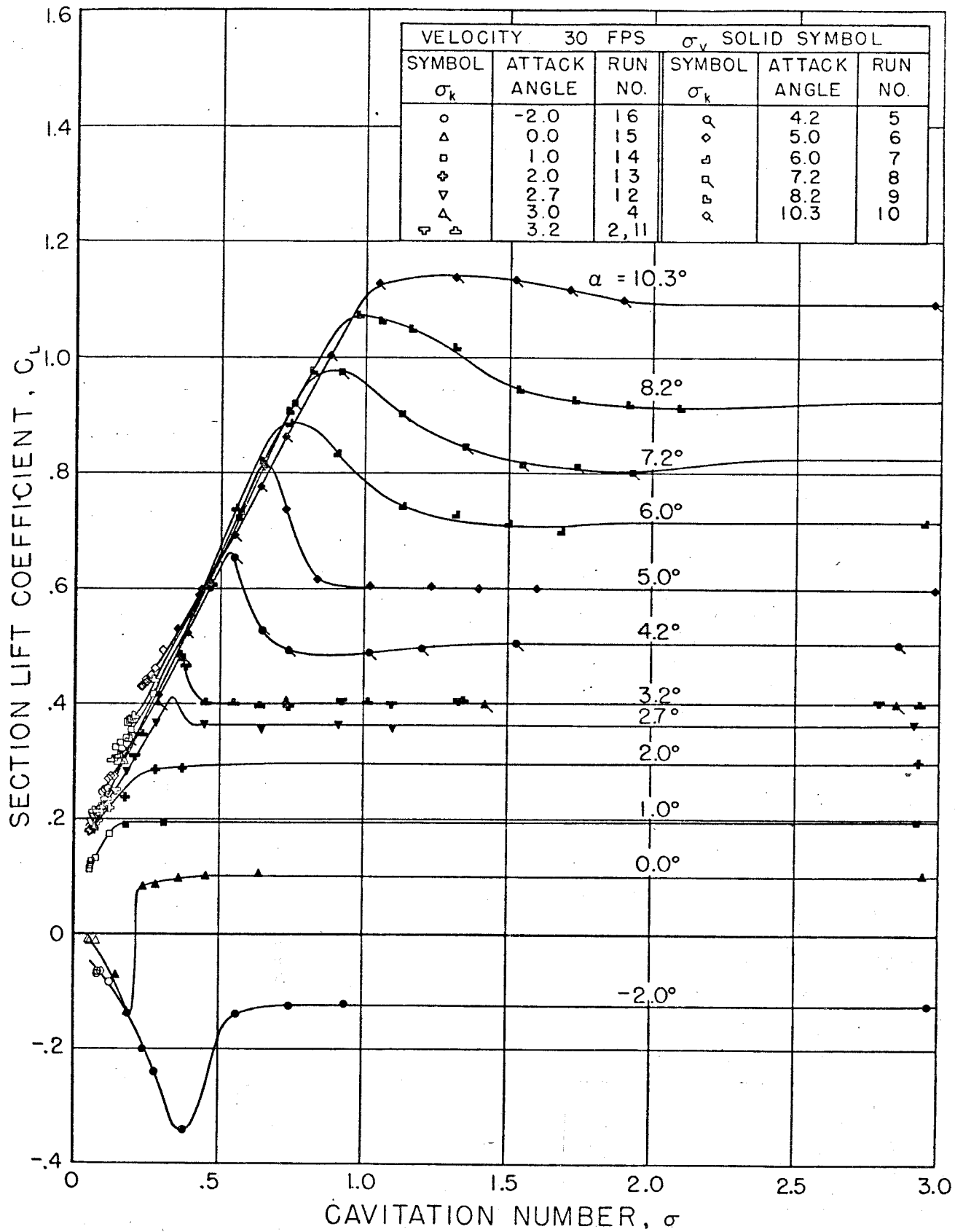


Fig. 6 Lift coefficient vs cavitation number.  $V = 30$  fps

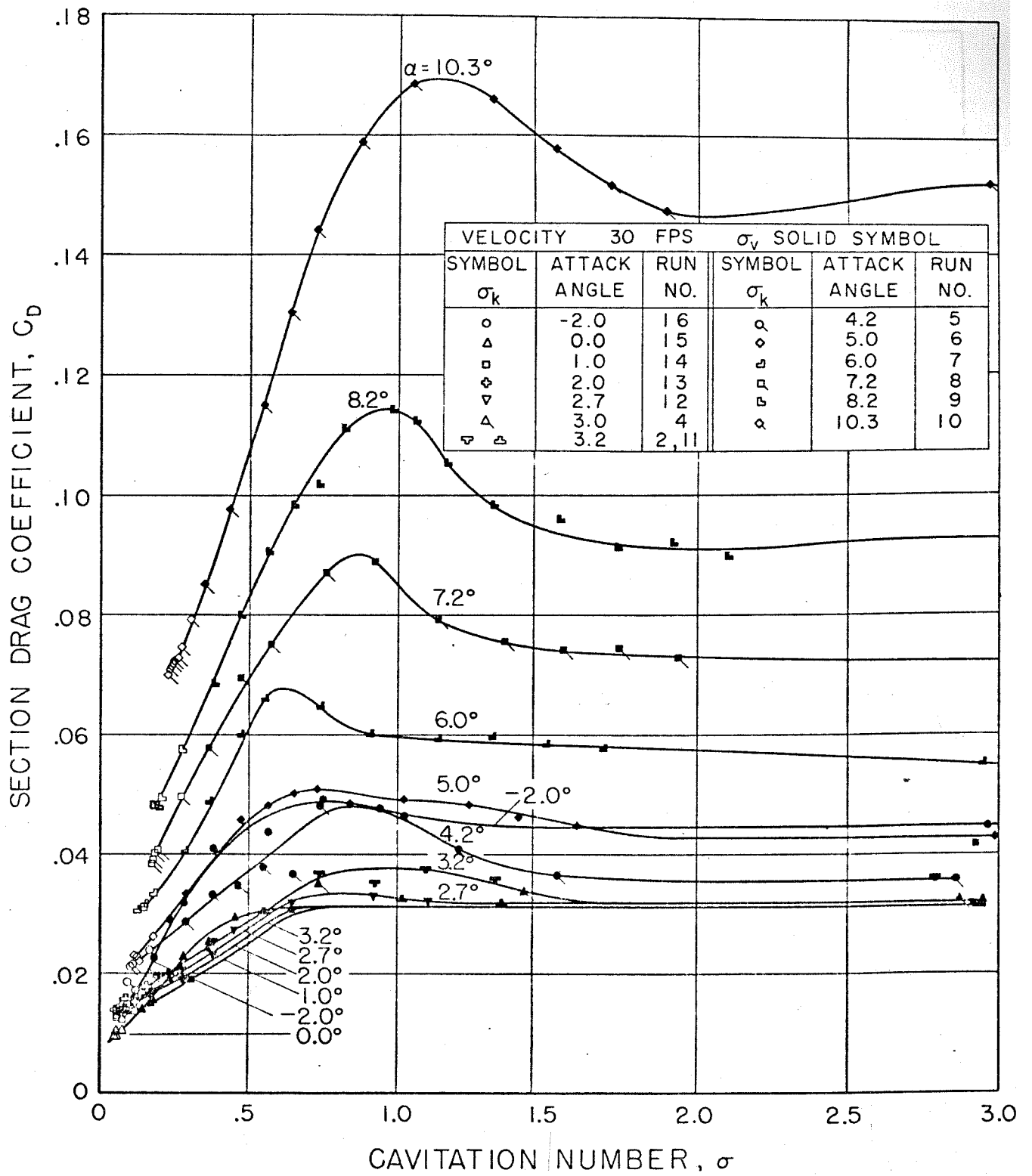


Fig. 7 Drag coefficient vs cavitation number. V = 30 fps

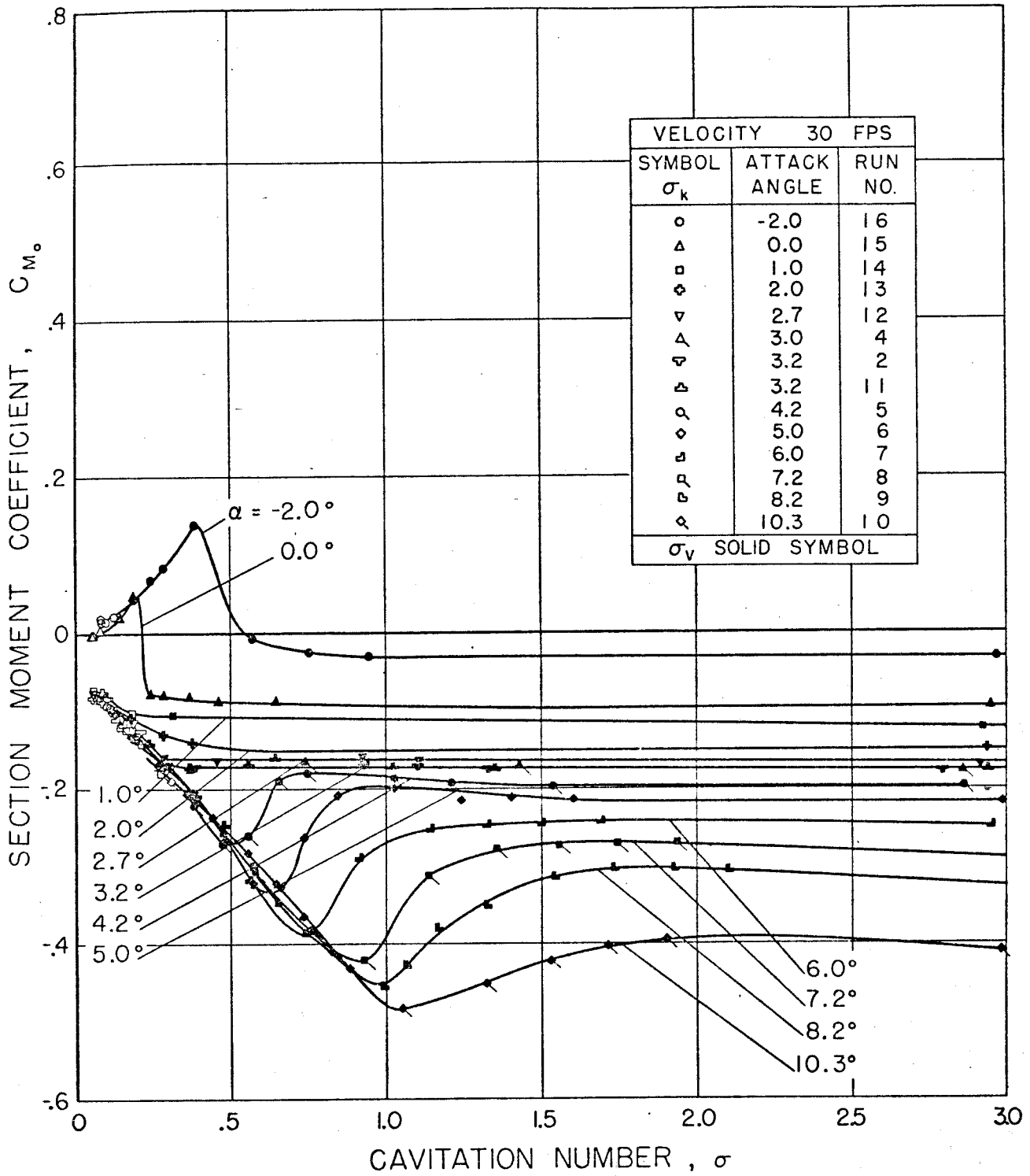


Fig. 8 Moment coefficient about leading edge vs cavitation number.  
 $V = 30$  fps

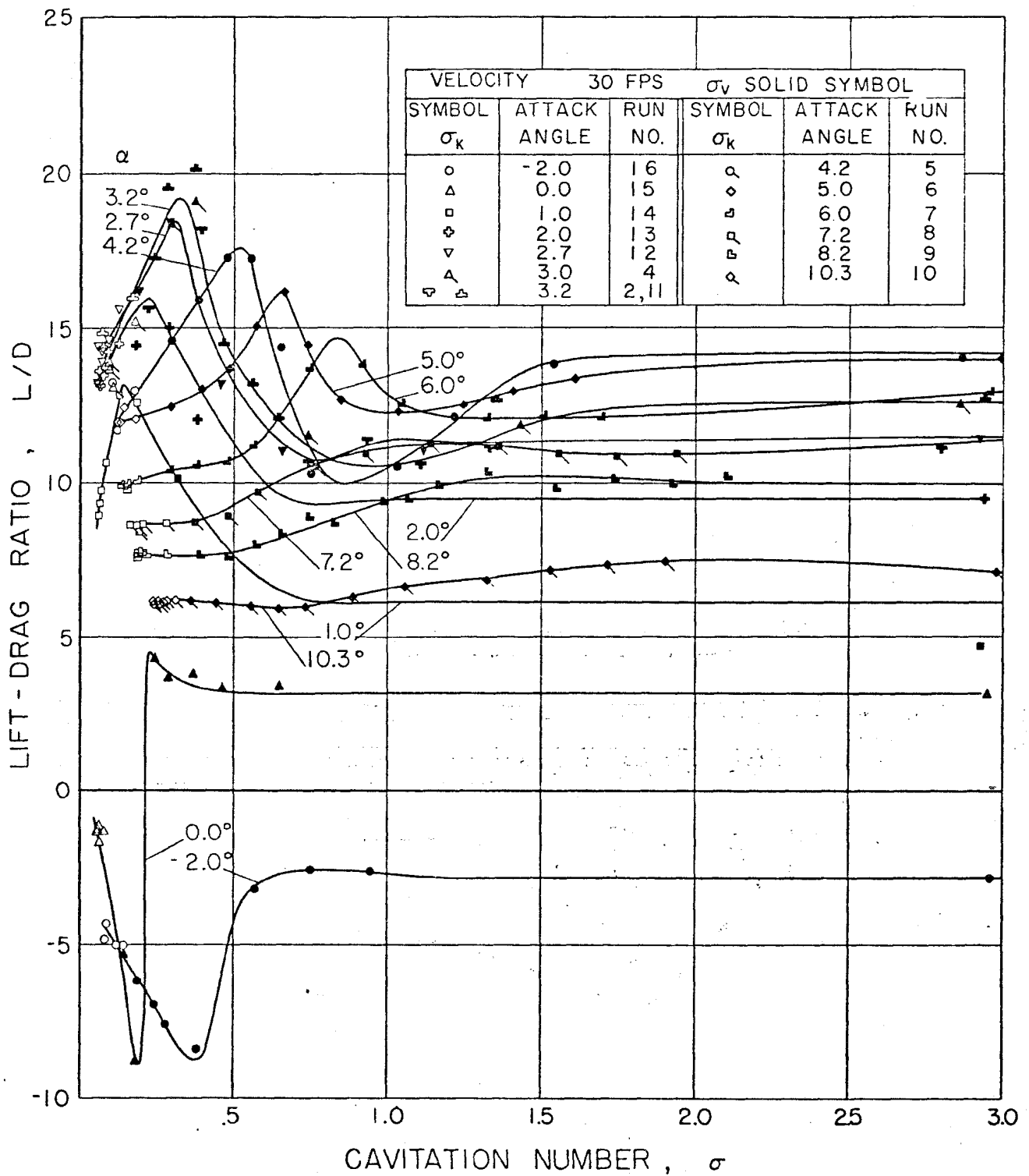


Fig. 9 Lift/drage ratio vs cavitation number.  $V = 30$  fps

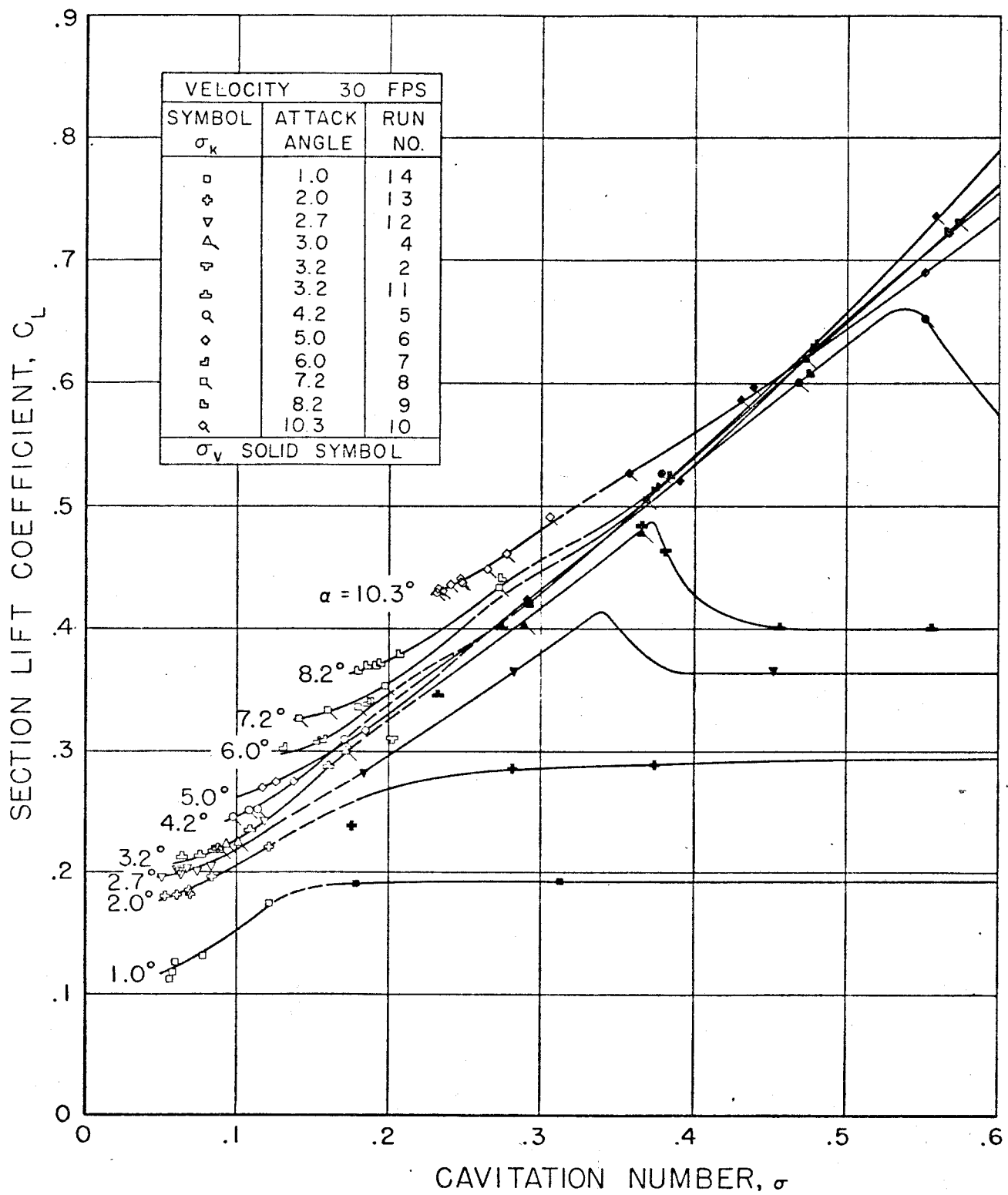


Fig. 10 Lift coefficients at small cavitation numbers. V = 30 fps

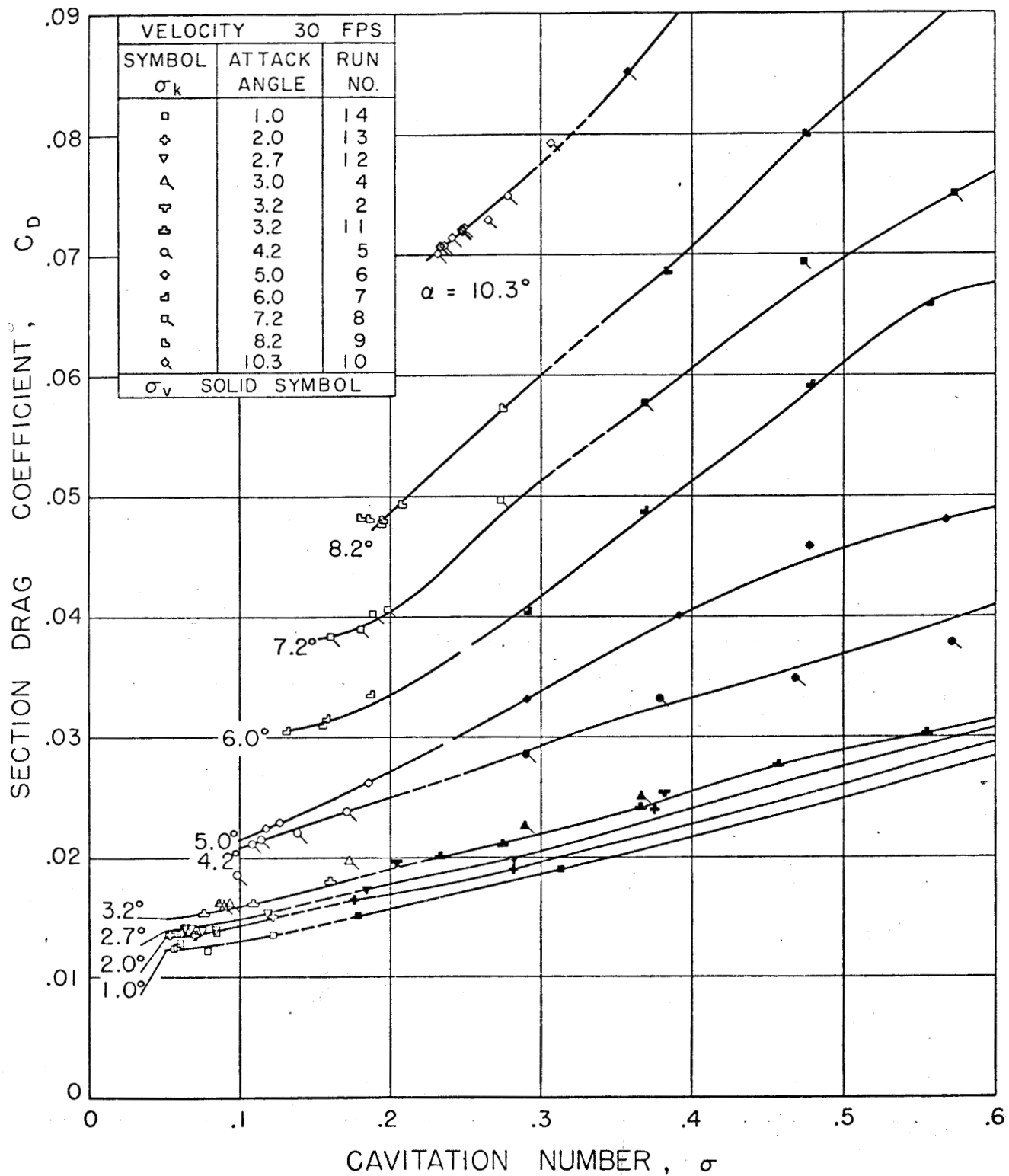


Fig. 11 Drag coefficients at small cavitation numbers.  $V = 30$  fps

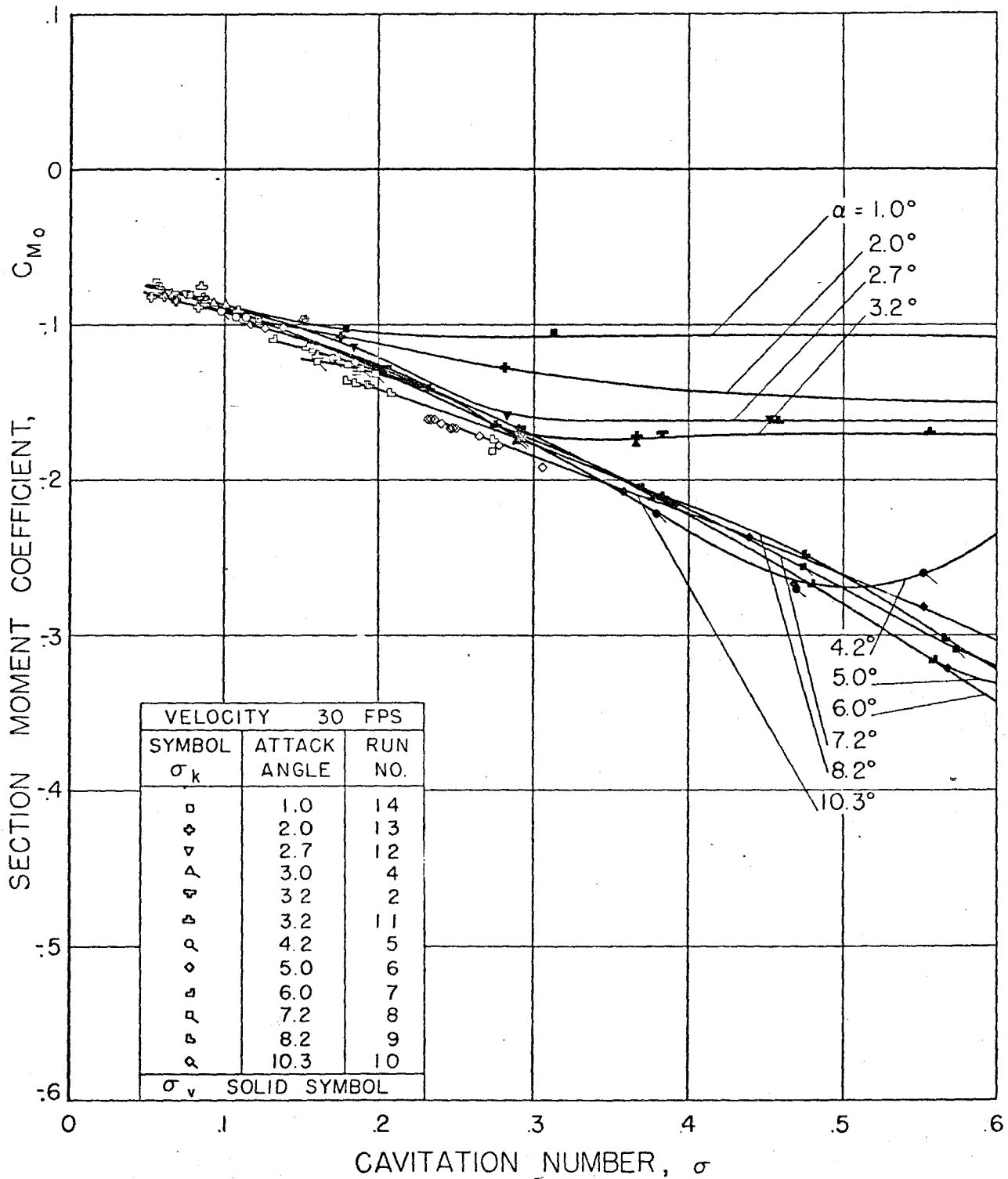


Fig. 12 Moment coefficient at small cavitation numbers.  $V = 30$  fps

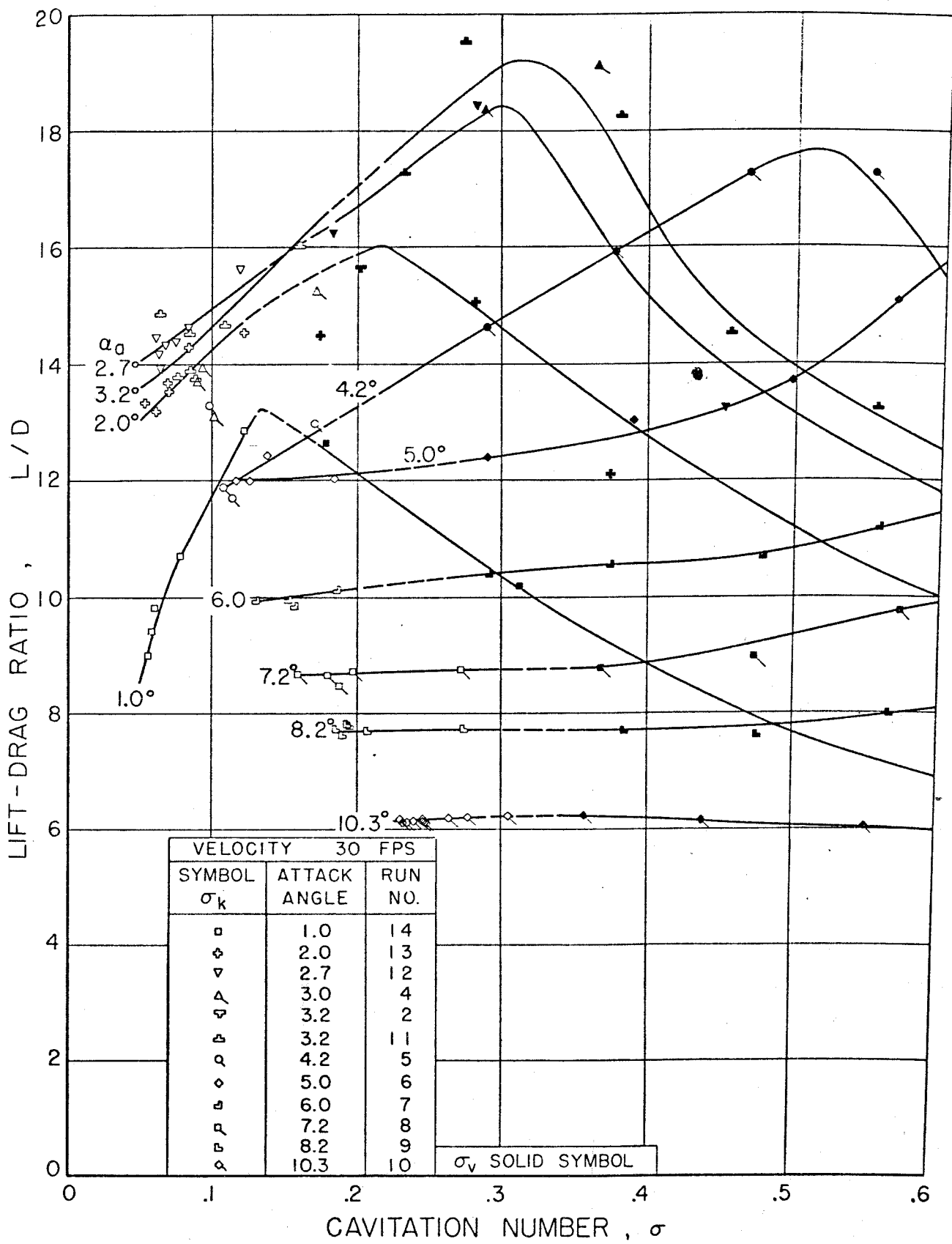


Fig. 13 Lift/drage ratio at small cavitation numbers. V = 30 fps

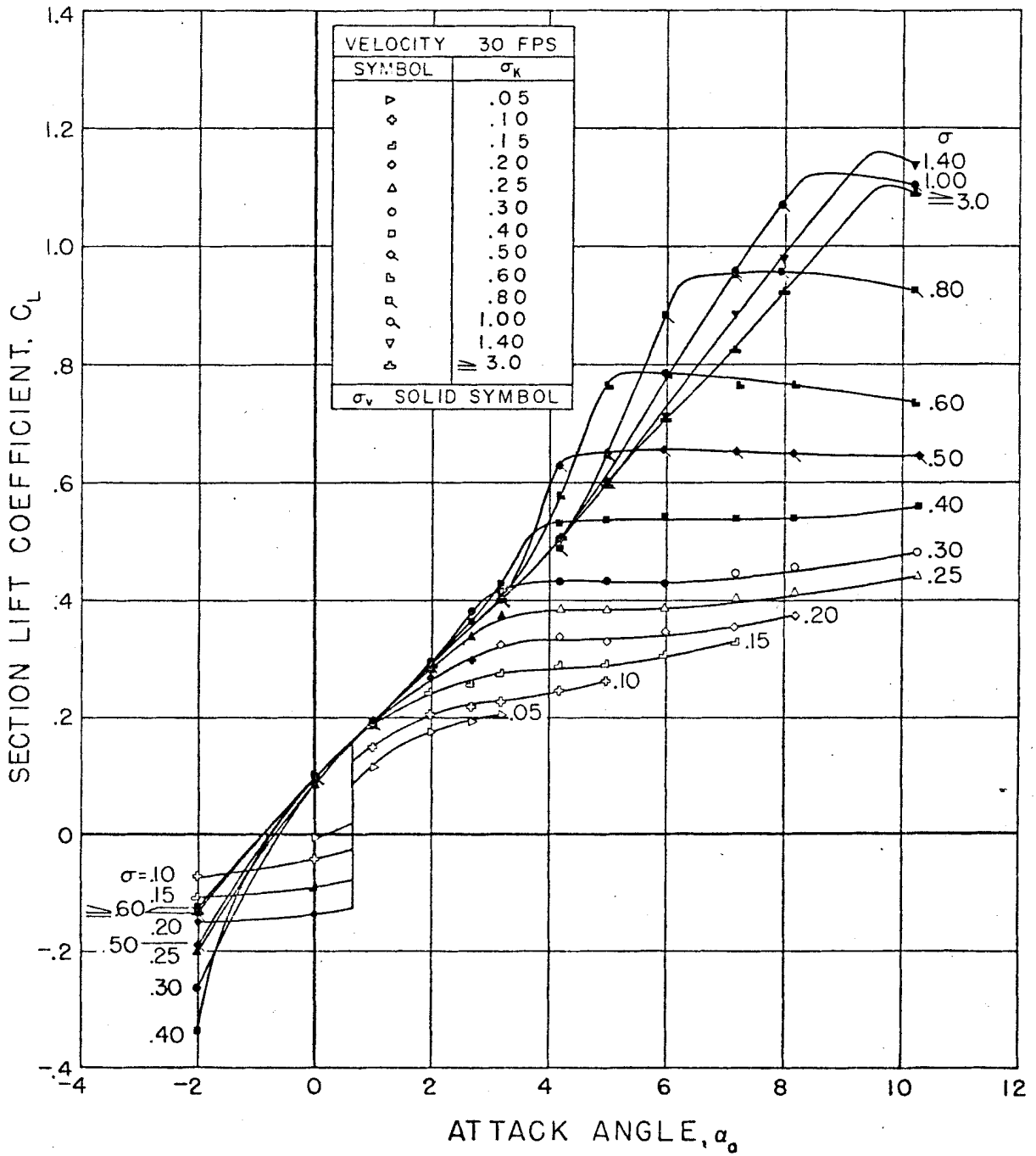


Fig. 14 Lift coefficient vs attack angle at constant cavitation numbers.  
 $V = 30$  fps

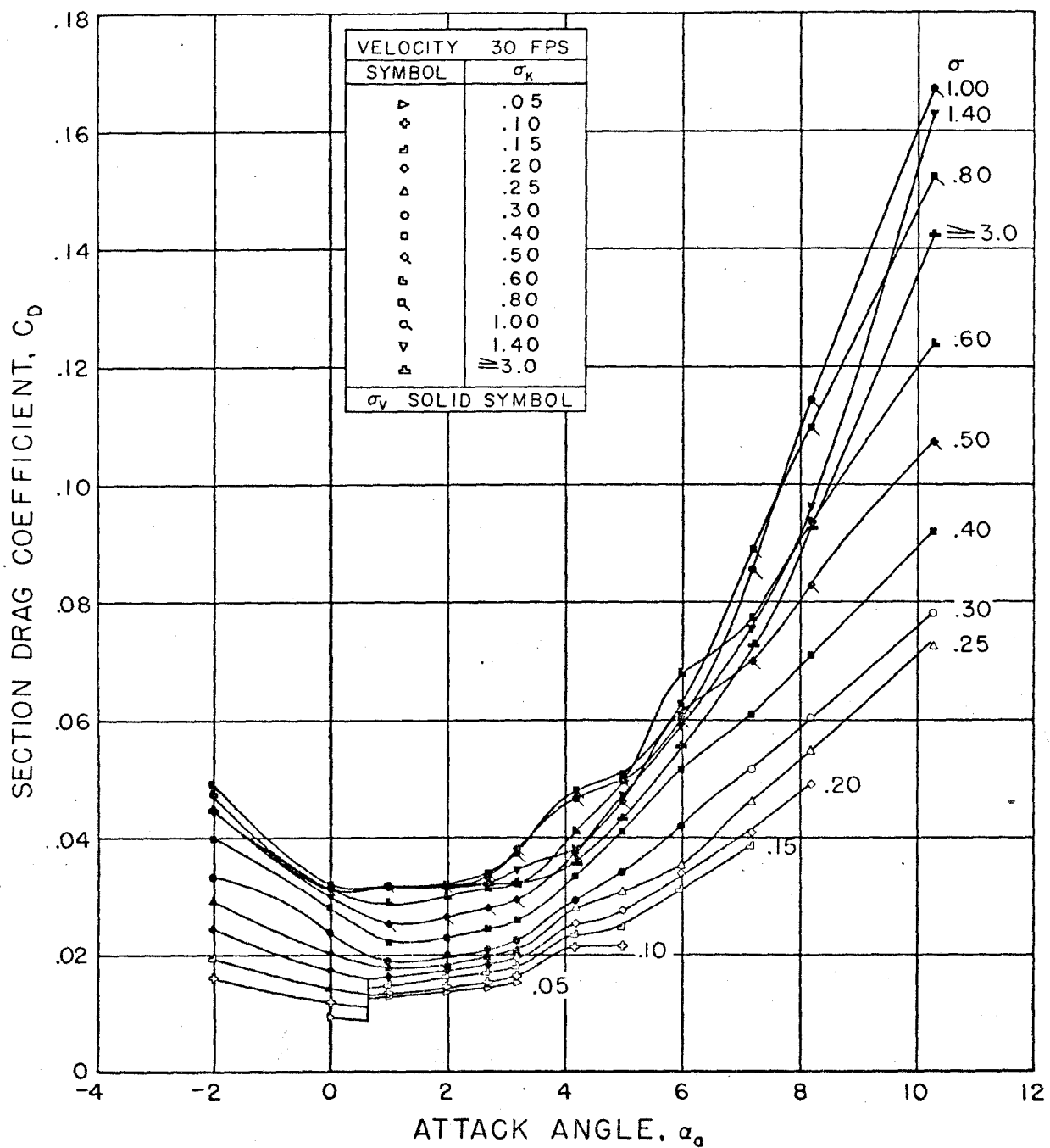


Fig. 15 Drag coefficient vs attack angle at constant cavitation numbers.  
 $V = 30$  fps

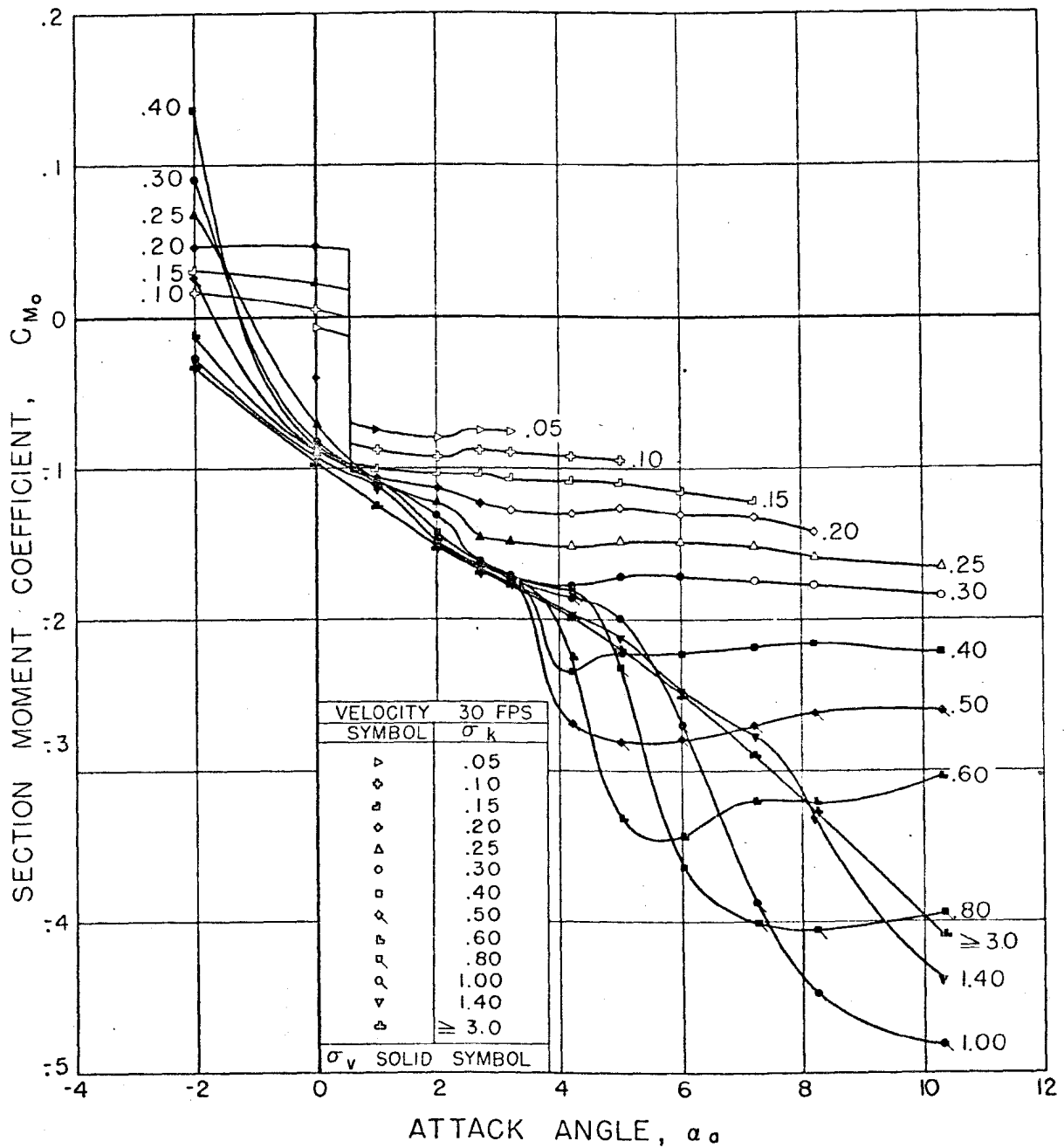


Fig. 16 Moment coefficient vs attack angle at constant cavitation numbers.  
 $V = 30$  fps

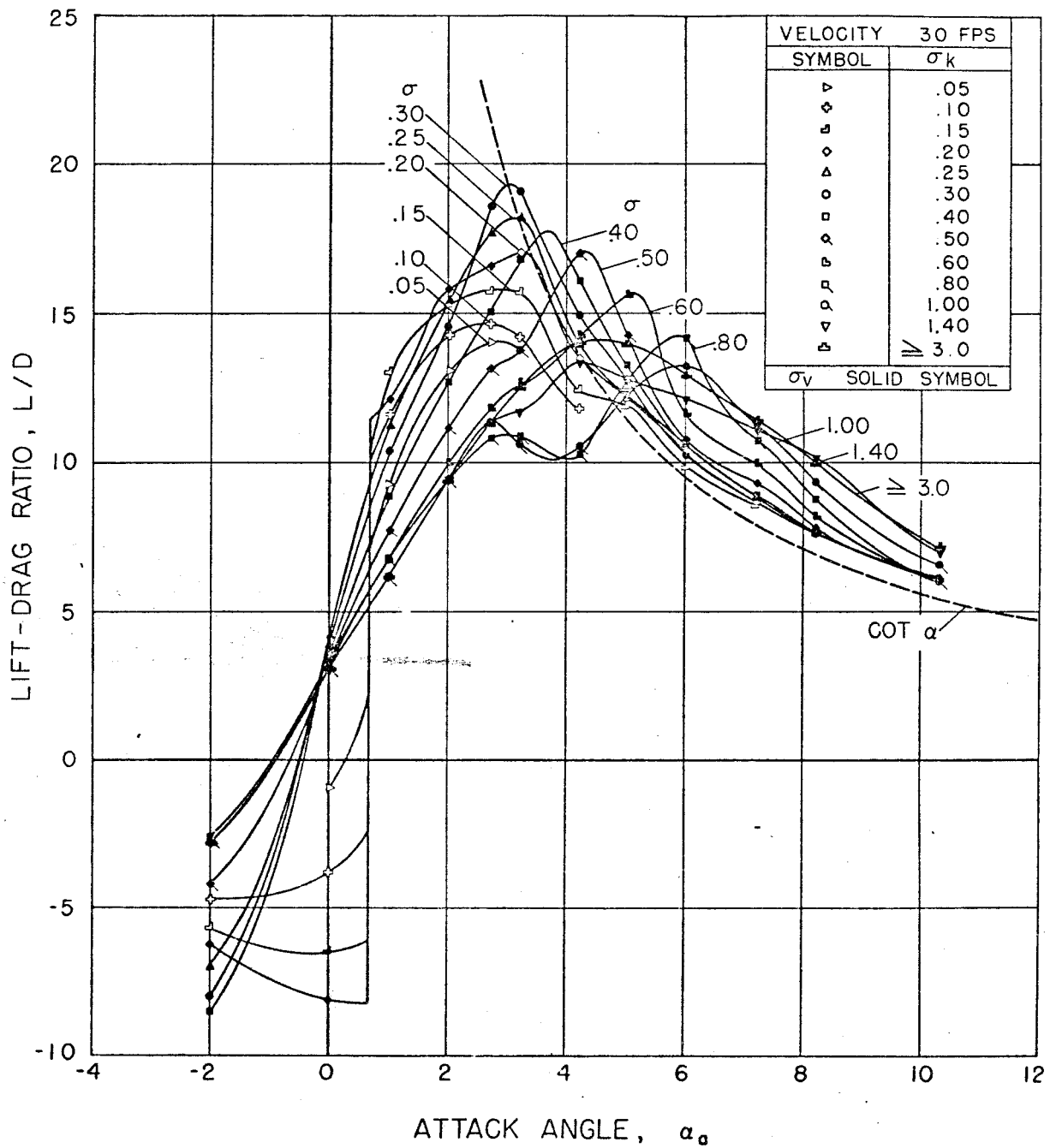


Fig. 17 Lift/drage ratio vs attack angle at constant cavitation numbers.  
 $V = 30 \text{ fps}$

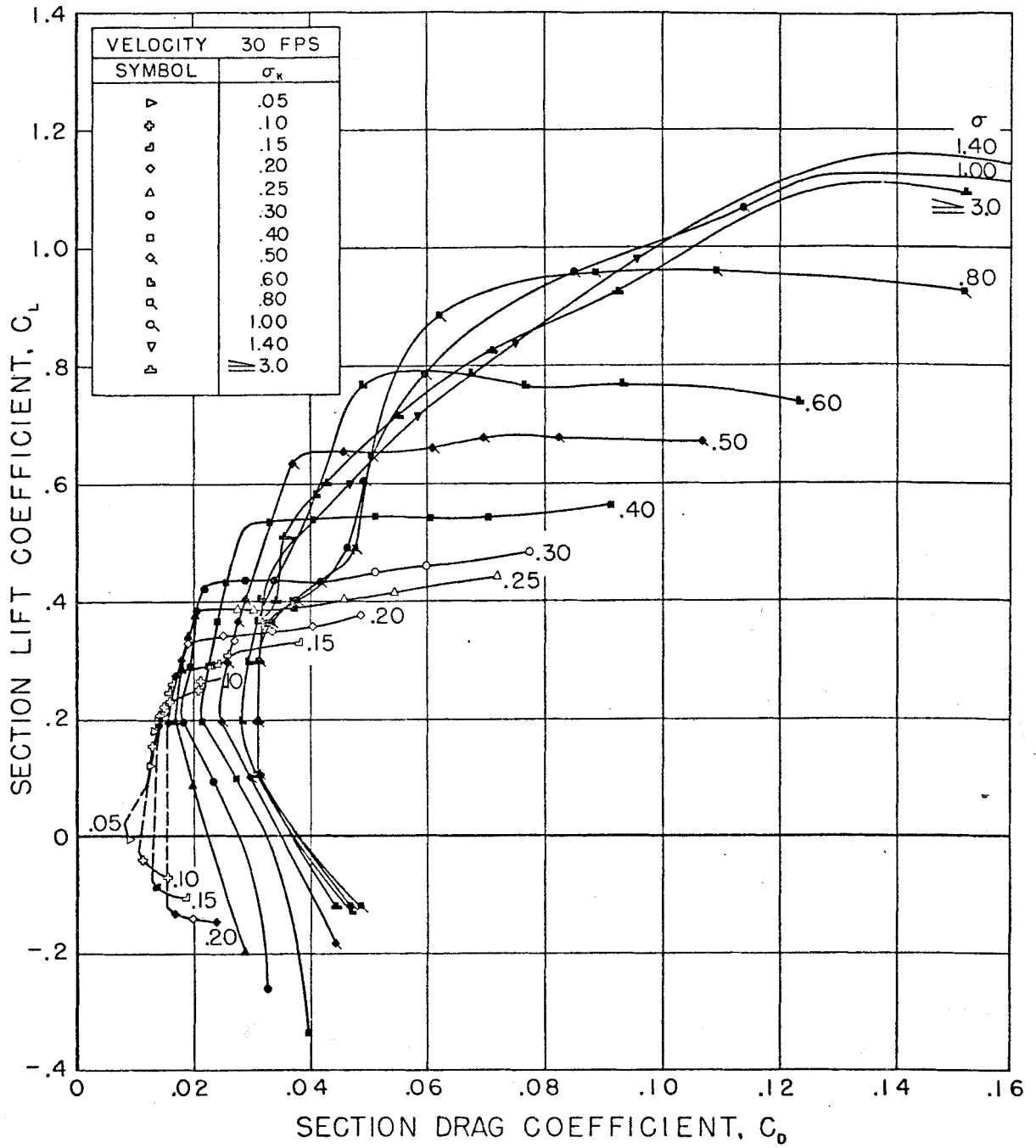


Fig. 18 Polar diagram at constant cavitation numbers.  $V = 30$  fps

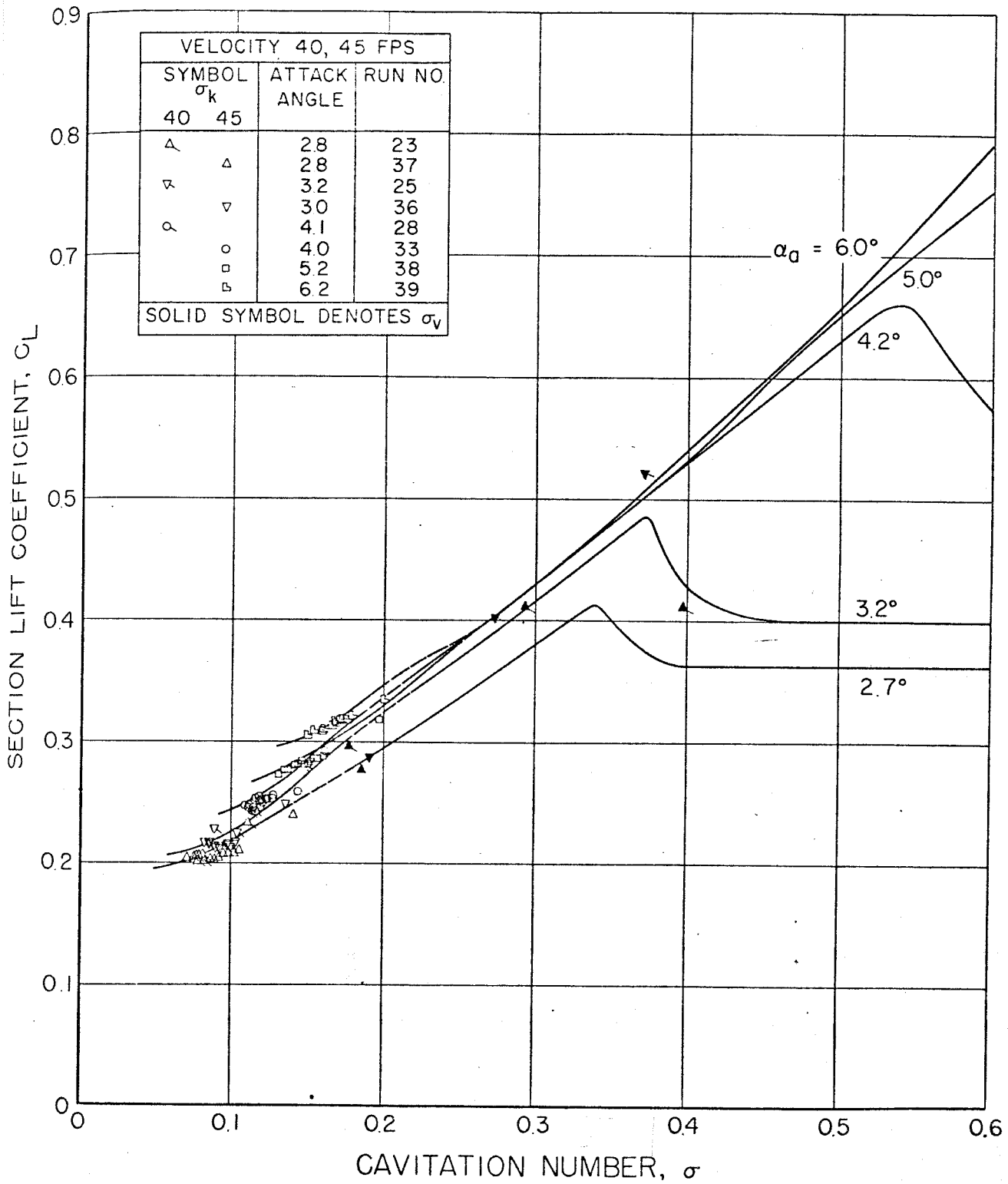


Fig. 19 Lift coefficients vs cavitation numbers at 30, 40, and 45 fps.

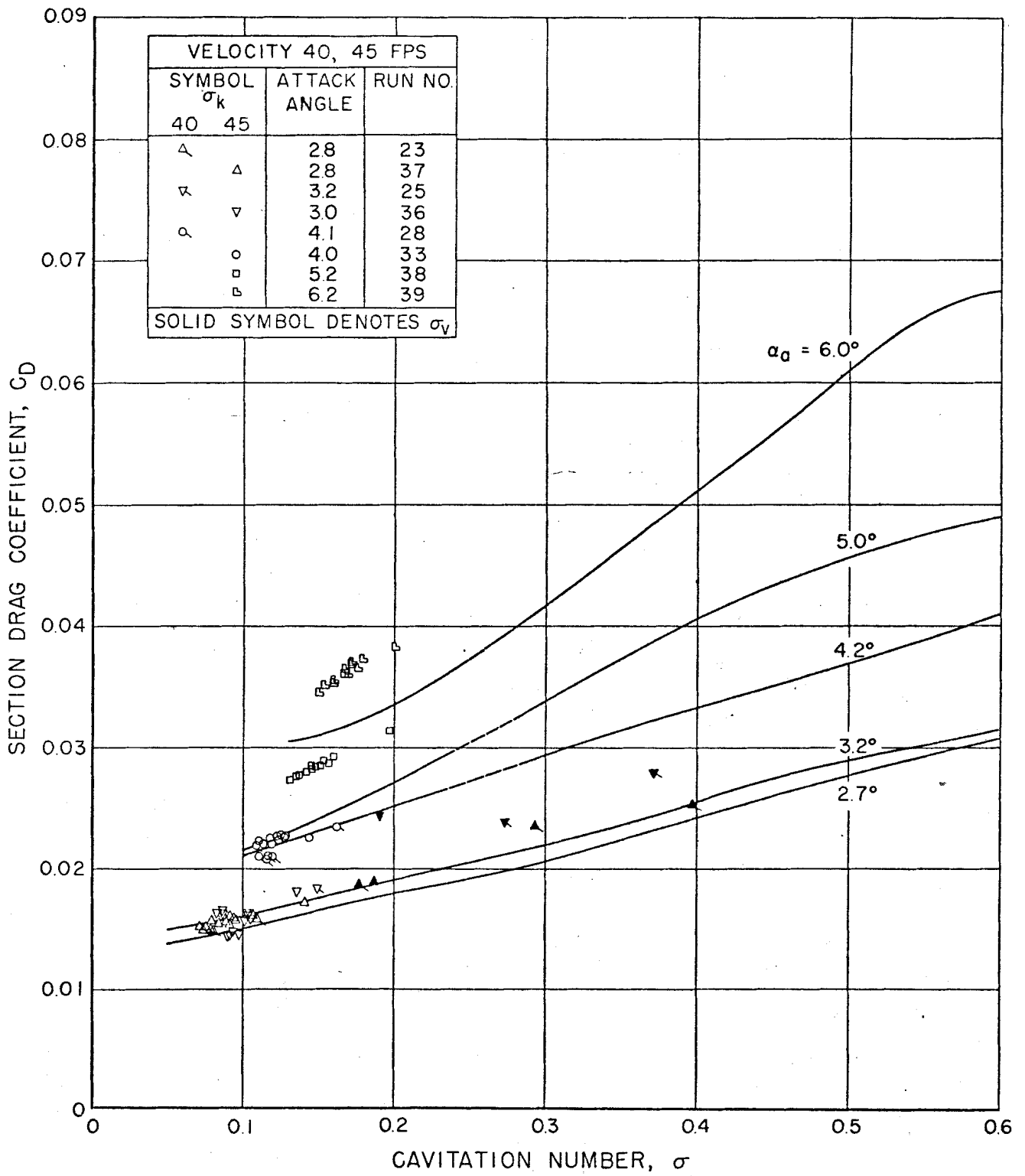


Fig. 20 Drag coefficients vs cavitation numbers at 30, 40, and 45 fps.

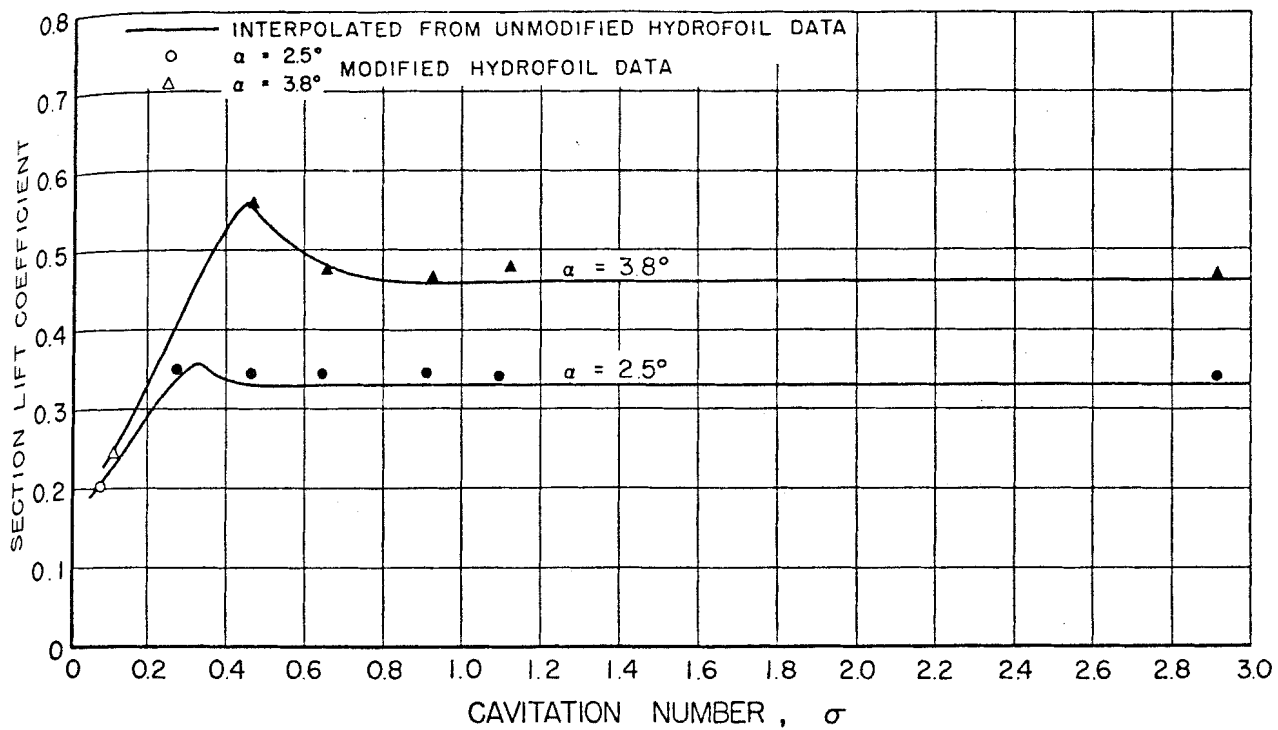


Fig. 21a Lift coefficient of modified and original models.  $V = 30$  fps.

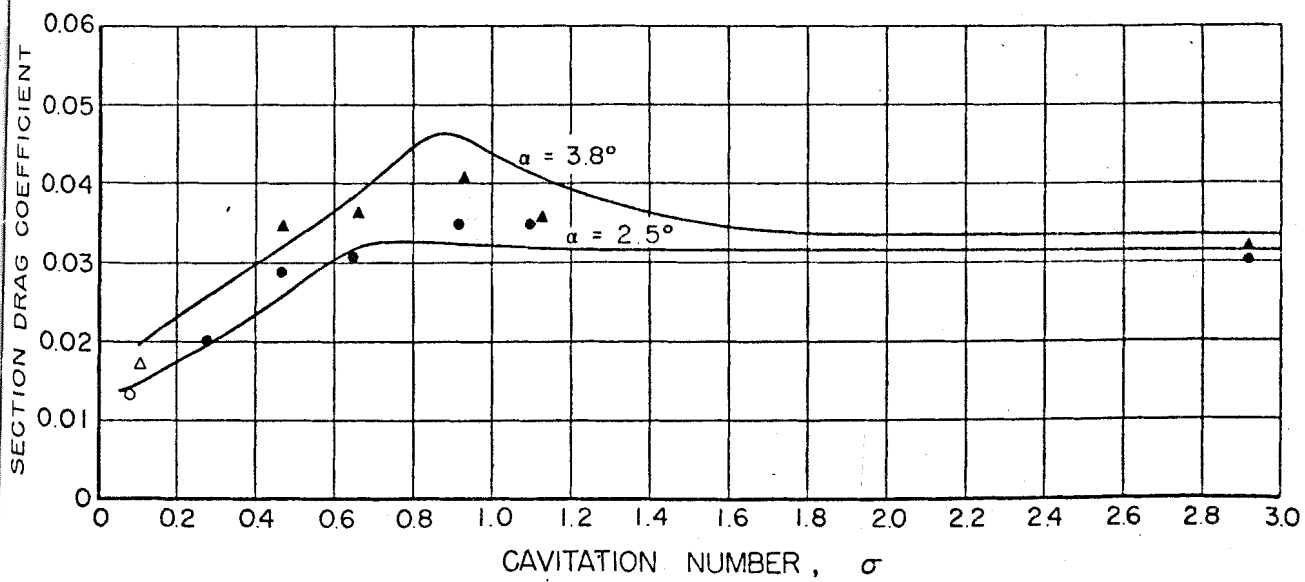


Fig. 21b Drag coefficient of modified and original models.  $V = 30$  fps



Fig. 22 Oblique view of wave-like cavitation.  $\alpha_a = 2.73^\circ$ ,  $\sigma_v = .37$ ,  $V = 31.0$  fps



Fig. 23 Oblique view of wave-like cavitation.  $\alpha_a = 2.73^\circ$ ,  $\sigma_v = .29$ ,  $V = 30.9$  fps



Fig. 24 Oblique view of wave-like cavitation.  $\alpha_a = 3.73^\circ$ ,  $\sigma_v = .47$ ,  $V = 30.9$  fps

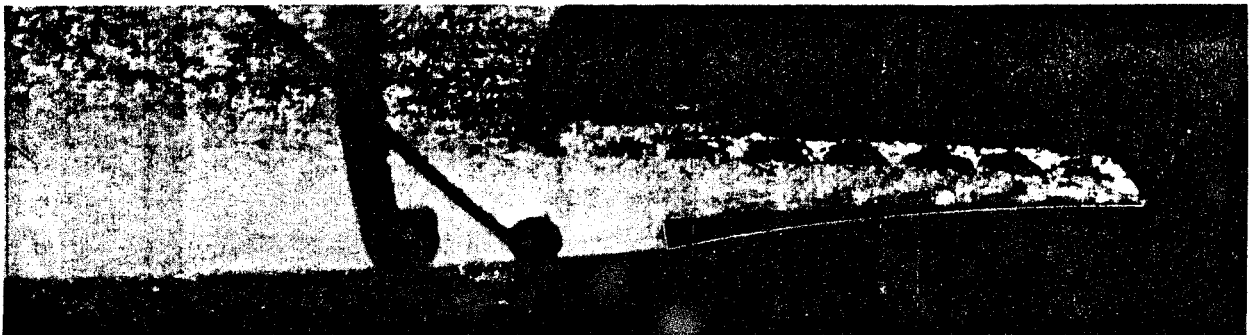


Fig. 25 Oblique view of wave-like cavitation.  $\alpha_a = 5.73^\circ$ ,  $\sigma_v = .20$ ,  $V = 30.8$  fps

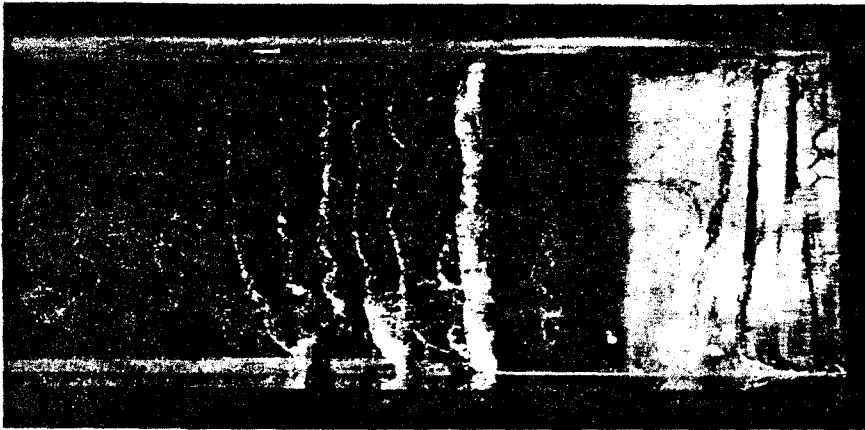


Fig. 26 Plan view of upper surface of supercavitating hydrofoil showing the cavitation pattern.  
 $\alpha_a = 2.73^\circ$ ,  $\sigma_v = .38$ ,  $V = 30.9$  fps

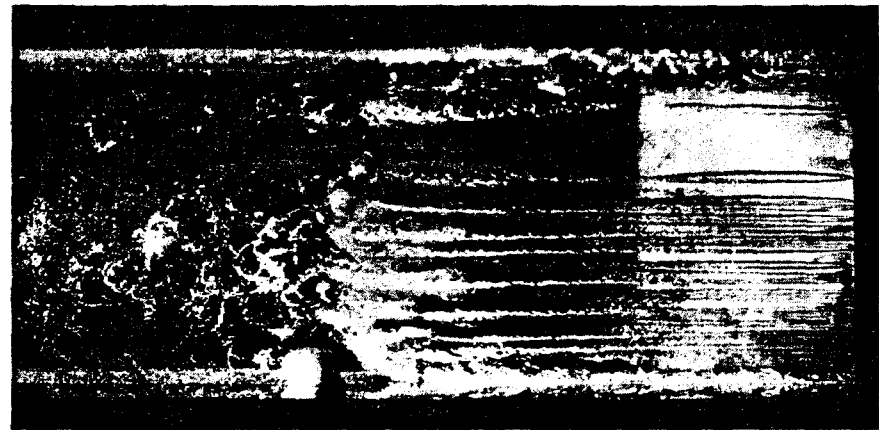


Fig. 28 Upper surface cavitation for  
 $\alpha_a = 2.73^\circ$ ,  $\sigma_v = .19$ ,  $V = 31.0$  fps.



Fig. 27 Upper surface cavitation for  
 $\alpha_a = 2.73^\circ$ ,  $\sigma_v = .37$ ,  $V = 31.0$  fps.



Fig. 29 Upper surface cavitation for  
 $\alpha_a = 2.73^\circ$ ,  $\sigma_v = .19$ ,  $V = 31.0$  fps.

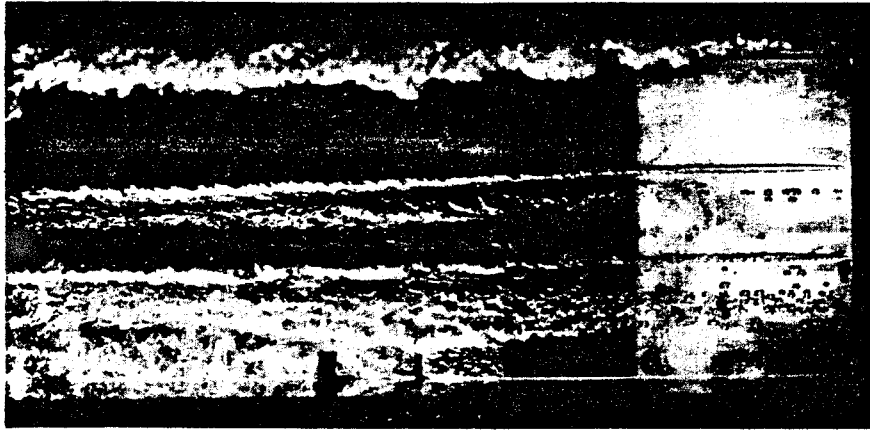


Fig. 30 Upper surface cavitation for  
 $\alpha_a = 2.73^\circ$ ,  $\sigma_v = .07$ ,  $V = 30.0$  fps.

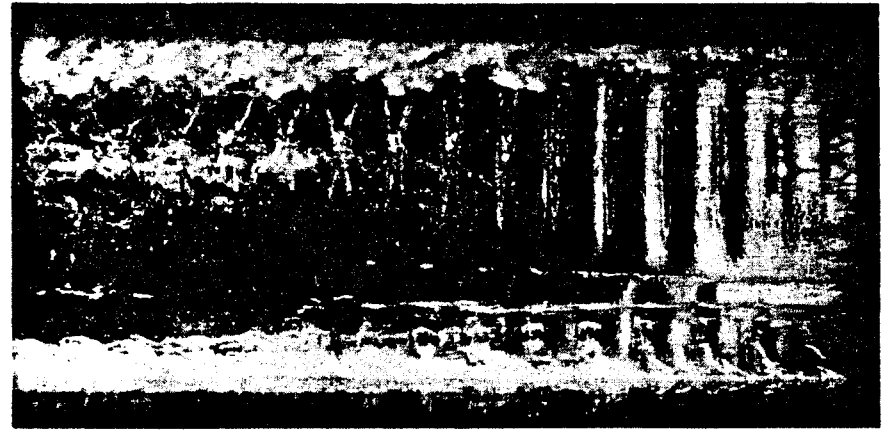


Fig. 32 Upper surface cavitation for  
 $\alpha_a = 5.73^\circ$ ,  $\sigma_v = .12$ ,  $V = 29.2$  fps.



Fig. 31 Upper surface cavitation for  
 $\alpha_a = 5.73^\circ$ ,  $\sigma_v = .20$ ,  $V = 30.8$  fps.

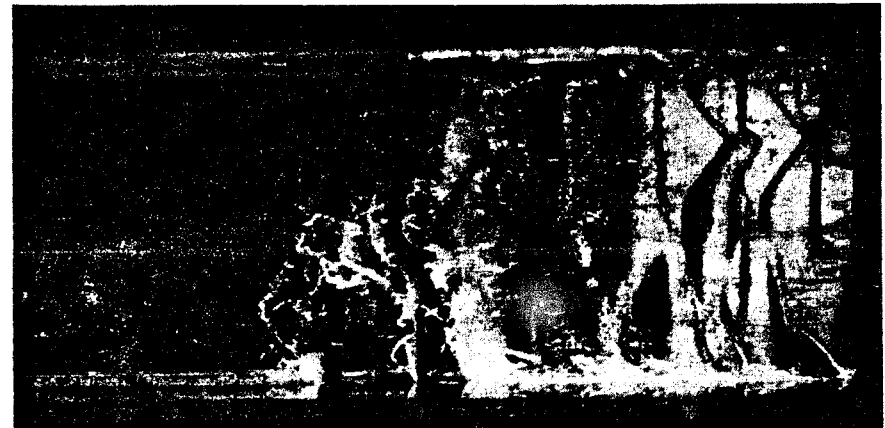


Fig. 33 Upper surface cavitation for  
 $\alpha_a = 2.456^\circ$ ,  $\sigma_v = .28$ ,  $V = 41.0$  fps.

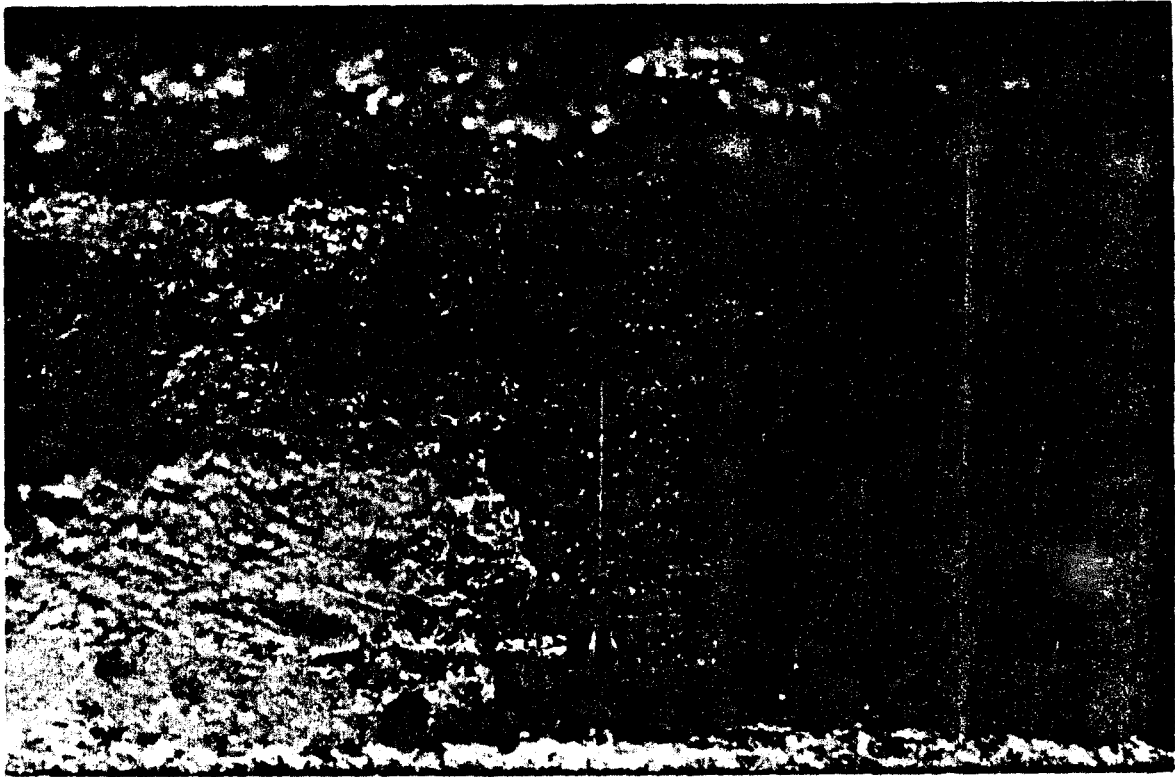


Fig. 34 Lower cavity surface waves as seen through upper cavity wall.  
 $\alpha_a = 7.73^\circ$ ,  $\sigma_v = .22$ ,  $V = 30.6$  fps

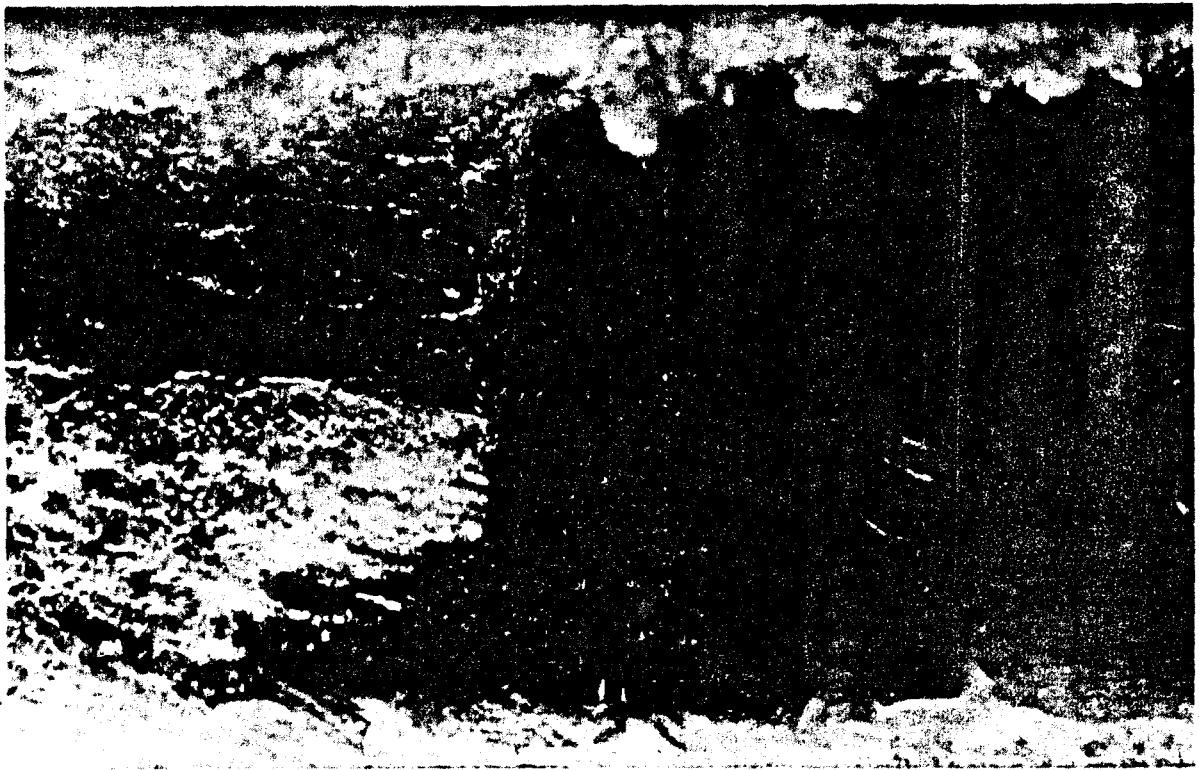


Fig. 35 Lower cavity surface waves as seen through upper cavity wall.  
 $\alpha_a = 9.73^\circ$ ,  $\sigma_v = .24$ ,  $V = 30.4$  fps

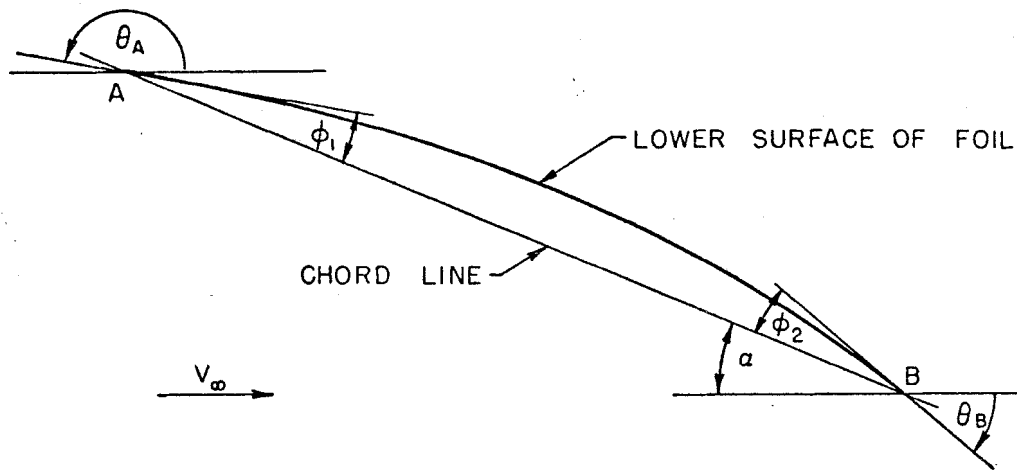


Fig. 36 Lower (wetted) surface of the supercavitating hydrofoil with definition of the boundary conditions.

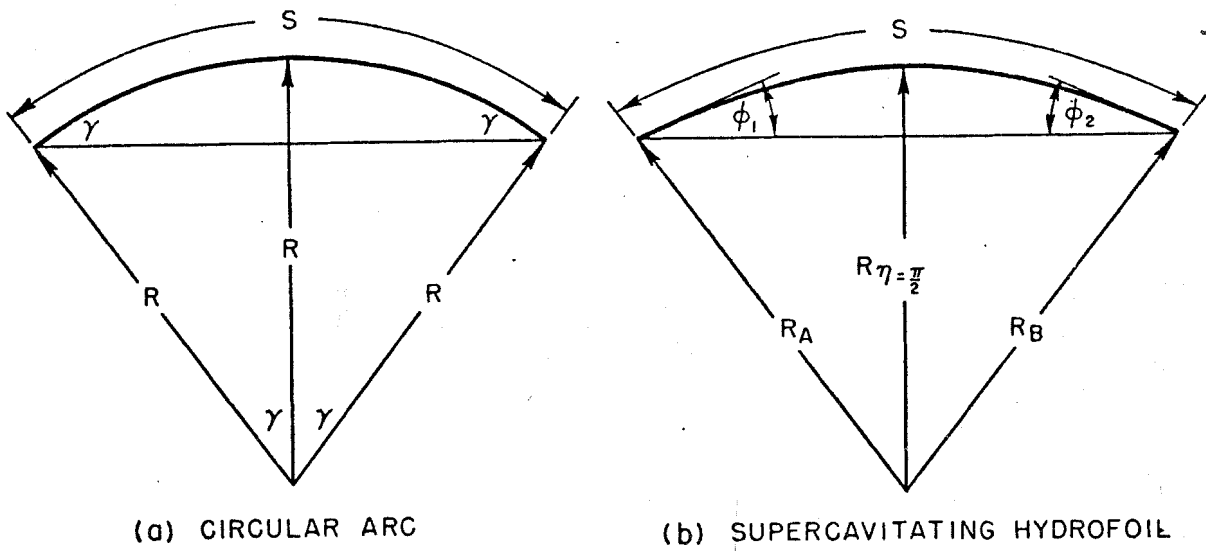


Fig. 37 Radius of curvature definitions:  
 (a) circular arc, (b) supercavitating hydrofoil.

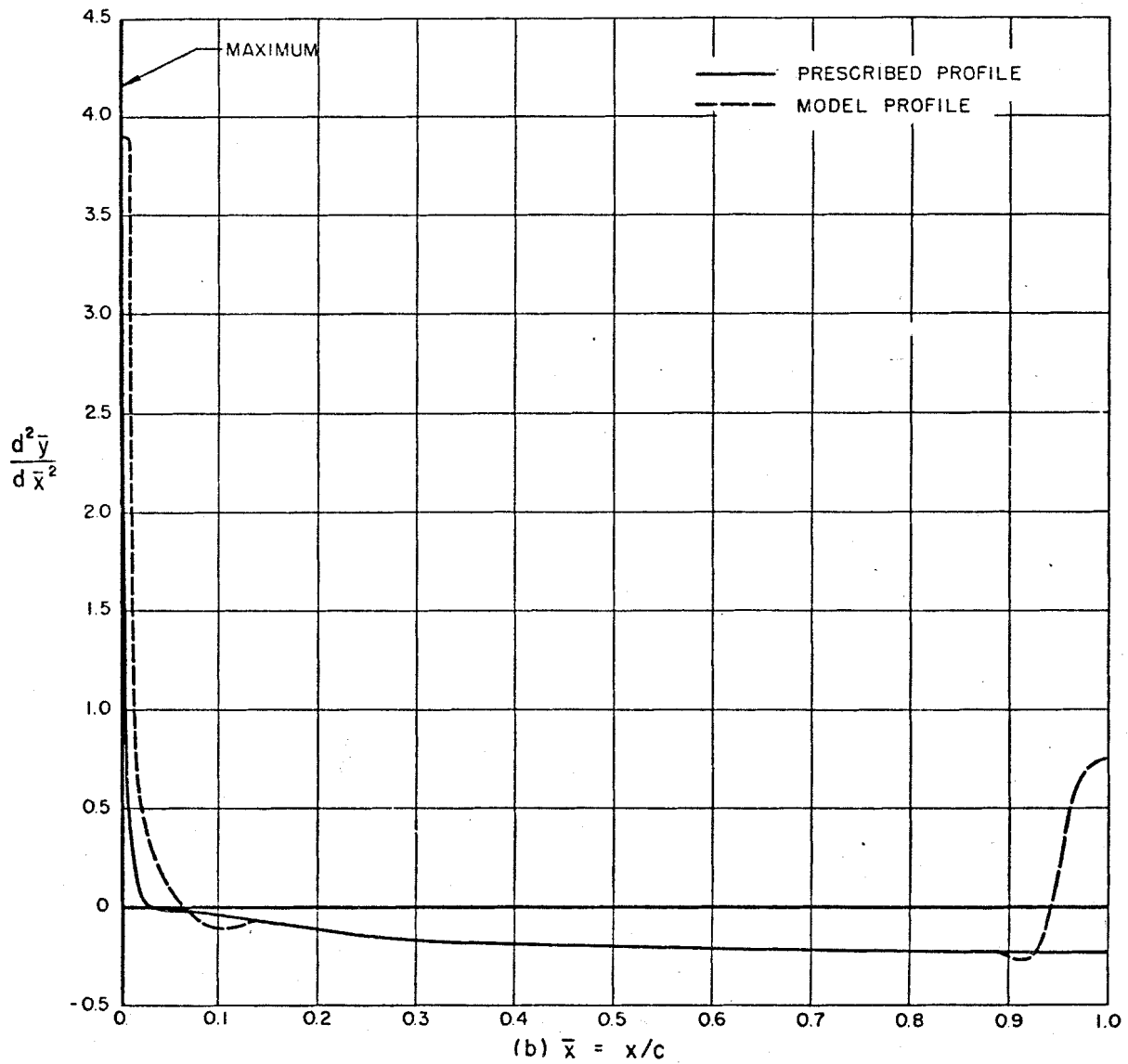
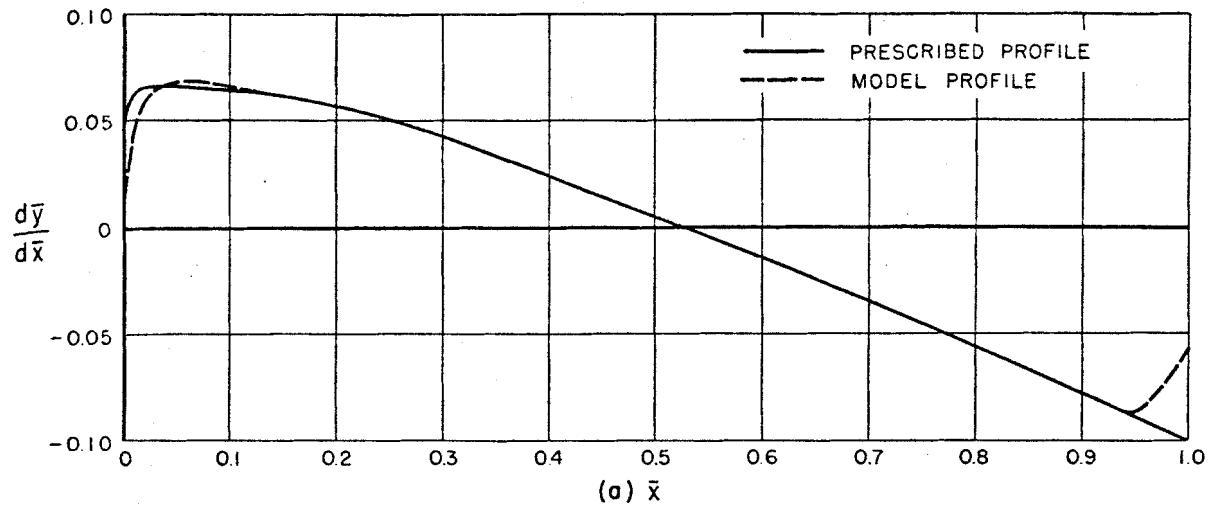
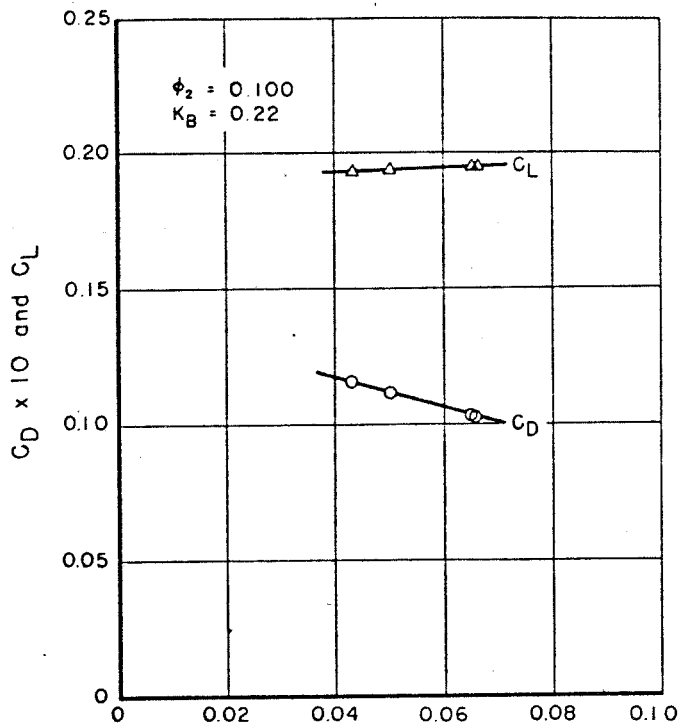
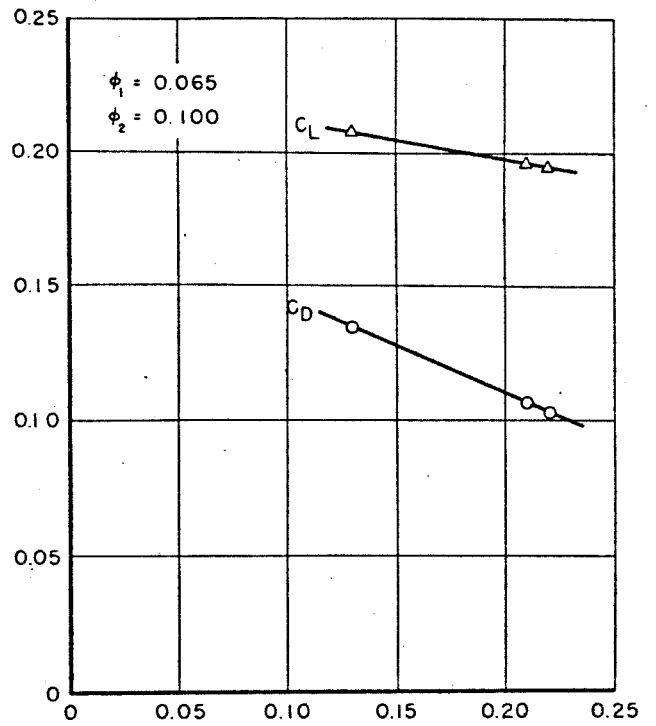


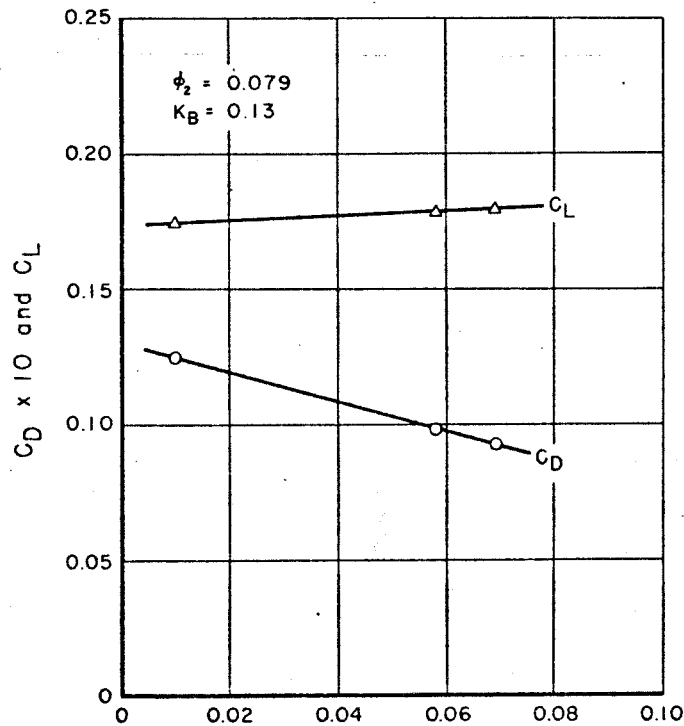
Fig. 38 Derivatives of the lower surfaces of the prescribed and model profiles:  
 (a) first derivative  $\frac{d\bar{y}}{d\bar{x}}$ , (b) second derivative  $\frac{d^2\bar{y}}{d\bar{x}^2}$



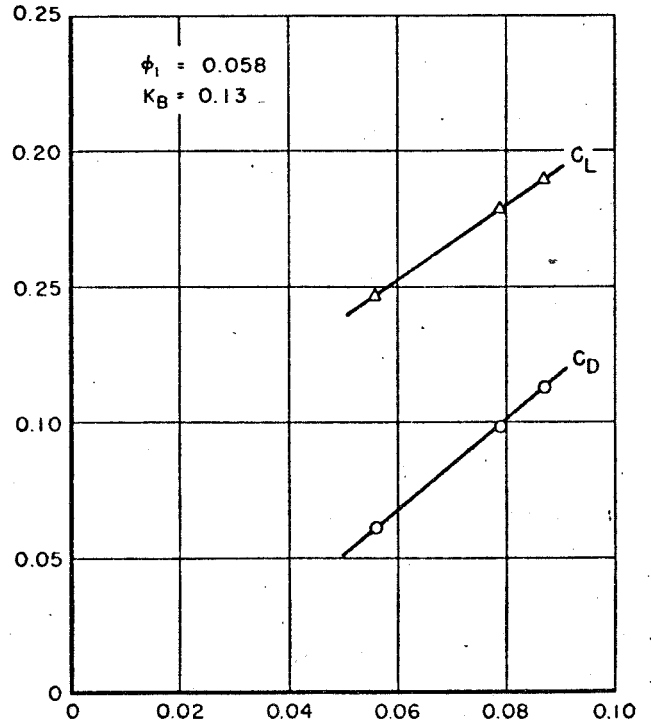
(a) PRESCRIBED  $\phi_1$



(b) PRESCRIBED  $K_B$



(c) MODEL,  $\phi_1$



(d) MODEL,  $\phi_2$

Fig. 39 Effects of the theoretical parameters  $\phi_1$ ,  $\phi_2$  and  $K_B$  on lift and drag coefficients for the prescribed (a,b) and model (c,d) profiles; (a) variations with  $\phi_1$ , (b) variations with  $K_B$ , (c) variations with  $\phi_1$ , (d) variations with  $\phi_2$ .

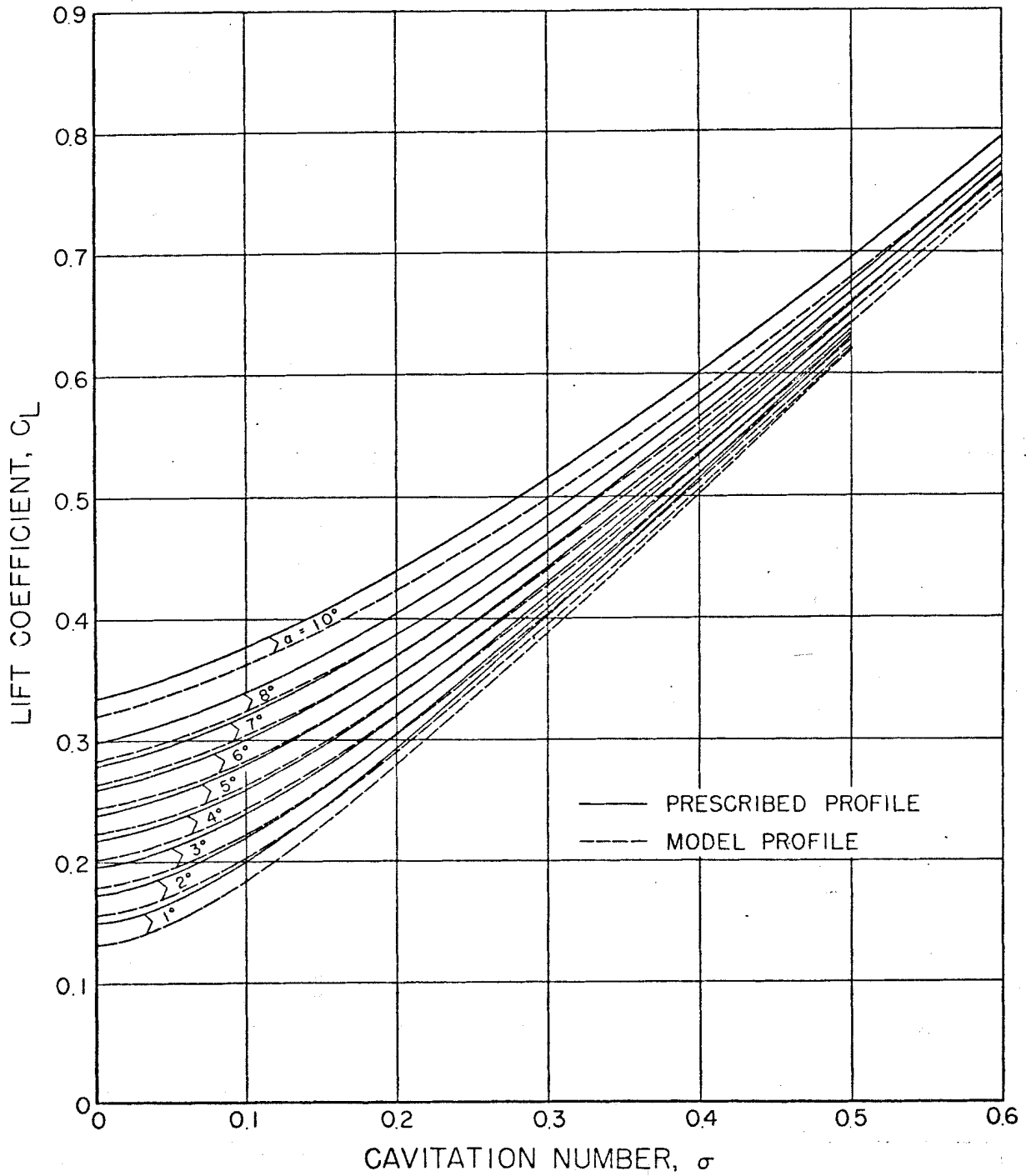


Fig. 40 Theoretical lift coefficient vs cavitation number for the prescribed and model profiles.

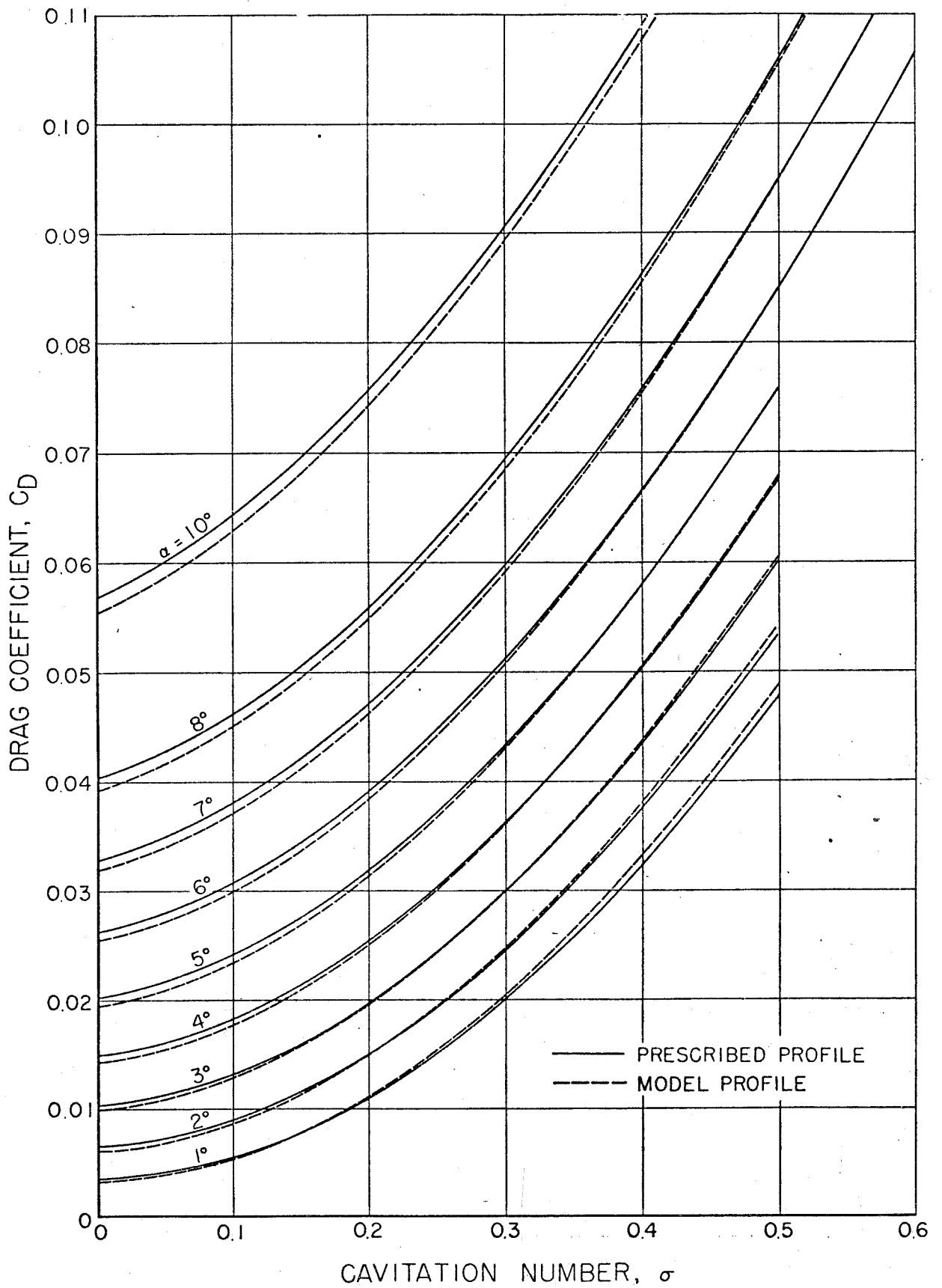


Fig. 41 Theoretical drag coefficient vs cavitation number for the prescribed and model profiles.

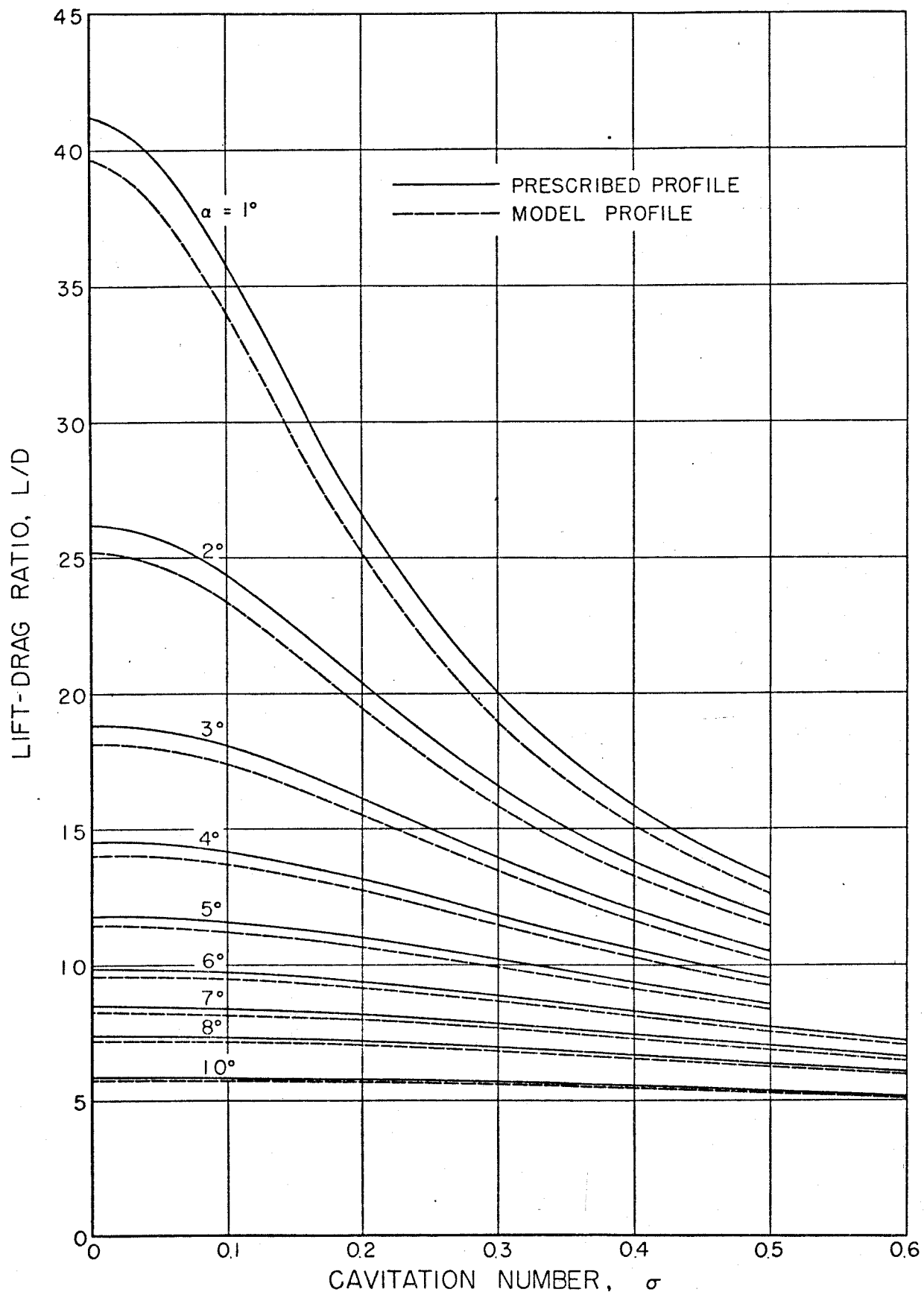


Fig. 42 Theoretical lift-drag ratio vs cavitation number for the prescribed and model profiles.

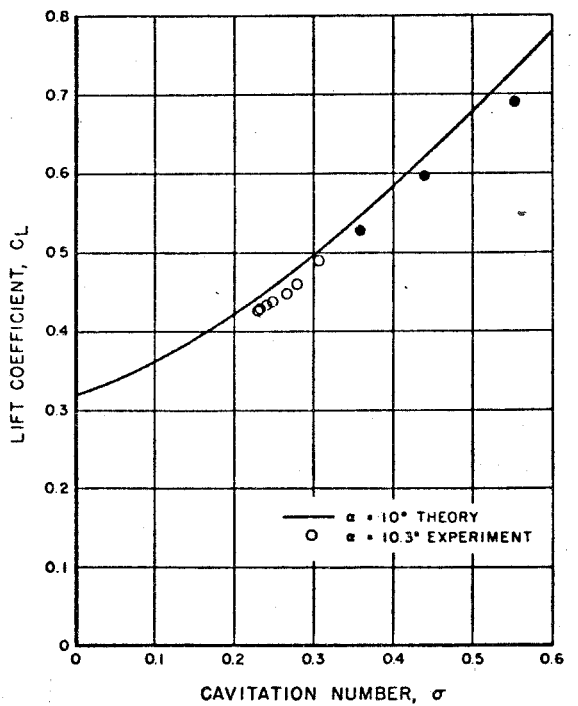
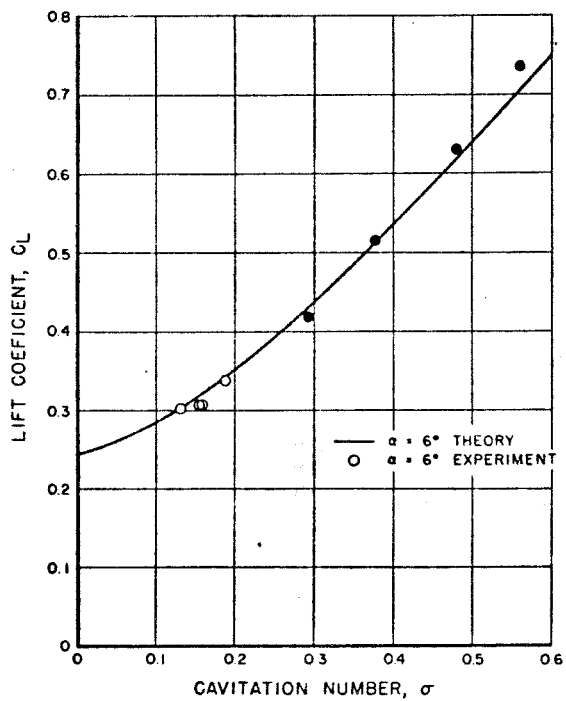
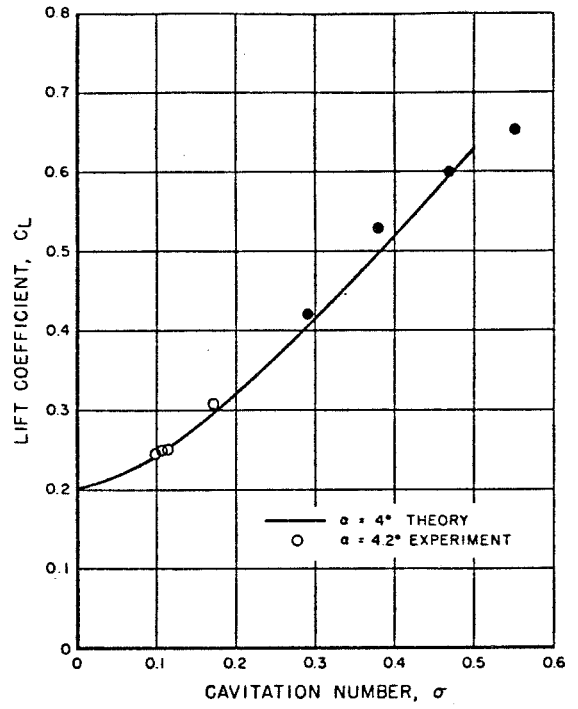
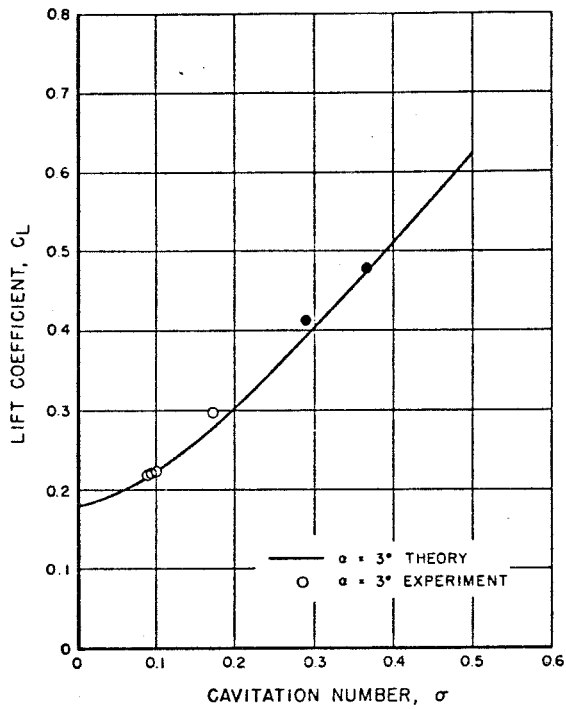


Fig. 43 Comparison of the experimental and theoretical section lift coefficients at low cavitation numbers.

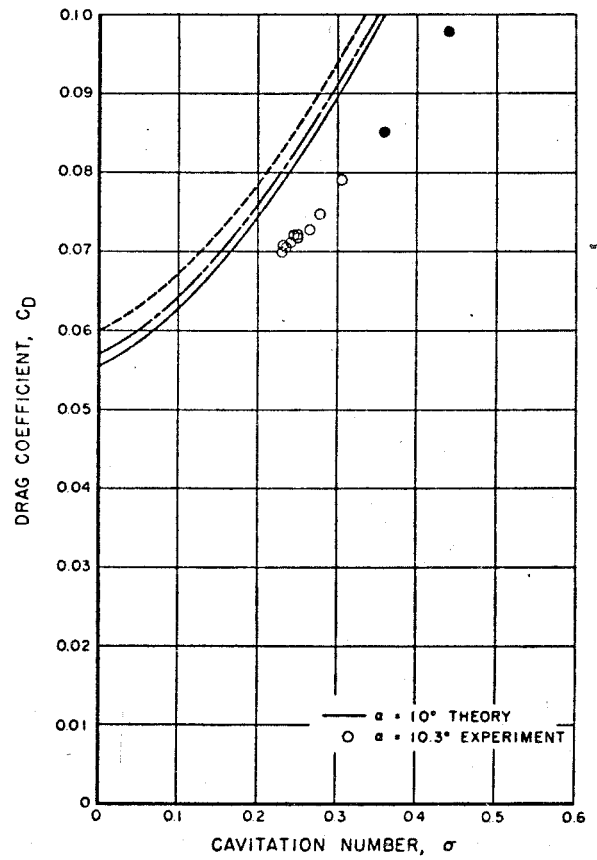
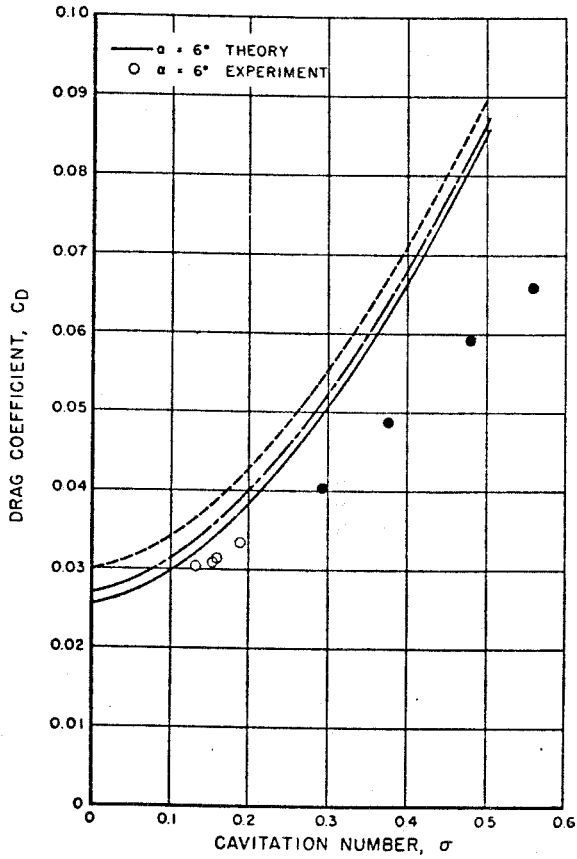
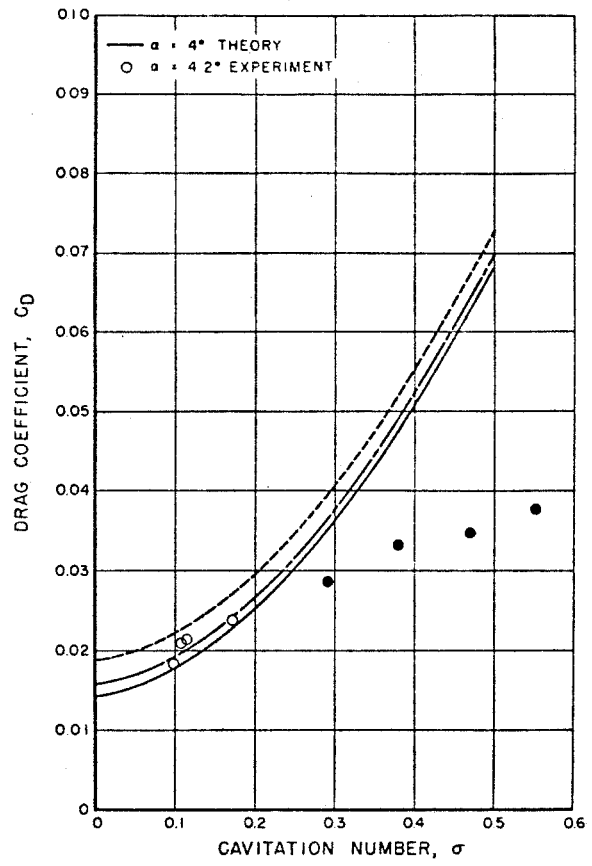
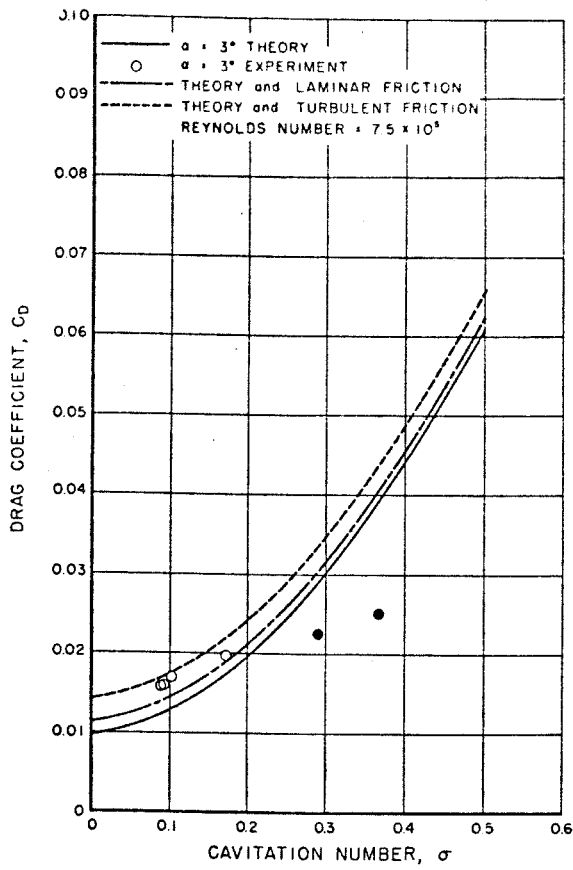


Fig. 44 Comparison of the experimental and theoretical section drag coefficients at low cavitation numbers.

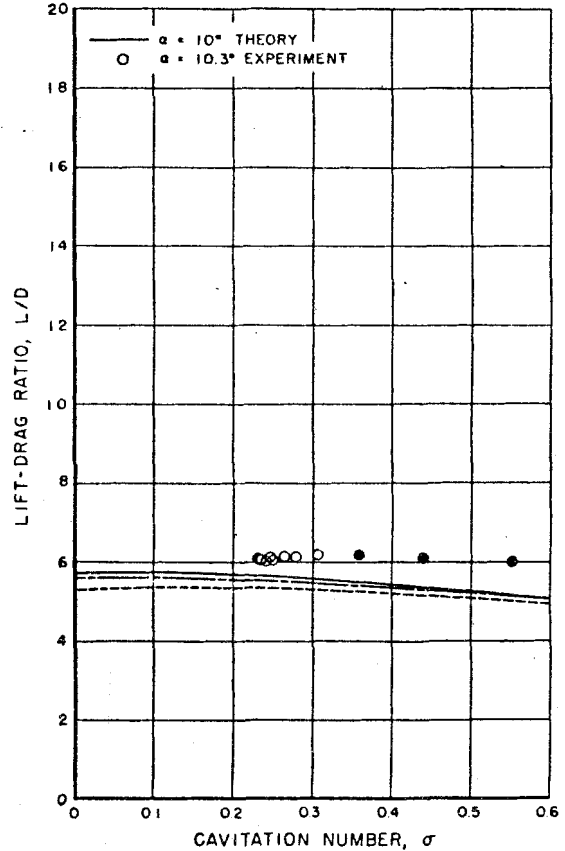
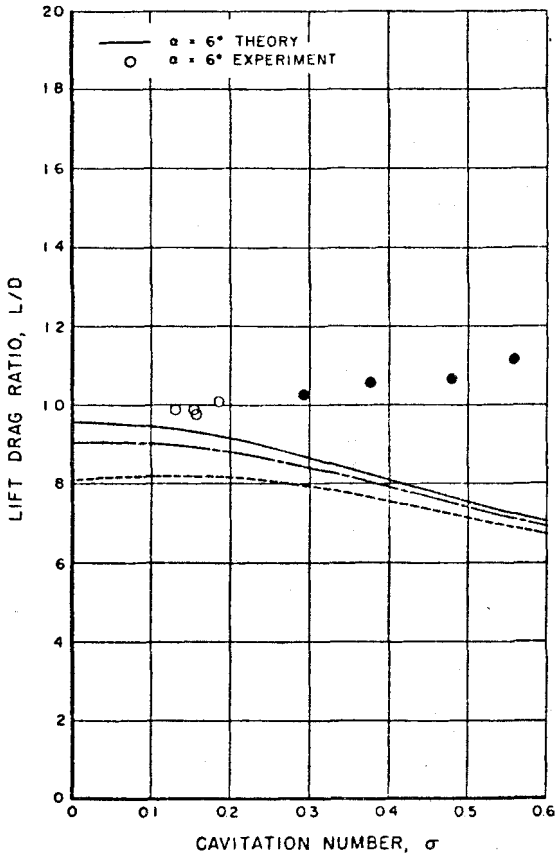
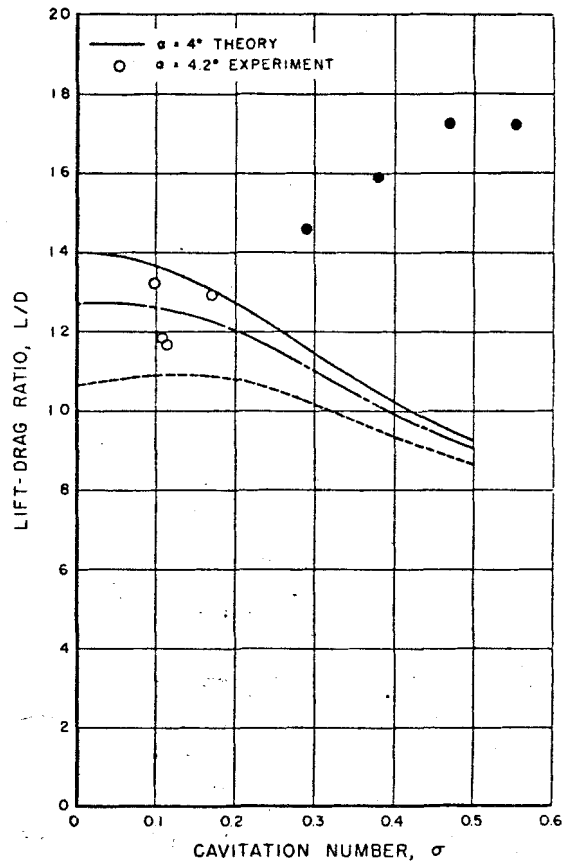
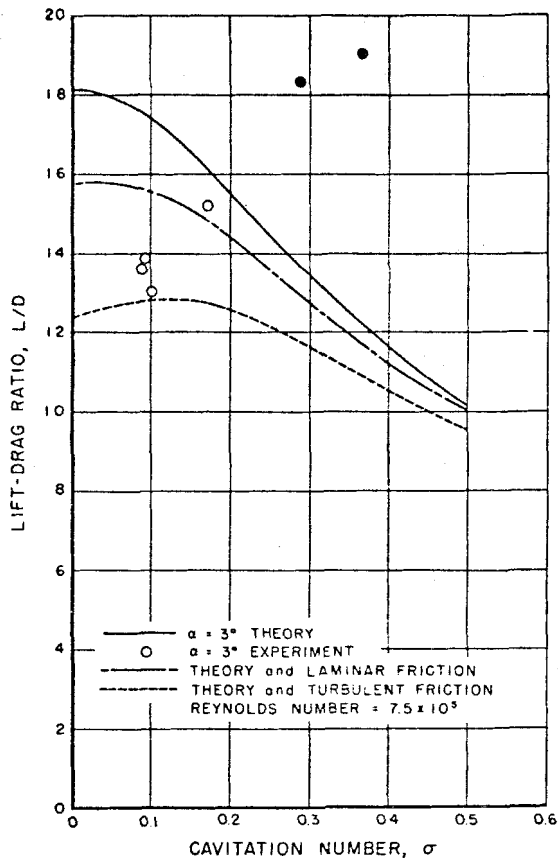


Fig. 45 Comparison of the experimental and theoretical section lift-drag ratios at low cavitation numbers.

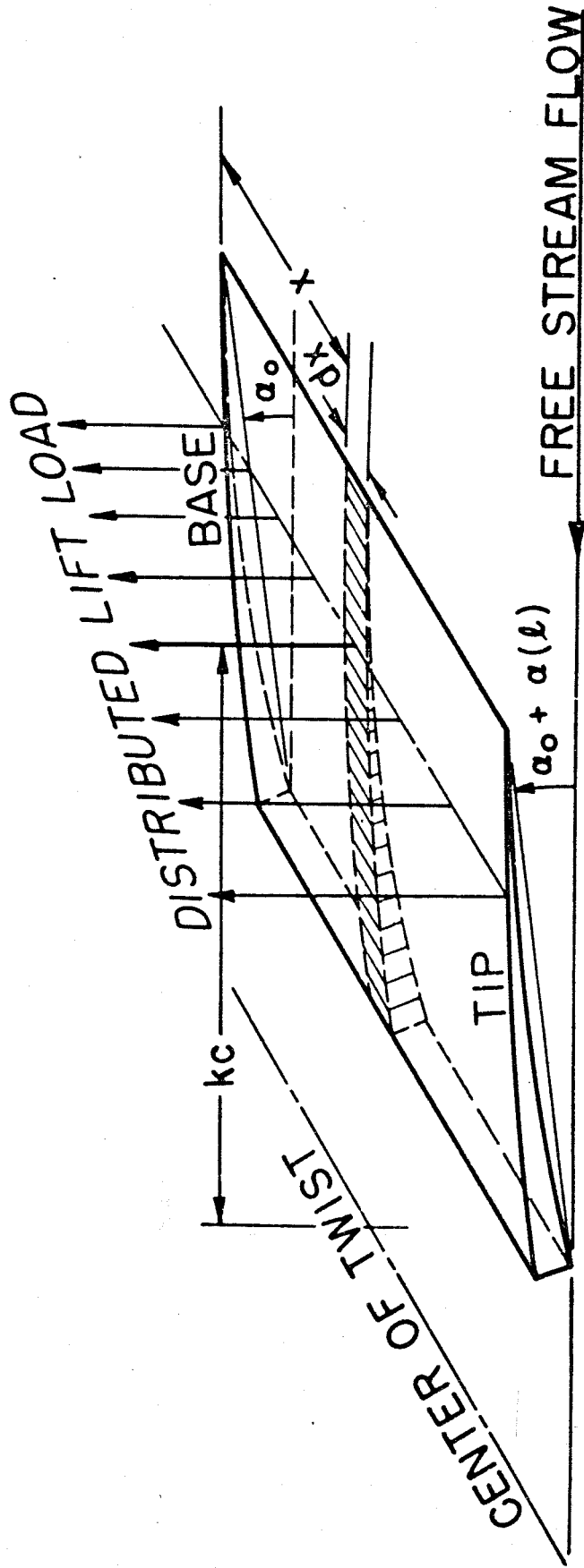


Fig. 46 Notation for hydrofoil twist corrections.

TABLE I - Ordinates for Supercavitating Hydrofoil

$\bar{x} = \frac{x}{c}$	$y = \frac{y_p}{c}$ (pressure side)	$y_c/c$ (cavity side)
0 (L. E.)	0	0
0.0075	.00043	.00145
0.0125	.00074	.00224
0.0500	.00323	.00713
0.1000	.00664	.01264
0.1500	.00980	.01783
0.2000	.01292	.02252
0.2500	.01557	.02706
0.3000	.01788	.03137
0.3500	.01974	.03580
0.4000	.02125	.04005
0.4500	.02235	.04432
0.5000	.02279	.04849
0.5500	.02285	.05255
0.6000	.02242	.05680
0.6500	.02146	.05990
0.7000	.02001	.06120
0.7500	.01802	.06175
0.8000	.01550	.06156
0.8500	.01243	.06090
0.9000	.00889	.05990
0.9500	.00472	.05857
1.0000 (T. E.)	0	.05691

TABLE II - Data for Supercavitating Hydrofoil

V=20 fps (fully wetted) - Run 1

Data No.	$\alpha$	$C_L$	$C_D$	$C_{M_0}$	$\alpha_{TLE}$	$\alpha_{T_e}$	$\alpha + \alpha_{T_e}$
1	0	0.0863	0.0291	-0.0845	-0.004	-0.003	-0.003
2	1	0.1917	0.0281	-0.1182	-0.004	-0.003	0.997
3	2	0.2872	0.0295	-0.1479	-0.053	-0.020	1.980
4	3	0.3854	0.0287	-0.1739	0.015	0.010	3.010
5	4	0.4860	0.0334	-0.1961	0.021	0.014	4.014
6	5	0.5881	0.0419	-0.2178	0.026	0.017	5.017
7	6	0.7162	0.0558	-0.2518	0.043	0.029	6.029
8	8	0.9468	0.0949	-0.3301	0.055	0.037	8.037
9	10	1.0738	0.1471	-0.4130	0.056	0.038	10.038
10	12	1.0146	0.1946	-0.4252	0.045	0.030	12.030
11	6	0.7216	0.0561	-0.2556	0.036	0.024	6.024
12	2	0.2891	0.0298	-0.1465	0.010	0.006	2.006
13	0	0.0866	0.0307	-0.0900	-0.001	0	0
14	-1	-0.0227	0.0352	-0.0613	-0.004	-0.003	-1.003
15	-2	-0.1512	0.0441	-0.0241	-0.016	-0.011	-2.011
16	-3	-0.3013	0.0588	0.0285	-0.015	-0.010	-3.010
17	-3	-0.3077	0.0598	0.0318	-0.026	-0.017	-3.017
18	-4	-0.4990	0.0827	0.1189	-0.026	-0.018	-4.018
19	-5	-0.6705	0.1054	0.2170	-0.028	-0.019	-5.019
20	0	0.0885	0.0326	-0.0887	0.001	0	0

Data No.	$\sigma_v$	$\sigma_k$	$C_L$	$C_D$	$C_{M_0}$	$\alpha_{TLE}$	$\alpha_{TM}$	$\alpha_{T_e}$	$C_L$	$C_D$	$C_{M_0}$	L/D
V = 30 fps, $\alpha = -2^\circ$ , $\alpha_a = -2.0$ , Run 16												
266	2.969		-0.1680	0.0477	-0.0182	-0.548		-0.365	-0.125	0.0446	-0.032	2.8
267	0.944		-0.1598	0.0516	-0.0154	-0.503		-0.335	-0.123	0.0476	-0.030	2.6
268	0.751		-0.1713	0.0542	-0.0103	-0.525		-0.350	-0.126	0.0491	-0.024	2.6
269	0.569		-0.2193	0.0517	0.0162	-0.763		-0.508	-0.140	0.0536	-0.007	3.2
270	0.383		-0.3736	0.0427	0.1516	-0.350		-0.233	-0.342	0.0408	0.139	8.4
271	0.283		-0.2418	0.0326	0.0899	-0.237		-0.158	-0.240	0.0317	0.084	7.6
272	0.241		-0.2031	0.0295	0.0726	-0.175		-0.117	-0.201	0.0289	0.069	7.0
273	0.188		-0.1409	0.0233	0.0439	-0.226		-0.150	-0.140	0.0226	0.043	6.2
274	0.143	0.124	-0.0871	0.0174	0.0214	-0.130		-0.086	-0.086	0.0171	0.022	5.0
275	0.112	0.095	-0.0679	0.0152	0.0147	-0.068		-0.045	-0.067	0.0150	0.015	4.5
276	0.101	0.086	-0.0667	0.0154	0.0154	-0.101		-0.067	-0.066	0.0152	0.015	4.3
277	0.103	0.087	-0.0667	0.0154	0.0157	-0.136		-0.090	-0.066	0.0152	0.016	4.3
278	0.102	0.082	-0.0724	0.0149	0.0192	-0.006		-0.004	-0.072	0.0149	0.019	4.8
279	0.103	0.088	-0.0666	0.0148	0.0169	-0.051		-0.034	-0.066	0.0147	0.017	4.5

V = 30 fps, $\alpha = 0^\circ$ , $\alpha_a = 0.0$ , Run 15												
251	2.947		0.0909	0.0322	-0.0934	-0.113		-0.075	0.100	0.0320	-0.096	3.1
252	0.643		0.0920	0.0307	-0.0837	-0.175		-0.116	0.103	0.0305	-0.088	3.4
253	0.458		0.0854	0.0298	-0.0811	-0.192		-0.128	0.098	0.0293	-0.088	3.3
254	0.365		0.0790	0.0255	-0.0792	-0.192		-0.128	0.094	0.0249	-0.083	3.8
255	0.282		0.0715	0.0232	-0.0759	-0.141		-0.094	0.083	0.0227	-0.080	3.7
256	0.239		0.0636	0.0194	-0.0737	-0.186		-0.124	0.081	0.0190	-0.079	4.3
257	0.183		-0.1400	0.0157	0.0506	-0.158		-0.105	-0.137	0.0155	0.048	-8.8
258	0.144		-0.0758	0.0139	0.0206	-0.113		-0.075	-0.074	0.0138	0.019	-5.4
259	0.097	0.078	-0.0156	0.0104	0.0047	-0.079		-0.053	-0.014	0.0104	0.003	-1.3
260	0.076	0.059	-0.0162	0.0104	-0.0026	-0.113		-0.075	-0.012	0.0104	-0.004	-1.2
261	0.070	0.057	-0.0165	0.0093	-0.0012	-0.034		-0.022	-0.016	0.0093	-0.002	-1.7
262	0.066	0.052	-0.0145	0.0092	-0.0018	-0.079		-0.053	-0.012	0.0092	-0.003	-1.3
263	0.064	0.052	-0.0155	0.0093	-0.0007	-0.073		-0.049	-0.013	0.0093	-0.002	-1.4

V = 30 fps, $\alpha = 1^\circ$ , $\alpha_a = 1.0$ , Run 14												
239	2.926		0.2051	0.0414	-0.1250	0.146		0.098	0.196	0.0414	-0.123	
240	0.313		0.1939	0.0189	-0.1054	0.045		0.030	0.192	0.0189	-0.105	10.2
241	0.179		0.1884	0.0151	-0.1022	-0.045		-0.030	0.190	0.0151	-0.103	12.6
242	0.138	0.122	0.1730	0.0135	-0.0971	0		0	0.173	0.0135	-0.097	12.8
243	0.093	0.078	0.1195	0.0121	-0.0785	-0.135		-0.090	0.130	0.0122	-0.081	10.7
244	0.072	0.060	0.1160	0.0127	-0.0760	-0.130		-0.087	0.125	0.0128	-0.078	9.8
245	0.072	0.058	0.1156	0.0125	-0.0756	-0.023		-0.015	0.117	0.0125	-0.076	9.4
246	0.069	0.056	0.1105	0.0124	-0.0731	-0.006		-0.004	0.111	0.0124	-0.073	9.0

V = 30 fps, $\alpha = 2^\circ$ , $\alpha_a = 2.0$ , Run 13												
227	2.936		0.3108	0.0315	-0.1540	0.164		0.110	0.300	0.0315	-0.151	9.5
228	0.375		0.3047	0.0239	-0.1462	0.265		0.177	0.287	0.0238	-0.141	12.1
229	0.282		0.3024	0.0193	-0.1351	0.265		0.177	0.284	0.0189	-0.128	15.0
230	0.176		0.2408	0.0166	-0.1084	0.158		0.106	0.237	0.0164	-0.107	14.4
231	0.138	0.122	0.2214	0.0152	-0.0981	0.085		0.057	0.219	0.0151	-0.098	14.5
232	0.098	0.084	0.1968	0.0138	-0.0890	0.119		0.079	0.195	0.0137	-0.089	14.2
233	0.083	0.069	0.1868	0.0136	-0.0855	0.107		0.072	0.184	0.0135	-0.085	13.6
234	0.084	0.070	0.1841	0.0135	-0.0839	0.057		0.038	0.182	0.0135	-0.084	13.5
235	0.074	0.061	0.1817	0.0137	-0.0823	0.040		0.027	0.180	0.0137	-0.082	13.1
236	0.066	0.053	0.1822	0.0136	-0.0820	0.091		0.061	0.179	0.0135	-0.082	13.3

V = 30 fps, $\alpha = 2.722^\circ$ , $\alpha_a = 2.722$ , Run 12												
210	2.919		0.3850	0.0319	-0.1722	0.301		0.200	0.365	0.0318	-0.170	11.5
211	1.108		0.3812	0.0329	-0.1620	0.357		0.237	0.358	0.0323	-0.163	11.1
212	0.923		0.3947	0.0361	-0.1667	0.470		0.313	0.364	0.0332	-0.158	11.0
213	0.651		0.3931	0.0333	-0.1620	0.566		0.377	0.356	0.0322	-0.162	11.1
214	0.453		0.3965	0.0277	-0.1600	0.351		0.234	0.365	0.0276	-0.161	13.2
215	0.283		0.4069	0.0206	-0.1714	0.413		0.275	0.365	0.0198	-0.158	18.4
216	0.184		0.2864	0.0176	-0.1156	0.261		0.174	0.282	0.0174	-0.114	16.2
217	0.139	0.119	0.2449	0.0157	-0.0971	0.238		0.158	0.242	0.0155	-0.097	15.6
218	0.102	0.084	0.2082	0.0143	-0.0825	0.192		0.128	0.206	0.0141	-0.083	14.6
219	0.085	0.068	0.2061	0.0144	-0.0799	0.186		0.124	0.203	0.0142	-0.080	14.3
220	0.080	0.063	0.2041	0.0144	-0.0782	0.158		0.106	0.201	0.0142	-0.078	14.2
221	0.081	0.064	0.2024	0.0145	-0.0810	0.186		0.124	0.199	0.0143	-0.081	13.9
222	0.081	0.061	0.2050	0.0142	-0.0781	0.226		0.151	0.202	0.0140	-0.078	14.4
224	0.093	0.075	0.2044	0.0142	-0.0792	0.175		0.117	0.201	0.0140	-0.079	14.4

TABLE II (Continued)

Data No.	$r_v$	$r_x$	$C_f$	$C_d$	$C_{m_0}$	$a_{TLE}$	$a_{TM}$	$a_{Tc}$	$C_L$	$C_D$	$C_{M_0}$	L/D
V = 40 fps, $\alpha = 2.722^\circ$ , $a_n = 2.8$ , Run 23												
368	2.148		0.3909	0.0302	-0.1698	0.532		0.355	0.359	0.0294	-0.161	12.2
369	1.269		0.3919	0.0316	-0.1702	0.583		0.389	0.357	0.0305	-0.160	11.7
370	1.124		0.3938	0.0336	-0.1707	0.515		0.344	0.363	0.0317	-0.161	11.5
371	1.012		0.3972	0.0323	-0.1701	0.578		0.385	0.366	0.0305	-0.160	12.0
372	0.803		0.4037	0.0333	-0.1684	0.634		0.423	0.367	0.0306	-0.160	12.0
373	0.397		0.4615	0.0275	-0.1833	0.866		0.578	0.412	0.0251	-0.170	15.2
374	0.293		0.4338	0.0248	-0.1887	0.493		0.329	0.411	0.0236	-0.180	17.5
375	0.177		0.2953	0.0195	-0.1248	0.481		0.321	0.296	0.0185	-0.124	16.0
376	0.121	0.111	0.2350	0.0165	-0.0989	0.374		0.250	0.233	0.0158	-0.099	14.7
377	0.087	0.078	0.2085	0.0155	-0.0869	0.329		0.220	0.207	0.0150	-0.087	13.8
378	0.083	0.074	0.2075	0.0154	-0.0858	0.436		0.291	0.205	0.0147	-0.086	13.9
379	0.088	0.081	0.2089	0.0152	-0.0865	0.317		0.214	0.207	0.0147	-0.086	14.1
380	0.083	0.075	0.2080	0.0155	-0.0856	0.436		0.191	0.206	0.0151	-0.085	13.6
381	0.083	0.075	0.2074	0.0153	-0.0852	0.369		0.246	0.204	0.0150	-0.085	13.6
382	0.079	0.071	0.2059	0.0154	-0.0839	0.278		0.186	0.204	0.0150	-0.084	13.6
383	0.087	0.080	0.2069	0.0154	-0.0853	0.385		0.257	0.204	0.0148	-0.085	13.8
384	0.086	0.079	0.2062	0.0155	-0.0846	0.385		0.257	0.203	0.0149	-0.084	13.6
*385	0.093	0.077	0.2094	0.0154	-0.0859	0.380		0.254	0.206	0.0148	-0.086	13.9
*386	0.095	0.074	0.2101	0.0152	-0.0861	0.215		0.144	0.208	0.0149	-0.086	14.0
*387	0.093	0.071	0.2105	0.0151	-0.0860	0.261		0.174	0.209	0.0148	-0.086	14.1
*388	0.093	0.072	0.2111	0.0154	-0.0861	0.250		0.167	0.209	0.0150	-0.086	13.9
389	0.086	0.080	0.2057	0.0161	-0.0835	0.261		0.174	0.204	0.0156	-0.083	13.1
V = 40 fps, $\alpha = 2.722^\circ$ , $a_n = 2.8$ , Run 24												
392	2.144		0.3957	0.0306	-0.1717	0.463		0.310	0.369	0.0299	-0.164	12.3
393	0.178		0.2982	0.0192	-0.1253	0.520		0.347	0.299	0.0182	-0.125	16.5
394	0.082	0.071	0.2046	0.0149	-0.0847	0.282		0.189	0.203	0.0144	-0.084	14.1
*395	0.093	0.067	0.2210	0.0141	-0.0918	0.333		0.223	0.219	0.0137	-0.092	15.9
*396	0.108	0.055	0.2195	0.0138	-0.0902	0.316		0.211	0.218	0.0133	-0.090	16.3
*397	0.119	0.053	0.2370	0.0135	-0.0976	0.367		0.245	0.235	0.0129	-0.097	18.1
*398	0.130	0.054	0.2365	0.0135	-0.0969	0.095		0.064	0.236	0.0133	-0.097	17.6
399	0.076	0.067	0.2015	0.0155	-0.0824	0.107		0.072	0.200	0.0154	-0.081	13.0
*400	0.097	0.065	0.2073	0.0151	-0.0853	0.152		0.102	0.206	0.0147	-0.085	14.0
*401	0.104	0.064	0.2117	0.0149	-0.0872	0.243		0.162	0.210	0.0145	-0.087	14.5
*402	0.112	0.061	0.2125	0.0148	-0.0884	0.169		0.114	0.211	0.0145	-0.088	14.5
403	0.075	0.070	0.2004	0.0157	-0.0813	0.175		0.117	0.199	0.0154	-0.081	12.9
*404	0.093	0.064	0.2079	0.0153	-0.0855	0.259		0.174	0.206	0.0148	-0.085	13.9
*405	0.107	0.069	0.2104	0.0153	-0.0867	0.254		0.170	0.209	0.0149	-0.086	14.0
*406	0.109	0.060	0.2097	0.0151	-0.0866	0.180		0.121	0.209	0.0149	-0.086	14.0
V = 40 fps, $\alpha = 2.722^\circ$ , $a_n = 2.9$ , Run 29												
464	2.125		0.4051	0.0301	-0.1742	0.373	0.096	0.064	0.399	0.0300	-0.172	13.3
465	0.377		0.5208	0.0280	-0.2268	0.820	0.171	0.114	0.481	0.0277	-0.218	17.4
466	0.324		0.4627	0.0259	-0.2025	0.955	0.282	0.188	0.426	0.0254	-0.195	16.8
467	0.284		0.4150	0.0241	-0.1797	0.707	0.282	0.188	0.398	0.0235	-0.173	16.8
468	0.171		0.2810	0.0192	-0.1181	0.413	0.193	0.129	0.281	0.0188	-0.117	14.9
469	0.120	0.117	0.2297	0.0168	-0.0960	0.430	0.204	0.136	0.229	0.0165	-0.096	13.9
470	0.100	0.098	0.2124	0.0162	-0.0884	0.385	0.160	0.107	0.211	0.0160	-0.088	13.2
471	0.090	0.088	0.2102	0.0159	-0.0871	0.243	0.039	0.026	0.210	0.0158	-0.087	13.3
472	0.079	0.078	0.2088	0.0158	-0.0850	0.243	0.216	0.144	0.208	0.0154	-0.085	13.5
473	0.075	0.072	0.2077	0.0156	-0.0839	0.187	0.105	0.070	0.207	0.0154	-0.084	13.4
474	0.069	0.065	0.2067	0.0152	-0.0827	0.147	0.149	0.099	0.205	0.0150	-0.083	13.7
475	0.068	0.064	0.2049	0.0151	-0.0814	0.192	0.116	0.077	0.204	0.0149	-0.081	13.7
476	0.049	0.044	0.2012	0.0143	-0.0788	0.215	0.094	0.063	0.200	0.0141	-0.079	14.2
V = 45 fps, $\alpha = 2.722^\circ$ , $a_n = 2.8$ , Run 37												
564	0.186		0.2807	0.0191	-0.1188	0.491	0.149	0.099	0.277	0.0188	-0.116	14.7
565	0.140	0.141	0.2420	0.0175	-0.1017	0.350	0.212	0.141	0.240	0.0171	-0.099	14.1
566	0.108	0.106	0.2107	0.0158	-0.0895	0.238	0.011	0.007	0.211	0.0158	-0.089	13.3
567	0.103	0.102	0.2093	0.0161	-0.0889	0.350	0.057	0.038	0.209	0.0157	-0.089	13.3
568	0.102	0.100	0.2091	0.0159	-0.0887	0.283	0.023	0.015	0.209	0.0158	-0.089	13.2
569	0.099	0.098	0.2087	0.0159	-0.0885	0.277	0.057	0.038	0.208	0.0156	-0.088	13.3
570	0.096	0.095	0.2070	0.0158	-0.0878	0.248	0.023	0.016	0.207	0.0157	-0.088	13.2
571	0.095	0.094	0.2066	0.0159	-0.0873	0.260	0.011	0.003	0.207	0.0159	-0.087	13.0
572	0.093	0.092	0.2061	0.0158	-0.0869	0.310	0.103	0.068	0.204	0.0156	-0.086	13.1
573	0.089	0.089	0.2036	0.0156	-0.0855	0.198	0.091	0.061	0.202	0.0155	-0.085	13.0
574	0.086	0.086	0.2029	0.0155	-0.0848	0.079	0	0	0.203	0.0155	-0.085	13.1
575	0.083	0.082	0.2014	0.0153	-0.0838	0.011	-0.081	-0.054	0.203	0.0154	-0.084	13.2
V = 30 fps, $\alpha = 3^\circ$ , $a_n = 3.2$ , Run 2												
23	2.792		0.4168	0.0365	-0.1809	0.227		0.152	0.401	0.0361	-0.178	11.1
24	1.329		0.4213	0.0369	-0.1760	0.301		0.201	0.402	0.0360	-0.173	11.2
25	1.102		0.4173	0.0389	-0.1719	0.290		0.193	0.397	0.0375	-0.169	10.6
26	0.929		0.4194	0.0385	-0.1705	0.256		0.171	0.401	0.0354	-0.168	11.3
27	0.738		0.4209	0.0412	-0.1669	0.272		0.282	0.392	0.0368	-0.162	10.6
28	0.382		0.5264	0.0265	-0.2259	0.414		0.876	0.463	0.0254	-0.170	18.2
29	0.203		0.3166	0.0203	-0.1278	0.380		0.254	0.308	0.0197	-0.126	15.6
30	0.140		0.2502	0.0169	-0.0968	0.193		0.129	0.247	0.0167	-0.097	14.8
V = 30 fps, $\alpha = 3^\circ$ , $a_n = 3.2$ , Run 3												
33	2.848		0.4217	0.0306	-0.1816	0.274		0.183	0.399	0.0305	-0.178	13.1
34	0.369		0.5087	0.0226	-0.2145	0.348		0.232	0.470	0.0218	-0.169	21.6
35	0.117		0.2218	0.0155	-0.0857	0.125		0.085	0.220	0.0154	-0.086	14.3
37	0.087		0.2132	0.0165	-0.0781	0.070		0.047	0.212	0.0164	-0.078	12.9
*38	0.091		0.2153	0.0156	-0.0798	0.002		0.002	0.215	0.0156	-0.080	13.8
V = 30 fps, $\alpha = 3^\circ$ , $a_n = 3.0$ , Run 4												
42	2.857		0.4280	0.0328	-0.1841	0.321		0.206	0.407	0.0322	-0.180	12.6
43	1.428		0.4186	0.0344	-0.1755	0.277		0.184	0.398	0.0335	-0.173	11.9
44	0.736		0.4270	0.0407	-0.1707	0.362		0.240	0.403	0.0350	-0.166	11.5
45	0.366		0.5040	0.0261	-0.2164	0.446		0.297	0.477	0.0250	-0.176	19.1
46	0.289		0.4179	0.0229	-0.1762	0.126		0.084	0.412	0.0225	-0.175	18.3
47	0.191	0.172	0.3020	0.0199	-0.1214	0.220		0.146	0.298	0.0196	-0.121	15.2
48	0.118	0.101	0.2251	0.0174	-0.0868	0.198		0.131	0.223	0.0171	-0.087	13.0
49	0.121	0.093	0.2250	0.0162	-0.0859	0.232		0.154	0.222	0.0160	-0.086	13.9
50	0.106	0.089	0.2199	0.0161	-0.0826	0.215		0.143	0.217	0.0159	-0.083	13.6
*51	0.115	0.076	0.2246	0.0159	-0.0839	0.237		0.158	0.222	0.0156	-0.084	14.2
*52	0.113	0.073	0.2208	0.0148	-0.0840	0.102		0.067	0.220	0.0147	-0.084	15.0

\* Added air to cavity.

TABLE II (Continued)

Data No.	$\sigma_v$	$\sigma_k$	$C_c$	$C_d$	$C_{m_0}$	$\alpha_{TLE}$	$\alpha_{TM}$	$\alpha_{Te}$	$C_L$	$C_D$	$C_{M_0}$	L/D
V = 30 fps, $\alpha = 3^\circ$ , $\alpha_a = 3.2$ , Run 11												
189	2.938		0.4171	0.0314	-0.1803	0.210		0.139	0.399	0.0313	-0.178	12.7
190	1.351		0.4269	0.0320	-0.1788	0.221		0.147	0.403	0.0318	-0.176	12.7
191	1.020		0.4260	0.0328	-0.1771	0.243		0.162	0.402	0.0324	-0.174	12.4
192	0.643		0.4298	0.0335	-0.1694	0.469		0.312	0.394	0.0326	-0.162	12.1
193	0.556		0.4294	0.0302	-0.1729	0.322		0.214	0.399	0.0302	-0.169	13.2
194	0.457		0.4398	0.0282	-0.1658	0.345		0.229	0.400	0.0276	-0.162	14.5
195	0.366		0.5099	0.0255	-0.2185	0.475		0.316	0.483	0.0240	-0.172	20.1
196	0.275		0.4029	0.0217	-0.1688	0.328		0.218	0.410	0.0210	-0.165	19.5
197	0.233		0.3499	0.0204	-0.1443	0.271		0.180	0.345	0.0200	-0.141	17.2
198	0.183	0.160	0.2588	0.0182	-0.1199	0.232		0.154	0.286	0.0179	-0.120	16.0
199	0.133	0.109	0.2349	0.0160	-0.0914	0.074		0.048	0.234	0.0160	-0.091	14.6
200	0.109	0.088	0.2188	0.0160	-0.0841	-0.010		-0.008	0.219	0.0160	-0.084	13.7
201	0.103	0.085	0.2164	0.0156	-0.0823	0		0	0.216	0.0156	-0.082	13.8
202	0.093	0.076	0.2142	0.0155	-0.0805	0.034		0.022	0.213	0.0155	-0.081	13.7
203	0.104	0.085	0.2020	0.0139	-0.0754	0.040		0.026	0.201	0.0139	-0.075	14.5
204	0.082	0.064	0.2118	0.0143	-0.0788	0.004		0.003	0.212	0.0143	-0.079	14.8
*205	0.110		0.2185	0.0143	-0.0826				(0.218)	(0.0143)	(-0.083)	(15.2)
*206	0.110	0.074	0.2194	0.0146	-0.0830	-0.010		-0.008	0.219	0.0146	-0.083	15.0
*207	0.133	0.084	0.2240	0.0144	-0.0855	0.034		0.022	0.224	0.0144	-0.086	15.6
V = 30 fps, $\alpha = 3^\circ$ , $\alpha_a = 3.0$ , Run 40												
610	0.295		0.4236	0.0236	-0.1790	0.305		0.203	0.413	0.0226	-0.174	18.3
611	0.199		0.2878	0.0190	-0.1145	0.298		0.132	0.285	0.0187	-0.114	15.2
613	0.157	0.150	0.2665	0.0169	-0.1072	0.224		0.150	0.264	0.0166	-0.107	15.9
614	0.124	0.121	0.2224	0.0160	-0.0866	0.291		0.127	0.220	0.0158	-0.087	13.9
615	0.110	0.106	0.2194	0.0154	-0.0842	0.179		0.120	0.217	0.0152	-0.084	14.3
**616	0.109	0.105	0.2178	0.0146	-0.0826	0.291		0.127	0.216	0.0144	-0.083	15.0
**617	0.293		0.4021	0.0210	-0.1680	0.360		0.241	0.400	0.0203	-0.164	19.7
**618	0.198	0.188	0.2891	0.0169	-0.1160	0.219		0.146	0.286	0.0166	-0.116	17.2
**619	0.124	0.120	0.2203	0.0148	-0.0856	0.179		0.120	0.218	0.0146	-0.086	14.9
**620	0.111	0.106	0.2178	0.0155	-0.0834	0.185		0.123	0.216	0.0153	-0.083	14.1
**621	0.105	0.101	0.2155	0.0153	-0.0811	0.117		0.078	0.215	0.0151	-0.081	14.2
V = 30 fps, $\alpha = 3^\circ$ , $\alpha_a = 3.2$ , Run 41												
624	0.106	0.103	0.2187	0.0142	-0.0811	0.165		0.111	0.217	0.0140	-0.081	15.5
625	0.102	0.098	0.2183	0.0149	-0.0804	0.080		0.054	0.217	0.0148	-0.080	14.7
V = 40 fps, $\alpha = 3^\circ$ , $\alpha_a = 3.2$ , Run 25												
409	2.127		0.4189	0.0299	-0.1745	0.503			0.395	0.0301	-0.169	13.4
410	0.902		0.4408	0.0439	-0.1774	0.734			0.418	0.0425	-0.173	9.8
411	0.372		0.5327	0.0289	-0.2347		0.310	0.207	0.522	0.0279	-0.231	18.7
412	0.274		0.4070	0.0246	-0.1743		0.298	0.199	0.403	0.0238	-0.175	16.9
413	0.162	0.150	0.2814	0.0187	-0.1175		0.230	0.153	0.282	0.0183	-0.118	15.1
414	0.109	0.104	0.2268	0.0160	-0.0928	0.480		0.100	0.226	0.0157	-0.093	14.4
415	0.094	0.089	0.2292	0.0157	-0.0939	0.344		0.138	0.229	0.0155	-0.094	14.7
*416	0.115	0.070	0.2254	0.0157	-0.0916	0.231		0.115	0.225	0.0155	-0.091	14.5
417	0.095	0.083	0.2187	0.0167	-0.0883		0.207	0.138	0.218	0.0163	-0.088	13.4
418	0.093	0.087	0.2188	0.0167	-0.0876	0.339		0.126	0.218	0.0165	-0.088	13.2
419	0.093	0.088	0.2183	0.0168	-0.0876	0.429		0.344	0.216	0.0161	-0.087	13.4
V = 45 fps, $\alpha = 3^\circ$ , $\alpha_a = 3.0$ , Run 36												
549	0.191		0.2906	0.0248	-0.1223	0.396	0.178	0.118	0.287	0.0244	-0.120	11.8
550	0.140	0.136	0.2487	0.0180	-0.1038	0.413	-0.034	-0.023	0.250	0.0181	-0.104	13.8
551	0.109	0.105	0.2182	0.0163	-0.0916	0.385	0.178	0.118	0.215	0.0160	-0.091	13.4
552	0.107	0.103	0.2184	0.0163	-0.0913	0.294	0.023	0.015	0.218	0.0163	-0.091	13.4
553	0.109	0.105	0.2168	0.0164	-0.0907	0.402	0.081	0.053	0.216	0.0163	-0.090	13.3
554	0.107	0.102	0.2185	0.0158	-0.0912	0.334	0.092	0.061	0.217	0.0156	-0.091	13.4
555	0.107	0.102	0.2172	0.0158	-0.0906	0.198	0.098	0.065	0.216	0.0156	-0.090	13.8
556	0.103	0.098	0.2161	0.0146	-0.0896	0.227	0.035	0.023	0.216	0.0145	-0.090	14.8
557	0.101	0.097	0.2152	0.0160	-0.0892	0.204	0.109	0.072	0.215	0.0158	-0.089	13.6
558	0.098	0.094	0.2143	0.0152	-0.0886	0.153	0.178	0.118	0.212	0.0148	-0.088	14.3
559	0.096	0.092	0.2135	0.0146	-0.0876	0.153	0.012	0.007	0.213	0.0146	-0.088	14.5
560	0.094	0.090	0.2121	0.0145	-0.0864	0.148	0.035	0.023	0.212	0.0144	-0.086	14.7
V = 45 fps, $\alpha = 3.5^\circ$ , $\alpha_a = 3.6$ , Run 35												
531	0.192		0.3052	0.0235	-0.1261	0.549	0.075	0.050	0.304	0.0232	-0.126	13.1
532	0.154	0.149	0.2691	0.0212	-0.1103	0.368	0.011	0.007	0.269	0.0211	-0.110	12.8
533	0.123	0.118	0.2412	0.0199	-0.0991	0.408	-0.033	-0.022	0.242	0.0200	-0.099	12.1
534	0.122	0.117	0.2404	0.0196	-0.0983	0.408	0.032	0.021	0.239	0.0195	-0.098	12.3
535	0.122	0.117	0.2401	0.0197	-0.0982	0.362	-0.033	-0.022	0.241	0.0198	-0.099	12.2
536	0.121	0.114	0.2393	0.0197	-0.0975	0.323	0.021	0.014	0.239	0.0197	-0.098	12.1
537	0.121	0.114	0.2389	0.0197	-0.0973	0.357	-0.044	-0.030	0.240	0.0198	-0.098	12.1
538	0.120	0.113	0.2383	0.0193	-0.0971	0.329	-0.174	-0.102	0.241	0.0197	-0.098	12.2
539	0.115	0.108	0.2363	0.0197	-0.0958	0.339	-0.033	-0.022	0.237	0.0199	-0.096	12.0
540	0.116	0.103	0.2364	0.0191	-0.0957	0.329	0.029	0.021	0.235	0.0190	-0.096	12.4
541	0.110	0.103	0.2353	0.0195	-0.0949	0.277	-0.066	-0.044	0.237	0.0197	-0.095	12.0
542	0.113	0.101	0.2345	0.0195	-0.0946	0.317	0.040	0.028	0.234	0.0194	-0.095	12.0
543	0.107	0.098	0.2325	0.0193	-0.0932	0.289	0	0	0.233	0.0193	-0.094	12.0
544	0.104	0.096	0.2320	0.0189	-0.0925	0.272	-0.123	-0.109	0.236	0.0194	-0.094	12.1
545	0.100	0.091	0.2301	0.0185	-0.0911	0.204	0	0	0.230	0.0185	-0.091	12.4
V = 30 fps, $\alpha = 4^\circ$ , $\alpha_a = 4.2$ , Run 5												
54	2.861		0.5327	0.0372	-0.2064	0.436		0.291	0.502	0.0357	-0.199	14.1
55	1.536		0.5321	0.0392	-0.2036	0.390		0.261	0.504	0.0365	-0.198	13.8
56	1.210		0.5476	0.0449	-0.2037	0.651		0.434	0.496	0.0408	-0.193	12.2
57	1.026		0.5443	0.0489	-0.1987	0.724		0.483	0.488	0.0464	-0.187	10.5
58	0.744		0.5491	0.0499	-0.1949	0.651		0.434	0.493	0.0480	-0.180	10.3
59	0.652		0.5924	0.0396	-0.2112	0.566		0.378	0.526	0.0366	-0.188	14.4
60	0.552		0.7220	0.0404	-0.3149	0.560		0.372	0.652	0.0378	-0.260	17.2
61	0.469		0.6273	0.0382	-0.2704	0.521		0.348	0.600	0.0348	-0.270	17.2
62	0.379		0.5202	0.0352	-0.2201	0.385		0.257	0.526	0.0331	-0.221	15.9
63	0.291		0.4165	0.0303	-0.1712	0.368		0.246	0.419	0.0287	-0.173	14.6
64	0.191	0.171	0.3065	0.0245	-0.1200	0.226		0.151	0.308	0.0238	-0.121	12.9
65	0.121	0.108	0.2517	0.0216	-0.0948	0.181		0.121	0.250	0.0211	-0.095	11.8
66	0.127	0.114	0.2524	0.0218	-0.0946	0.130		0.087	0.251	0.0215	-0.095	11.7
67	0.112	0.098	0.2461	0.0188	-0.0913	0.130		0.087	0.245	0.0185	-0.091	13.2
*69	0.122	0.026	0.2433	0.0188	-0.0893	0.153		0.102	0.241	0.0185	-0.089	13.0
*70	0.124	0.085	0.2393	0.0185	-0.0877	0.198		0.133	0.237	0.0182	-0.088	13.0

\* Added air to cavity.

\*\* Large tip clearance.

TABLE II (Continued)

Data No.	$\sigma_v$	$\sigma_k$	$C_L$	$C_D$	$C_{m_0}$	$\alpha_{TLE}$	$\alpha_{TM}$	$\alpha_{Te}$	$C_L$	$C_D$	$C_{M_0}$	L/D
V = 40 fps, $\alpha = 4^\circ$ , $\alpha_a = 4.2$ , Run 26												
422	2.253		0.5659	0.0414	-0.2123	0.946			0.532	0.0394	-0.205	13.5
423	1.200		0.5640	0.0443	-0.2102	0.934	0.367	0.245	0.530	0.0414	-0.204	12.8
424	0.978		0.5744	0.0450	-0.2065	0.956	0.424	0.283	0.530	0.0440	-0.199	12.0
425	0.326		0.4253	0.0335	-0.1796	0.725	0.298	0.199	0.429	0.0318	-0.181	13.5
426	0.272		0.3538	0.0286	-0.1465	0.691	0.333	0.222	0.353	0.0272	-0.147	13.0
427	0.216	0.207	0.3110	0.0255	-0.1279	0.566	0.218	0.146	0.311	0.0247	-0.128	12.6
428	0.189	0.179	0.2782	0.0233	-0.1134	0.532	0.264	0.176	0.278	0.0224	-0.113	12.4
429	0.162	0.157	0.2624	0.0225	-0.1064	0.385	0.195	0.130	0.261	0.0217	-0.106	12.0
* 430	0.167	0.100	0.2558	0.0223	-0.1026	0.419	0.287	0.191	0.254	0.0214	-0.102	11.9
* 431	0.167	0.120	0.2558	0.0213	-0.1023	0.340	0.230	0.153	0.254	0.0207	-0.102	12.3
* 432	0.167	0.111	0.2548	0.0211	-0.1015	0.425	0.172	0.115	0.253	0.0207	-0.101	12.2
V = 40 fps, $\alpha = 4^\circ$ , $\alpha_a = 4.3$ , Run 27												
435	2.163		0.2372	0.396	-0.2027	0.820	0.250	0.167	0.526	0.0378	-0.200	13.9
436	0.180	0.171	0.2986	0.248	-0.1232	0.424	-0.024	-0.016	0.298	0.0249	-0.124	12.0
437	0.153	0.146	0.2842	0.234	-0.1168	0.328	0.136	0.091	0.284	0.0230	-0.117	12.3
438	0.126	0.119	0.2523	0.213	-0.1021	0.220	0.171	0.114	0.251	0.0208	-0.101	12.1
439	0.084	0.076	0.2428	0.210	-0.0958	0.300	0.080	0.053	0.241	0.0207	-0.095	11.7
* 440	0.103	0.070	0.2393	0.201	-0.0944	0.238	-0.012	-0.008	0.239	0.0201	-0.094	11.9
* 441	0.107	0.063	0.2371	0.200	-0.0934	0.333	0.102	0.068	0.236	0.0198	-0.092	11.9
V = 40 fps, $\alpha = 4^\circ$ , $\alpha_a = 4.1$ , Run 28												
444	2.189		0.5559	0.0400	-0.2054	1.024	0.218	0.145	0.536	0.0379	-0.202	14.2
445	0.167	0.162	0.2935	0.0235	-0.1211	0.436	0	0	0.293	0.0234	-0.121	12.5
446	0.124	0.120	0.2532	0.0208	-0.1026	0.300	-0.022	-0.015	0.253	0.0209	-0.103	12.1
* 447	0.158	0.107	0.2578	0.0200	-0.1009	0.306	-0.010	-0.007	0.248	0.0200	-0.101	12.4
* 448	0.172	0.124	0.2577	0.0198	-0.1002	0.396	0.127	0.085	0.246	0.0194	-0.100	12.7
449	0.119	0.117	0.2513	0.0209	-0.1015	0.277	-0.022	-0.015	0.251	0.0210	-0.102	12.0
* 450	0.149	0.105	0.2468	0.0202	-0.1001	0.194	0.012	0.008	0.246	0.0202	-0.100	12.2
* 451	0.160	0.107	0.2471	0.0199	-0.0998	0.249	0.058	0.039	0.246	0.0197	-0.100	12.5
* 452	0.171	0.108	0.2458	0.0197	-0.0993	0.255	0.046	0.031	0.245	0.0196	-0.099	12.5
* 453	0.183	0.107	0.2464	0.0195	-0.0988	0.317	-0.114	-0.076	0.247	0.0198	-0.099	12.5
454	0.120	0.116	0.2512	0.0206	-0.1018	0.249	-0.079	-0.053	0.253	0.0208	-0.102	12.2
455	0.116	0.113	0.2498	0.0212	-0.1000	0.243	-0.033	-0.022	0.250	0.0213	-0.100	11.7
* 456	0.141	0.109	0.2480	0.0202	-0.1000	0.317	-0.033	-0.022	0.248	0.0203	-0.100	12.2
* 457	0.154	0.105	0.2457	0.0202	-0.1001	0.221	-0.068	-0.045	0.246	0.0204	-0.100	12.1
458	0.113	0.111	0.2485	0.0208	-0.0984	0.388	-0.022	-0.015	0.248	0.0209	-0.098	11.9
* 459	0.137	0.107	0.2472	0.0208	-0.0986	0.249	-0.056	-0.037	0.247	0.0210	-0.099	11.8
* 460	0.153	0.106	0.2440	0.0200	-0.0976	0.204	-0.148	-0.099	0.245	0.0204	-0.098	12.0
461	0.111	0.109	0.2479	0.0217	-0.0972	0.187	-0.011	-0.007	0.248	0.0219	-0.097	11.4
V = 40 fps, $\alpha = 4^\circ$ , $\alpha_a = 4.2$ , Run 30												
479	2.128		0.5452	0.0390	-0.2040	0.927	0.267	0.178	0.522	0.0373	-0.199	14.0
480	0.191		0.3033	0.0246	-0.1255	0.367	0.044	0.029	0.303	0.0244	-0.126	12.4
481	0.140	0.134	0.2548	0.0213	-0.1042	0.362	-0.045	-0.030	0.255	0.0214	-0.105	11.9
482	0.168	0.117	0.2507	0.0205	-0.1019	0.486	0.066	0.044	0.250	0.0204	-0.101	12.3
483	0.176	0.121	0.2528	0.0207	-0.1021	0.322	-0.067	-0.045	0.254	0.0210	-0.102	12.1
484	0.116	0.105	0.2464	0.0215	-0.0978	0.316	-0.022	-0.015	0.246	0.0216	-0.098	11.4
485	0.144	0.100	0.2439	0.0205	-0.0971	0.339	0	0	0.243	0.0205	-0.097	11.9
V = 40 fps, $\alpha = 4^\circ$ , $\alpha_a = 4.1$ , Run 31												
489	0.256	0.139	0.2539	0.0204	-0.1019	0.526	0.261	0.174	0.252	0.0197	-0.101	12.8
490	0.266	0.125	0.2569	0.0206	-0.1021	0.300	0.068	0.045	0.256	0.0204	-0.102	12.6
491	0.259	0.130	0.2559	0.0211	-0.1012	0.311	0.125	0.083	0.255	0.0207	-0.101	12.3
492	0.280	0.129	0.2540	0.0208	-0.1005	0.418	0.170	0.113	0.253	0.0203	-0.100	12.5
V = 45 fps, $\alpha = 4^\circ$ , $\alpha_a = 4.0$ , Run 32												
495	0.162	0.156	0.2827	0.0241	-0.1153	0.419	0.146	0.098	0.282	0.0236	-0.115	11.9
496	0.142	0.134	0.2589	0.0227	-0.1061	0.509	0.191	0.128	0.256	0.0220	-0.105	11.6
497	0.141	0.134	0.2585	0.0225	-0.1058	0.497	0.179	0.120	0.256	0.0219	-0.105	11.7
498	0.135	0.128	0.2569	0.0224	-0.1051	0.357	0.123	0.083	0.255	0.0220	-0.104	11.6
499	0.135	0.128	0.2566	0.0226	-0.1049	0.368	0.033	0.022	0.256	0.0224	-0.104	11.4
500	0.135	0.128	0.2559	0.0227	-0.1046	0.441	0.123	0.083	0.254	0.0223	-0.104	11.4
501	0.131	0.127	0.2555	0.0227	-0.1043	0.300	0.067	0.046	0.255	0.0224	-0.104	11.4
* 502	0.178	0.122	0.2610	0.0224	-0.1048	0.498	0.169	0.113	0.257	0.0219	-0.104	11.7
* 503	0.183	0.123	0.2596	0.0223	-0.1046	0.351	0.123	0.083	0.258	0.0219	-0.104	11.8
* 504	0.195	0.127	0.2609	0.0221	-0.1048	0.469	0.191	0.128	0.256	0.0215	-0.104	11.9
V = 45 fps, $\alpha = 4^\circ$ , $\alpha_a = 4.2$ , Run 33												
507	0.153	0.144	0.2602	0.0228	-0.1075	0.491	0.079	0.053	0.259	0.0225	-0.107	11.5
508	0.134	0.128	0.2553	0.0227	-0.1051	0.373	-0.011	-0.007	0.256	0.0227	-0.105	11.2
509	0.132	0.127	0.2542	0.0228	-0.1045	0.424	0.079	0.053	0.253	0.0225	-0.104	11.2
510	0.132	0.127	0.2538	0.0225	-0.1043	0.430	0	0	0.254	0.0225	-0.104	11.3
511	0.130	0.125	0.2538	0.0225	-0.1042	0.415	0	0	0.254	0.0225	-0.104	11.3
512	0.129	0.124	0.2526	0.0225	-0.1035	0.362	0.046	0.030	0.252	0.0223	-0.103	11.3
513	0.129	0.123	0.2524	0.0225	-0.1033	0.379	-0.022	-0.015	0.253	0.0226	-0.103	11.2
514	0.124	0.121	0.2513	0.0225	-0.1022	0.413	0.147	0.098	0.249	0.0220	-0.101	11.3
515	0.122	0.118	0.2505	0.0224	-0.1013	0.334	0.012	0.007	0.250	0.0224	-0.101	11.2
516	0.117	0.111	0.2487	0.0222	-0.1001	0.423	-0.011	-0.007	0.249	0.0222	-0.100	11.2
517	0.118	0.114	0.2474	0.0221	-0.0991	0.305	0.023	0.015	0.247	0.0220	-0.099	11.2
518	0.116	0.109	0.2473	0.0221	-0.0987	0.339	0.068	0.045	0.246	0.0219	-0.099	11.2
V = 45 fps, $\alpha = 4^\circ$ , $\alpha_a = 4.0$ , Run 34												
521	0.110	0.104	0.2469	0.0213	-0.0994	0.316	0	0	0.247	0.0213	-0.099	11.6
522	0.104	0.097	0.2456	0.0212	-0.0980	0.345	-0.033	-0.022	0.247	0.0213	-0.099	11.6
523	0.097	0.090	0.2424	0.0208	-0.0953	0.254	-0.066	-0.044	0.244	0.0210	-0.096	11.6
524	0.122	0.114	0.2493	0.0214	-0.1009	0.282	-0.033	-0.022	0.250	0.0220	-0.101	11.6
525	0.132	0.112	0.2488	0.0210	-0.1009	0.292	-0.066	-0.044	0.250	0.0212	-0.101	11.8
526	0.133	0.112	0.2482	0.0209	-0.1005	0.277	-0.045	-0.030	0.249	0.0211	-0.100	11.8
527	0.141	0.108	0.2472	0.0206	-0.0998	0.237	-0.033	-0.022	0.248	0.0207	-0.100	12.0

\* Added air to cavity

TABLE II (Continued)

Data No.	$\sigma_v$	$\sigma_k$	$C_f$	$C_d$	$C_{m0}$	$\alpha_{TLE}$	$\alpha_{TM}$	$\alpha_{Te}$	$C_L$	$C_D$	$C_{M0}$	L/D
V = 30 fps, $\alpha = 5^\circ$ , $\alpha_a = 5.0$ , Run 6												
73	2.989		0.6516	0.0486	-0.2342	0.787		0.525	0.597	0.0426	-0.219	14.0
74	1.604		0.6444	0.0502	-0.2293	0.663		0.442	0.599	0.0449	-0.216	13.3
75	1.405		0.6414	0.0516	-0.2238	0.651		0.434	0.599	0.0462	-0.212	13.0
76	1.241		0.6572	0.0524	-0.2289	0.673		0.449	0.602	0.0481	-0.216	12.5
77	1.026		0.6650	0.0521	-0.2284	0.708		0.472	0.604	0.0490	-0.201	12.3
78	0.841		0.7019	0.0514	-0.2427	0.719		0.480	0.614	0.0485	-0.210	12.7
79	0.657		0.8310	0.0563	-0.3568	0.623		0.415	0.811	0.0501	-0.328	16.2
80	0.568		0.7337	0.0537	-0.3167	0.504		0.336	0.722	0.0480	-0.321	15.0
81	0.478		0.6240	0.0495	-0.2644	0.453		0.302	0.626	0.0458	-0.267	13.7
82	0.391		0.5187	0.0421	-0.2146	0.430		0.286	0.520	0.0400	-0.216	13.0
83	0.291		0.4132	0.0347	-0.1662	0.294		0.196	0.413	0.0334	-0.166	12.4
84	0.204	0.185	0.3194	0.0276	-0.1239	0.362		0.242	0.315	0.0262	-0.124	12.0
85	0.145	0.126	0.2746	0.0236	-0.1034	0.175		0.117	0.273	0.0228	-0.102	12.0
86	0.126	0.117	0.2707	0.0236	-0.1004	0.283		0.188	0.268	0.0224	-0.100	12.0
87	0.733		0.8508	0.0570	-0.3504	0.702		0.468	0.735	0.0508	-0.264	14.5
88	0.149	0.138	0.2755	0.0232	-0.1015	0.277		0.185	0.273	0.0220	-0.101	12.4
* 89	1.007	0.040	0.3154	0.0275	-0.1175	0.203		0.136	0.313	0.0267	-0.117	11.7
* 90	0.145	0.145	0.2463	0.0232	-0.0960	0.198		0.132	0.242	0.0226	-0.095	10.7
V = 45 fps, $\alpha = 5^\circ$ , $\alpha_a = 5.2$ , Run 38												
579	0.200	0.197	0.3209	0.0327	-0.1317	0.629	0.286	0.191	0.319	0.0313	-0.131	10.2
580	0.165	0.160	0.2900	0.0298	-0.1181	0.590	0.271	0.115	0.289	0.0292	-0.117	9.9
581	0.161	0.157	0.2884	0.0297	-0.1173	0.590	0.276	0.183	0.287	0.0286	-0.116	10.0
582	0.160	0.154	0.2878	0.0295	-0.1170	0.391	0.143	0.096	0.287	0.0289	-0.117	9.9
583	0.157	0.152	0.2864	0.0291	-0.1160	0.498	0.338	0.226	0.284	0.0277	-0.115	10.2
584	0.151	0.146	0.2846	0.0288	-0.1151	0.397	0.149	0.099	0.284	0.0282	-0.114	10.1
585	0.152	0.148	0.2840	0.0290	-0.1145	0.459	0.149	0.099	0.283	0.0284	-0.114	10.0
586	0.149	0.145	0.2827	0.0288	-0.1136	0.369	0.086	0.057	0.282	0.0284	-0.113	9.9
587	0.147	0.142	0.2814	0.0284	-0.1127	0.289	0.131	0.088	0.281	0.0279	-0.112	10.1
588	0.141	0.137	0.2796	0.0283	-0.1116	0.340	0.171	0.115	0.278	0.0276	-0.111	10.1
589	0.137	0.135	0.2783	0.0278	-0.1104	0.363	0.074	0.040	0.277	0.0275	-0.110	10.1
590	0.134	0.131	0.2754	0.0271	-0.1085	0.228	0.074	0.040	0.274	0.0268	-0.108	10.2
V = 30 fps, $\alpha = 6^\circ$ , $\alpha_a = 6.0$ , Run 7												
93	2.953		0.7608	0.0617	-0.2617	0.637		0.425	0.713	0.0550	-0.250	13.0
94	1.693		0.7475	0.0637	-0.2545	0.596		0.398	0.696	0.0575	-0.243	12.1
95	1.505		0.7736	0.0668	-0.2609	0.846		0.564	0.710	0.0583	-0.246	12.2
96	1.510		0.7657	0.0664	-0.2517				0.710	0.0579	-0.239	12.3
97	1.327		0.7868	0.0675	-0.2640	0.761		0.507	0.725	0.0596	-0.248	12.2
98	1.142		0.8136	0.0679	-0.2751	0.790		0.526	0.740	0.0590	-0.253	12.5
99	0.914		0.9221	0.0730	-0.3486	0.716		0.477	0.830	0.0600	-0.292	13.8
100	0.744		0.9062	0.0785	-0.3880	0.658		0.439	0.885	0.0646	-0.386	13.7
101	0.559		0.7331	0.0698	-0.3137	0.579		0.275	0.735	0.0658	-0.317	11.2
102	0.480		0.6301	0.0622	-0.2649	0.449		0.288	0.631	0.0590	-0.267	10.7
103	0.376		0.5143	0.0515	-0.2108	0.454		0.292	0.514	0.0487	-0.212	10.6
104	0.293		0.4199	0.0421	-0.1680	0.380		0.242	0.418	0.0403	-0.168	10.4
105	0.207	0.187	0.3397	0.0349	-0.1315	0.330		0.208	0.337	0.0334	-0.131	10.1
106	0.170	0.158	0.3107	0.0323	-0.1179	0.216		0.133	0.307	0.0314	-0.117	9.8
108	0.169	0.154	0.3086	0.0318	-0.1159	0.222		0.137	0.306	0.0309	-0.115	9.9
109	0.146	0.132	0.3026	0.0313	-0.1109	0.199		0.121	0.301	0.0304	-0.110	9.9
*110	0.181	0.140	0.3000	0.0303	-0.1117	0.199		0.121	0.298	0.0292	-0.111	10.2
V = 45 fps, $\alpha = 6^\circ$ , $\alpha_a = 6.2$ , Run 39												
593	0.204	0.200	0.3366	0.0393	-0.1380	0.846	0.223	0.149	0.334	0.0382	-0.137	8.7
594	0.183	0.179	0.3218	0.0376	-0.1316	0.488	0.075	0.057	0.321	0.0372	-0.131	8.6
595	0.181	0.176	0.3203	0.0372	-0.1306	0.505	0.177	0.118	0.318	0.0364	-0.130	8.7
596	0.179	0.172	0.3192	0.0372	-0.1299	0.477	0.069	0.042	0.318	0.0369	-0.130	8.6
597	0.176	0.171	0.3177	0.0368	-0.1289	0.477	0.034	0.023	0.317	0.0367	-0.129	8.6
598	0.174	0.169	0.3166	0.0366	-0.1283	0.437	0.131	0.088	0.315	0.0359	-0.128	8.8
599	0.173	0.167	0.3157	0.0364	-0.1274	0.374	0	0	0.316	0.0364	-0.128	8.7
600	0.173	0.166	0.3143	0.0362	-0.1265	0.403	0.069	0.042	0.313	0.0359	-0.126	8.7
601	0.167	0.160	0.3120	0.0359	-0.1250	0.212	0.098	0.078	0.310	0.0354	-0.125	8.8
602	0.165	0.159	0.3110	0.0355	-0.1241	0.374	0.075	0.057	0.309	0.0351	-0.124	8.8
603	0.161	0.154	0.3088	0.0350	-0.1225	0.340	0	0	0.309	0.0350	-0.123	8.8
604	0.158	0.150	0.3068	0.0347	-0.1210	0.334	0.064	0.049	0.305	0.0344	-0.121	8.9
V = 30 fps, $\alpha = 7^\circ$ , $\alpha_a = 7.2$ , Run 8												
114	3.047		0.8791	0.0816	-0.2992	0.790		0.527	0.824	0.0721	-0.291	11.4
115	1.934		0.8557	0.0831	-0.2865	0.836		0.558	0.801	0.0729	-0.271	11.0
116	1.741		0.8658	0.0852	-0.2881	0.870		0.580	0.809	0.0744	-0.272	10.9
117	1.555		0.8823	0.0863	-0.2940	0.961		0.641	0.813	0.0742	-0.274	11.0
118	1.356		0.9301	0.0883	-0.3151	0.944		0.629	0.845	0.0756	-0.279	11.2
119	1.136		0.9899	0.0932	-0.3572	0.899		0.599	0.900	0.0792	-0.313	11.4
120	0.925		1.0450	0.1053	-0.4371	0.842		0.561	0.974	0.0889	-0.422	11.0
121	0.760		0.9185	0.0982	-0.3824	0.660		0.440	0.919	0.0870	-0.383	10.6
122	0.573		0.7247	0.0834	-0.3056	0.574		0.383	0.740	0.0750	-0.309	9.9
123	0.474		0.6182	0.0733	-0.2553	0.529		0.353	0.619	0.0693	-0.256	8.9
124	0.369		0.5062	0.0599	-0.2036	0.324		0.216	0.504	0.0577	-0.204	8.7
125	0.291	0.273	0.4353	0.0518	-0.1821	0.369		0.246	0.432	0.0496	-0.181	8.7
126	0.211	0.198	0.3563	0.0428	-0.1325	0.252		0.274	0.352	0.0406	-0.131	8.7
127	0.197	0.188	0.3445	0.0419	-0.1291	0.313		0.208	0.339	0.0402	-0.128	8.4
128	0.186	0.180	0.3395	0.0404	-0.1260	0.396		0.197	0.335	0.0389	-0.125	8.6
129	0.151	0.141	0.3301	0.0397	-0.1200				0.325	0.0380	-0.120	8.6
130	0.177	0.160	0.3358	0.0394	-0.1236	0.211		0.140	0.332	0.0384	-0.123	8.6
*131	0.200	0.180	0.3376	0.0397	-0.1247	0.205		0.136	0.336	0.0386	-0.124	8.7
*132	0.174	0.152	0.3293	0.0391	-0.1208	0.175		0.117	0.327	0.0382	-0.120	8.6

\* Added air to cavity

TABLE II (Continued)

Data No.	$\sigma_v$	$\sigma_k$	$C_f$	$C_d$	$C_{m0}$	$\sigma_{TLE}$	$\sigma_{TM}$	$\sigma_{Te}$	$C_L$	$C_D$	$C_{M0}$	L/D
V = 30 fps, $\alpha = 8^\circ$ , $\alpha_a = 8.2$ , Run 9												
135	3.114		1.0190	0.1105	-0.3601	0.901		0.601	0.924	0.0926	-0.329	10.0
136	2.097		0.9493	0.1090	-0.3408	0.976		0.650	0.910	0.0897	-0.307	10.4
137	1.920		0.9915	0.1103	-0.3370	0.936		0.623	0.916	0.0919	-0.305	10.0
138	1.731		1.0162	0.1090	-0.3359	0.964		0.643	0.923	0.0912	-0.305	10.1
139	1.540		1.0344	0.1148	-0.3562	0.924		0.616	0.941	0.0960	-0.316	9.8
140	1.320		1.0950	0.1191	-0.3990	0.958		0.639	1.016	0.0983	-0.351	10.3
141	1.164		1.1128	0.1284	-0.4314	1.044		0.696	1.045	0.1056	-0.382	9.9
142	1.060		1.1100	0.1315	-0.4543	0.901		0.601	1.060	0.1122	-0.429	9.4
143	0.982		1.0881	0.1320	-0.4597	0.833		0.555	1.071	0.1140	-0.452	9.4
144	0.821		0.9700	0.1225	-0.4100	0.730		0.487	0.972	0.1120	-0.410	8.7
145	0.736		0.8982	0.1147	-0.3845	0.725		0.483	0.904	0.1016	-0.387	8.9
146	0.649		0.8129	0.1070	-0.3451	0.594		0.395	0.818	0.0982	-0.348	8.3
147	0.566		0.7183	0.0959	-0.3003	0.571		0.380	0.722	0.0906	-0.302	8.0
148	0.475		0.6053	0.0835	-0.2466	0.474		0.315	0.606	0.0799	-0.248	7.6
149	0.384		0.5264	0.0710	-0.2111	0.388		0.259	0.524	0.0685	-0.211	7.6
150	0.290	0.274	0.4430	0.0592	-0.1744	0.342		0.228	0.440	0.0572	-0.174	7.7
151	0.217	0.207	0.3809	0.0511	-0.1452	0.314		0.209	0.377	0.0493	-0.144	7.6
152	0.200	0.193	0.3723	0.0496	-0.1403	0.325		0.217	0.368	0.0476	-0.139	7.7
153	0.178	0.179	0.3709	0.0492	-0.1369	0.211		0.141	0.364	0.0481	-0.136	7.6
154	0.215	0.194	0.3734	0.0491	-0.1403	0.223		0.148	0.370	0.0479	-0.139	7.7
155	0.202	0.185	0.3708	0.0494	-0.1394	0.240		0.160	0.368	0.0480	-0.138	7.7
*156	0.244		0.3750	0.0480	-0.1398	0.228		0.152	0.372	0.0468	-0.139	7.9
*157	0.197	0.167	0.3619	0.0475	-0.1336	0.195		0.129	0.359	0.0463	-0.133	7.8
*158	0.265	0.220	0.3772	0.0495	-0.1409	0.172		0.114	0.375	0.0486	-0.140	7.7
*159	0.196	0.152	0.3583	0.0480	-0.1324	0.217		0.144	0.354	0.0469	-0.131	7.5
V = 30 fps, $\alpha = 10^\circ$ , $\alpha_a = 10.3$ , Run 10												
162	2.980		1.0771	0.1696	-0.4220	0.871		0.580	1.091	0.1522	-0.410	7.17
163	1.899		1.1110	0.1636	-0.4078	0.963		0.641	1.099	0.1470	-0.396	7.48
164	1.712		1.1258	0.1687	-0.4140	0.934		0.622	1.115	0.1516	-0.404	7.36
165	1.528		1.1402	0.1726	-0.4302	0.986		0.657	1.131	0.1576	-0.424	7.18
166	1.321		1.1334	0.1815	-0.4528	0.906		0.603	1.135	0.1660	-0.453	6.84
167	1.053		1.1230	0.1861	-0.4813	1.038		0.691	1.123	0.1688	-0.484	6.65
168	0.882		0.9959	0.1695	-0.4289	0.860		0.573	1.001	0.1589	-0.432	6.30
169	0.730		0.8568	0.1483	-0.3605	0.642		0.427	0.860	0.1441	-0.364	5.97
170	0.642		0.7699	0.1345	-0.3187	0.545		0.363	0.774	0.1306	-0.323	5.93
171	0.552		0.6882	0.1198	-0.2803	0.585		0.389	0.690	0.1149	-0.282	6.00
172	0.431		0.5879	0.1013	-0.2349				0.586	0.0979	-0.234	5.99
173	0.439		0.5974	0.1015	-0.2385	0.722		0.347	0.596	0.0977	-0.237	6.10
174	0.358		0.5301	0.0877	-0.2085	0.384		0.256	0.527	0.0851	-0.207	6.19
175	0.321	0.306	0.4942	0.0816	-0.1927	0.390		0.259	0.490	0.0791	-0.192	6.19
176	0.293	0.278	0.4637	0.0772	-0.1783	0.467		0.244	0.460	0.0748	-0.177	6.15
177	0.275	0.265	0.4520	0.0753	-0.1727	0.356		0.236	0.448	0.0728	-0.171	6.15
178	0.258	0.247	0.4419	0.0741	-0.1677	0.316		0.210	0.439	0.0720	-0.166	6.10
179	0.256	0.248	0.4399	0.0736	-0.1663	0.270		0.179	0.437	0.0718	-0.165	6.09
180	0.256	0.249	0.4400	0.0740	-0.1661	0.270		0.179	0.437	0.0722	-0.165	6.65
181	0.250	0.241	0.4379	0.0734	-0.1647	0.310		0.206	0.434	0.0713	-0.163	6.1
182	0.246	0.233	0.4335	0.0727	-0.1618	0.275		0.183	0.430	0.0708	-0.160	6.1
183	0.248	0.236	0.4329	0.0725	-0.1616	0.264		0.175	0.429	0.0707	-0.160	6.1
184	0.248	0.232	0.4321	0.0715	-0.1609	0.235		0.156	0.428	0.0700	-0.160	6.1
*185	0.266	0.247	0.4329	0.0714	-0.1616	0.281		0.187	0.428	0.0696	-0.160	6.1
*186	0.252	0.206	0.4225	0.0697	-0.1571	0.191		0.133	0.418	0.0683	-0.156	6.1
V = 30 fps, $\alpha = 2.722^\circ$ , $\alpha_a = 2.456$ , Run 51												
718	2.915		0.3569	0.0304	-0.1647	0.215	0.040	0.143	0.342	0.0303	-0.161	11.3
720	1.093		0.3601	0.0357	-0.1588	0.294	0.097	0.196	0.340	0.0350	-0.158	9.7
721	0.912		0.3638	0.0354	-0.1590	0.282	0.109	0.188	0.347	0.0348	-0.158	10.0
722	0.645		0.3619	0.0308	-0.1561	0.276	0.183	0.184	0.345	0.0307	-0.152	11.2
723	0.464		0.3649	0.0288	-0.1535	0.282	0.029	0.188	0.345	0.0288	-0.150	12.0
724	0.272		0.3609	0.0206	-0.1492	0.203	0.155	0.136	0.350	0.0201	-0.143	17.4
725	0.099		0.2139	0.0138	-0.0856							
726	0.084	0.077	0.2098	0.0136	-0.0830	0.322		0.215	0.205	0.0133	-0.083	15.4
V = 30 fps, $\alpha = 4^\circ$ , $\alpha_a = 3.833$ , Run 52												
729	2.915		0.4973	0.0332	-0.1988	0.481	0.281	0.254	0.470	0.0320	-0.193	14.7
730	1.121		0.5004	0.0374	-0.1919	0.413	0.103	0.221	0.478	0.0356	-0.187	13.4
731	0.927		0.5193	0.0444	-0.1932	0.831	0.504	0.488	0.466	0.0406	-0.183	11.5
732	0.659		0.5415	0.0396	-0.1936	0.707	0.327	0.405	0.474	0.0362	-0.176	13.1
733	0.467		0.6429	0.0370	-0.2773	0.729	0.281	0.420	0.560	0.0344	-0.260	16.2
734	0.281		0.4086	0.0294	-0.1661							
735	0.121	0.114	0.2518	0.0194	-0.0940							
736	0.111	0.105	0.2496	0.0190	-0.0916		0.361					
737	0.109	0.102	0.2467	0.0173	-0.0887	0.288	0.246	0.126	0.245	0.0170	-0.089	14.4
V = 30 fps, $\alpha = 4^\circ$ , Run 53												
740	0.462		0.6208	0.0345	-0.2679							
741	0.417		0.5763	0.0347	-0.2472							
742	0.373		0.5096	0.0326	-0.2155							
743	0.322		0.4548	0.0292	-0.1890							
744	0.284		0.4132	0.0286	-0.1691							
745	0.237	0.227	0.3602	0.0246	-0.1439							
746	0.189	0.180	0.3013	0.0211	-0.1164							
747	0.148	0.139	0.2603	0.0178	-0.0977							

\* Added air to cavity

TABLE IIIa

## Prescribed Profile -

$\varphi_1$	Source	$K_A$	Source
.0646	rms, $\bar{x} = 0$ to .05 chord	-.819	rms, $\bar{x} = 0$ to .05 chord
.043	$\bar{x} = 0$	-.24	rms, $\bar{x} = 0$ to .5
.066	$\bar{x} = .02$ , peak near l.e.	.84	6M, $\bar{x} = 0$ to .5

$\varphi_2$	Source	$K_B$	Source
.100	$\bar{x} = 1.0$	.224	$\bar{x} = 1.0$ chord
		.21	rms and 6M, $\bar{x} = .5$ to 1.0

## Model Profile -

$\varphi_1$	Source	$K_A$	Source
.0583	rms, $\bar{x} = 0$ to .05 chord	-1.80	rms, $\bar{x} = 0$ to .05 chord
.010	$\bar{x} = 0$	-.55	rms, $\bar{x} = 0$ to .5
.069	$\bar{x} = .06$ , peak near l.e.	.01	6M, $\bar{x} = 0$ to .5

$\varphi_2$	Source	$K_B$	Source
.0790	rms, $\bar{x} = .9$ to 1.0 chord	-.406	rms, $\bar{x} = .9$ to 1.0 chord
.056	$\bar{x} = 1.0$	.12	rms, $\bar{x} = .5$ to 1.0
.087	$\bar{x} = .94$ , peak near t.e.	.13	6M, $\bar{x} = .5$ to 1.0

TABLE IIIb

$\varphi_1$	$\varphi_2$	$K_A$	$K_B$	$C_D$	$C_L$	$K_{\eta=\pi/2}$
(prescribed profile, $\alpha = 3^\circ$ , $\sigma = 0$ )						
.0646	.100	-.819	.224	.01024	.1946	.145
.043	.100	.84	.22	.01158	.1934	.115
.050	.100	.84	.22	.01118	.1940	.125
.065	.100	.84	.22	.01037	.1953	.147
.065	.100	.84	.21	.01070	.1967	.152
.065	.100	-.24	.21	.01069	.1966	.152
.065	.100	-.24	.22	.01036	.1953	.148
.065	.100	0	.13	.01352	.2077	.185
.066	.100	.84	.22	.01032	.1954	.149
(model profile, $\alpha = 3^\circ$ , $\sigma = 0$ )						
.0583	.0790	-1.80	-.406	.03376	.2505	.364
.058	.056	.01	.13	.00609	.1462	.110
.058	.079	-.55	.13	.00982	.1786	.144
.058	.079	.01	.13	.00983	.1786	.144
.058	.087	.01	.13	.01132	.1896	.156
.010	.079	.01	.13	.01250	.1745	.074
.069	.079	.01	.13	.00927	.1796	.159
.069	.087	.01	.13	.01072	.1906	.171
$\alpha = 10^\circ$ , $\sigma = 0$						
.010	.079	0	.13	.06125	.3149	.077
.058	.079	0	.13	.05541	.3193	.147

DISTRIBUTION LIST FOR TECHNICAL REPORTS ISSUED UNDER  
CONTRACT NONR-220(12)

<u>Item</u>	<u>Address</u>	<u>No. Copies</u>
1	Commanding Officer and Director, David Taylor Model Basin, Washington 7, D. C., Attn: Code 580	75
2	Chief of Naval Research, Office of Naval Research, Department of the Navy, Washington 25, D. C., Attn: Mechanics Branch (Code 438)	6
3	Commanding Officer, Branch Office, Office of Naval Research, 495 Summer St., Boston 10, Mass.	1
4	Commanding Officer, Branch Office, Office of Naval Research, 346 Broadway, New York 13, N. Y.	1
5	Commanding Officer, Branch Office, Office of Naval Research, The John Crerar Library Bldg., 10th Floor, 86 E. Randolph St., Chicago 1, Ill.	1
6	Commanding Officer, Branch Office, Office of Naval Research, 1000 Geary St., San Francisco 9, Calif.	1
7	Commanding Officer, Branch Office, Office of Naval Research, 1030 E. Green Street, Pasadena 1, Calif.	2
8	Asst. Naval Attache for Research, Office of Naval Research, American Embassy, London, England, Navy 100, F. P. O. New York, N. Y.	2
9	Director, Naval Research Laboratory, Office of Naval Research, Washington 25, D. C. Attn: Librarian	9
10	Bureau of Aeronautics, Dept. of the Navy, Washington 25, D. C., Attn: Aero and Hydro Branch (Code AD3)	2
11	Bureau of Ordnance, Dept. of the Navy, Washington 25, D. C., Attn: Code Re9 Code Re6 Code Re3	1 1 1
12	Commander, U. S. Naval Ordnance Laboratory, U. S. Navy Bureau of Ordnance, White Oak, Silver Spring 19, Maryland	2
13	Underwater Ordnance Dept., Naval Ordnance Test Station, 3202 E. Foothill Blvd., Pasadena, Calif. Attn: Pasadena Annex Library (Code P 5507)	3
14	Chief, Bureau of Ships, Dept. of the Navy, Washington 25, D. C. Attn: Technical Library (Code 312) for additional distribution to:	10

Distribution List (continued)

<u>Item</u>	<u>Address</u>	<u>No. Copies</u>
	(Bureau of Ships distribution) Research and Development (Code 300) Ship Design (Code 410) Preliminary Design (Code 420) Hull Design (Code 440) Hull Scientific (Code 442) Propeller Design (Code 554)	
15	Mr. R. H. Kent, Ballistic Research Laboratories, Dept. of the Army, Aberdeen Proving Ground, Maryland	1
16	Director of Research, National Advisory Committee for Aeronautics, 1512 H Street, N. W., Washington 25, D. C.	1
17	Director, Langley Aeronautical Lab., National Advisory Committee for Aeronautics, Langley Field, Virginia	1
18	Commander, Naval Ordnance Test Station, Inyokern, China Lake, Calif., Attn: Library (Code 5507)	1
19	Dr. K.S.M. Davidson, Experimental Towing Tank, Stevens Institute of Technology, Hoboken, N. J.	1
20	Dr. J.H. McMillen, National Science Foundation, 1520 H Street, N. W., Washington 25, D. C.	1
21	Dr. A. Miller, Bureau of Ordnance (Code Re3d) Navy Dept. Washington 25, D. C.	1
22	Dr. H. Rouse, Iowa Institute of Hydraulic Research, State University of Iowa, Iowa City, Iowa	1
23	Dr. R.G. Folsom, Director, Engineering Research Institute, University of Michigan, East Engineering Bldg. Ann Arbor, Michigan	1
24	Dr. V.L. Streeter, Engineering Dept., University of Michigan, Ann Arbor, Michigan	1
25	Dr. G.F. Wislicenus, Pennsylvania State University, Ordnance Research Laboratory, University Park, Pa.	1
26	Dr. A.T. Ippen, Dept. of Civil and Sanitary Engineering, Massachusetts Institute of Technology, Cambridge 39, Mass.	1
27	Dr. L.G. Straub, St. Anthony Falls Hydraulic Laboratory, University of Minnesota, Minneapolis 14, Minn.	1
28	Prof. K.E. Schoenherr, University of Notre Dame, College of Engineering, Notre Dame, Indiana	1
29	Director, Ordnance Research Laboratory, Pennsylvania State University, University Park, Pa.	1

Distribution List (continued)

<u>Item</u>	<u>Address</u>	<u>No. Copies</u>
30	Society of Naval Architects and Marine Engineers 74 Trinity Place, New York 6, N. Y.	1
31	Prof. J. K. Vennard, Stanford University, Dept. of Civil Engineering, Stanford, California	1
32	Prof. J. L. Hooper, Worcester Polytechnic Institute, Alden Hydraulic Laboratory, Worcester 6, Mass.	1
33	Prof. J. M. Robertson, Dept. of Theoretical and Applied Mechanics, University of Illinois, Urbana, Ill.	1
34	Dr. A. B. Kinzel, President, Union Carbide and Carbon Research Lab., Inc., 30 E. 42nd St., New York, N. Y.	1
35	Goodyear Aircraft Corp., Akron 15, Ohio, Attn: Security Officer	1
36	Prof. H. R. Henry, Hydraulics Laboratory, Michigan State College, East Lansing, Michigan	1
37	British Joint Services Mission, Navy Staff, P. O. Box 165 Benjamin Franklin Station, Washington, D. C., Via David Taylor Model Basin	9
38	Commander, Submarine Development Group TWO, Box 70, U. S. Naval Submarine Base, New London, Conn.	1
39	Commanding Officer and Director, U. S. Navy Engineering Experiment Station, Annapolis, Maryland	1
40	Library of Congress, Washington 25, D. C., Attn: ASTIA	1
41	Dr. P. R. Garabedian, Stanford University, Applied Mathematics and Statistics Laboratory, Stanford, California	1
42	Armed Services Technical Information Agency, Knott Building, Dayton, Ohio	5
43	Mr. J. G. Baker, Baker Manufacturing Company, Evansville, Wisconsin	1
44	Mr. T. M. Buerman, Gibbs and Cox, Inc., 21 West St., New York 6, New York	1
45	Dynamic Developments, Inc., St. Mark's Lane, Islip, Long Island, New York, Attn: Mr. W. P. Carl, Jr.	1
46	Hydrodynamics Research Laboratory, Consolidated- Vultee Aircraft Corporation, San Diego 12, California	1

Distribution List (continued)

<u>Item</u>	<u>Address</u>	<u>No. Copies</u>
47	Mr. R.K. Johnston, Miami Shipbuilding Corporation, 615 S.W. Second Avenue, Miami 36, Florida	1
48	Mr. J.D. Pierson, The Glenn L. Martin Company, Baltimore 3, Maryland	1
49	Mr. W.R. Ryan, Edo Corporation, College Point 56, Long Island, New York	1
50	Dr. Robert C. Seamans, Radio Corporation of America, Waltham, Massachusetts	1
51	Dr. A.G. Strandhagen, Department of Engineering Mechanics, University of Notre Dame, Notre Dame, Ind.	1
52	Dr. H.W.E. Lerbs, Hamburgische Schiffbau-Versuchsanstalt Hamburg 33, Bramfelderstrasse 164	1
53	Commander, Air Research and Development Command, P.O. Box 1395, Baltimore, Maryland. Attn: RDTDED	1
54	Avco Manufacturing Corp., Advanced Development Div., 2385 Revere Beach Parkway, Everett 49, Mass. Atten: Technical Librarian	1
55	Dr. L. Landweber, Iowa Inst. of Hydraulic Research, State University of Iowa, Iowa City, Ia.	1
56	The Naval Member, Canadian Joint Staff, 2001 Connecticut Ave., N.W., Washington 8, D.C. VIA David Taylor Model Basin -	3
57	Professor H. Reichardt, Max Planck Institut Fur Stromungsforschung, Gottingen, Germany	1